



Norwegian University of
Science and Technology

Linking Skyscrapers

A Conceptual Study on Skybridges' Effects on
the Structural Behaviour of Tall Buildings
Subject to Quasi-Static Wind Loads

Tormod Taraldsen

Civil and Environmental Engineering

Submission date: June 2017


Supervisor: Anders Rönquist, KT

Norwegian University of Science and Technology
Department of Structural Engineering



MASTER THESIS 2017

SUBJECT AREA: Engineering Architecture	DATE: 11.06.2017	NO. OF PAGES: 144
---	------------------	-------------------

TITLE: Linking Skyscrapers Sammenkoblede høyhus	
BY: Tormod Taraldsen	

SUMMARY: Increasing urbanisation has led to many cities now featuring 100m+ skyscrapers located right next to each other. Thus, the development of tall buildings will have a large impact on our future cities. In this thesis, the structural systems of tall buildings are studied and the general effect on the structural behaviour of two towers linked together by skybridges subject to wind loading is investigated. The general trends for deformations and stress distributions for skybridges of different structural configurations and height along the towers are reported. Among other findings, it was seen that by applying the structural links at heights of about 0,3 times the total height of the towers, the load on one of the towers could be shared equally amongst the base of both towers. Additionally, the displacement at the link was found to vary approximately linearly with link height, with the magnitude varying with link stiffness. The reported findings will hopefully be a useful tool in the conceptual design stage of a linked building system.

RESPONSIBLE TEACHER: Anders Rönquist
SUPERVISOR(S)
CARRIED OUT AT: Department of Structural Engineering, NTNU

Abstract

Increasing urbanisation has led to many cities now featuring 100m+ skyscrapers located right next to each other. Thus, the development of tall buildings will have a large impact on our future cities. In this thesis, the structural systems of tall buildings are studied and the general effect on the structural behaviour of two towers linked together by skybridges subject to wind loading is investigated. The trends for deformations and stress distributions for skybridges of different structural configurations and height along the towers are reported. Among other findings, it was seen that by applying the structural links at heights of about 0,3 times the total height of the towers, the load on one of the towers could be shared equally amongst the base of both towers. Additionally, the displacement at the link was found to vary approximately linearly with link height, with the magnitude varying with link stiffness. The reported findings will hopefully be a useful tool in the conceptual design stage of a linked building system.

Sammendrag

Økende urbanisering har ført til at mange byer nå innehar flere 100m+ høye skyskraper rett ved siden av hverandre. På grunn av dette vil utviklingen av høyhus ha en stor påvirkning på våre fremtidige byer. I denne oppgaven blir bæresystemet til høye bygninger studert og oppførselen til to høyhus koblet sammen med en bru påsatt vindlast er undersøkt. Overordnede fordelinger av deformasjoner og spenninger i bygningene for forskjellige brutyper og lokasjoner er rapportert. Blant flere funn, kan man se at ved å knytte husene sammen med en bru ved ca. 0,3 ganger husenes høyde, så kan man fordele lasten som opprinnelig bare virker på det ene tårnet til å bli fordelt til grunnen av begge tårnene. I tillegg ble det funnet at forskyvningen ved brulokasjonen varierer tilnærmet lineært med høyden opp til bruen, hvor størrelsen på forskyvningene varierer med brustivheten. De rapporterte funnene vil forhåpentligvis vise seg å være et brukbart verktøy i den konseptuelle designfasen av et sammenkoblet høyhussystem.

Problem formulation

This thesis is written for the subject group “Engineering Architecture” at the department of structural engineering at NTNU. The problem formulation given at the start of the project was:

For å utvikle nye og gode konstruksjoner i et samfunn under stadig utvikling er det stort behov for kunnskap om, og interesse for konseptuell design og formgivning av ulike konstruksjoner. Dette betyr at det også stilles større krav på ingeniørers evner til å håndtere funksjonelle og kontekstuelle parametere i tillegg til de tradisjonelle prosjekteringsfagene. For at vi som ingeniører skal bidra på beste måte i dette må vi også trene oss i å håndtere disse komplekse kravene.

Design av skyskraper

En naturlig del av arbeidet vil være å sette seg godt inn i aktuelle referansebygg og sentral arkitektur innen design av skyskraper som er valgt her. I tillegg til konstruktive egenskaper vil begrep som funksjonalitet, drift av bygning, effektivisering av etasjeplaner og form som visuelt uttrykk stå sentralt i oppgaven.

- Design av skyskraper, i perspektiv fra ingeniør, arkitekt, miljø og samfunn.*
- Hvordan finne form: direkte inngrep med arkitektonisk formgivning – frigjøre potensiale i komplekse konstruksjoner.*
- Formens funksjonalitet: lete etter og utnytte former i naturen til nye konstruktive elementer i bygninger – dine konsepter.*

Det er opp til kandidaten å selv velge og vektlegge problemstillinger relevant for oppgaven.

Based on this, a specific problem formulation for this thesis was agreed upon:

Oppgaven tar inspirasjon fra «Vertical Cities», dvs. skyskrapere som inneholder alle byfunksjoner vertikalt. Oppgaven vil legge vekt på studie av skyskraperes konstruksjon, relevante referanseprosjekter, og vil vurdere fordeler og ulemper ved forskjellige type

bærekonstruksjoner som skal sammenkoble skyskraperne, ved hjelp av rammeprogramanalyser.

Thesis supervisor: Anders Rönquist, NTNU

Preface

This master thesis was written during the spring semester of 2017, during the final year of my Master of Science degree at the Norwegian University of Science and Technology.

Ever since I took a basic mechanics course at the start of my university studies, I have been fascinated by spectacular structures such as large bridges or tall buildings, and how they distribute forces through their vast network of structural members. At the same time, the focus of my courses at university has been primarily on detailed design, usually limited to simple beams and frames or structural connections. The behaviour of more complex structural systems has rarely been the topic in class. I think this is a shame, because I believe that the qualitative force distribution of a complex indeterminate system requires more understanding of structural behaviour than the detailed design of weld sizes for a beam-to-column joint according to EC3-1-8, or the exact force distribution in a simple bar divided into five finite elements, all while being more interesting.

Thus, as I was choosing a topic for my Master's thesis, I immediately became interested in the possibility to write about skyscrapers, and better yet, to write about what I thought was interesting about them. Finally, I could use my university time to study the behaviour of a complex system in a more general way. I am very grateful to Anders and the group at Engineering Architecture for giving me this opportunity.

As stated in the problem formulation, the work in this thesis is concerned with the structural behaviour of skyscrapers, and how different link types to connect them will affect this. The goal is to obtain knowledge that will be relevant at a conceptual design stage for such linked building systems, by gaining an understanding of the probable distribution of load effects and deformations throughout the structure of tall buildings, compared to a similar unlinked system. This way the results can be used to better understand and identify which design parameters will be critical in the following, detailed analyses.

The thesis begins with a short introduction to why tall buildings are relevant today, and why the usage of structural links to connect skyscrapers at height has potential to better our cities. This is chapter 1.

Chapter 2 contains the history of how tall buildings have developed, and how structural systems have been invented to respond to buildings growing ever taller. It also contains a description of existing buildings that utilize structural links to improve their projects.

Chapter 3 describes the computer model used for analyses, and details the wind load calculation for the tall buildings.

Chapter 4 presents the results of the computer analysis on several models with different link types and locations, with a following discussion of the results, and how they can be used at a conceptual design stage.

Finally, chapter 5 ends the thesis with some concluding remarks, and my own ideas for further work within this field.

I would like to thank Anders for the support and guidance during my work on this thesis, without it I might not have reached the end.

TABLE OF CONTENTS

ABSTRACT.....	III
SAMMENDRAG	V
PROBLEM FORMULATION	VII
PREFACE	IX
1 INTRODUCTION	1
2 TALL BUILDINGS – DEVELOPMENT AND STRUCTURE	3
2.1 THE HISTORY OF TALL BUILDINGS	3
2.2 EXISTING LINKED SKYSCRAPERS.....	12
3 STRUCTURAL MODEL AND LOADING.....	19
3.1 STRUCTURAL MODEL.....	19
3.2 LOADING	21
3.3 BUILDING ACCELERATION	33
3.4 BASE MODEL LOAD CALCULATION	35
3.5 LOADS APPLIED TO OTHER MODELS	37
3.6 VERIFICATION OF MODEL	41
4 STRUCTURAL BEHAVIOUR.....	43
4.1 PORTAL FRAMES	43
4.2 SINGLE TOWER	46
4.3 STRUCTURAL LINKS	52
4.4 LINKS AT $H'=160M$	54
4.5 LINKS AT $H'=120M$	67
4.6 LINKS AT $H'=80M$	78
4.7 INITIAL OBSERVATIONS AND CONCLUSIONS	88
4.8 LINKS SPACING FOR EQUAL BEHAVIOUR.....	101
4.9 ERRORS.....	106
5 CONCLUDING REMARKS	107

1 Introduction

The increasing urbanisation of the global population coupled with increased sustainability demands have led to a large increase of tall buildings in the world, especially in densely populated countries in East-Asia. Tall building usage confer many benefits, such as reducing transportation demands and land usage, freeing up space for other purposes. However, as buildings have grown in height, the means of transportation between them has not changed.

While some cities now feature multiple skyscrapers of 40-50 stories practically right next to each other, Hong-Kong and Singapore being prime examples, the main method for getting to the 30th floor of one building from the 40th floor of the building next to it is by the ground floor. It is almost absurd that to move maybe 50 meters in the horizontal direction requires lifts carrying individuals 100-200 meters in the vertical directions. To enable a way to move directly from the 30th floor of one building to the 30th floor of the building adjacent, the most obvious solution is adding skybridges. By connecting skyscrapers together by skybridges, a new way of transportation can be utilized, letting people walk across the city without touching the ground, using “streets in the sky”.



Figure 1.1 Moses King's vision of future New York from 1908: a city filled with skyscrapers interconnected by bridges. Picture from [p, 1].

It may seem strange that the use of skybridges is not already a common occurrence in cities with a tall skyline. After all, interconnected skyscrapers are a standard fare in most science fiction works, and was already conceived as the future vision of the urban city back in 1908 in King's Dream of New York, see Figure 1.1. There are however, some significant challenges that must be overcome to make King's vision a reality. Antony Wood, the current director of CTBUH, the Council on Tall Buildings and Urban Habitat, describe some:

“If skybridges are to become an accepted element in high-rise design, not only between two towers but perhaps as an extensive network within a city, the first, and perhaps the biggest, challenge is the effect that this would have on project briefs. The clients/building owners need to agree to the idea of physical connection to a neighbour at height, and accept the necessary implications. In the case of most, if not all, buildings currently employing skybridges around the world, the two buildings are in common ownership and, even if the building is occupied on a multi-let basis, the landlord is effectively the same. Crucially also, this would have been the case when the buildings were conceived, designed and constructed; the skybridge would have been an integral part of the vision for the building; psychologically, constructionally and operationally. In the vast majority of our tall buildings today, connection occurs only at ground floor: the ‘pavement’ matrix within which the towers sit is usually owned by a separate, city authority body. Who would own the ‘pavement in the sky’, and thus be responsible for its construction, maintenance and security?” (Wood, 2003)

These obstacles seem too large to solve for a lowly engineering student, and will thus not be discussed much in this thesis. However, assuming they will be overcome, the use of skybridges also further complicate the already very complex structural behaviour of tall buildings. To gain knowledge on this seems within reason, and is the subject of this thesis.

2 Tall buildings – development and structure

Let us begin with a chapter on how the structure of tall buildings have evolved with time and technological advancement, to get an idea of how they work, and how they handle the structural challenges imposed upon them.

2.1 The history of tall buildings

The information presented in this chapter up to year 2000 is taken from the excellent book “Development in Structural Form”, by Rowland Mainstone (1998), pages 294-315, unless another source is cited.

The tall buildings we know today as «skyscrapers» first originated in Chicago after the city fire in 1871. These structures brought with them the separation of structure and façade, with the invention of load-bearing iron or steel frames and “curtain walls”, essentially facades that were hung like curtains off the structural frames. These new structural types outperformed the older buildings which didn’t separate structure and façade, namely buildings that utilized load bearing masonry walls to carry loads and to ensure lateral stability, one of the key challenges in tall building design. The slender frames created additional usable floor space while also bringing less self-weight, saving on loads needing to be transferred to the foundations, while at the same time being structurally sound.



Figure 2.1 The Monadnock Building (left) and Reliance Building (right). Note the 2m thick bottom walls for the Monandnock building. Photos from [p, 2] and [p, 3].

The 17-storey Monadnock Building is regarded as the limit of what can be achieved in tall-building design using load bearing masonry walls, requiring the walls to be nearly 2 m thick on the ground floor. For comparison, a 17-storey building built with a steel frame could get away with walls as slim as 0,4 to 0,5 m. The Reliance Building, completed in 1895, is regarded as the finest example of this new building type from this era, with 14 storeys going up to 60 meters in height. See Figure 2.1.

The steel frame buildings continued to grow in size and scope, and the development moved from Chicago to New York. The Empire State Building was completed in 1931, with a height of 381 meters and 102 storeys. The structure is a column-and-beam frame made in steel, with rigid connections ensuring the lateral stability of the building.

One of the first buildings to depart from the rigid-frame approach to lateral stability was the 13-storey IBM Office Building in Pittsburgh. Instead of vertical and horizontal columns and beams, it utilized an outer grid of diagonal members, usually referred to as “diagrid”, on each façade to carry all vertical and lateral loads. This system is much stiffer than the standard frame solution.

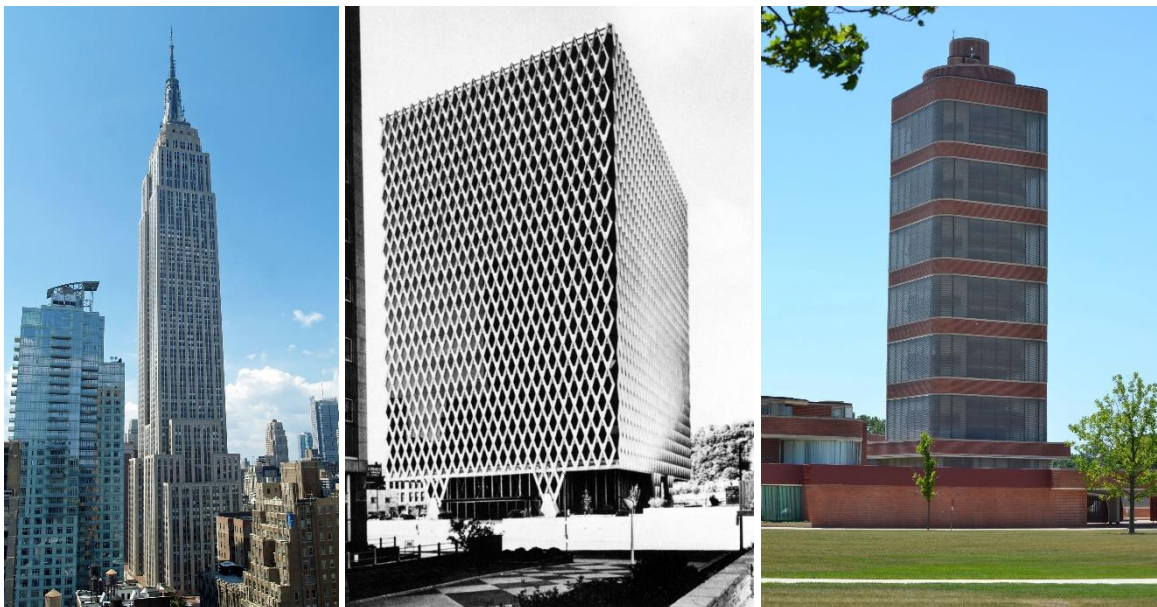


Figure 2.2 The Empire State Building (left), IBM Offices in Pittsburgh (centre), and Johnson Wax Research Tower (right). Photos from [p, 4], [p, 5], and [p, 6].

2. Tall buildings – development and structure

Another structural form that emerged was that of buildings using reinforced concrete cores. Utilizing solid concrete walls around lift shafts, stair and service runs, these cores with very few openings would act as vertical “tubes”, which is an inherently stiff form that was excellent at tackling lateral loads. The first building to use this structural system as the sole support was the Johnson Wax Research Tower from 1939, which had 14 floors individually cantilevered outwards from the central core, that transferred all vertical and lateral loads into the ground.

Some twenty years after this, the first building to use a bridge between two tall towers was completed (Wood, 2003). Oscar Niemeyer’s 1958 National Congress Complex in Brasilia featured two 92m high towers, connected by a three-storey bridge at the 14th to 16th floors, approximately halfway up its 28 floors total.

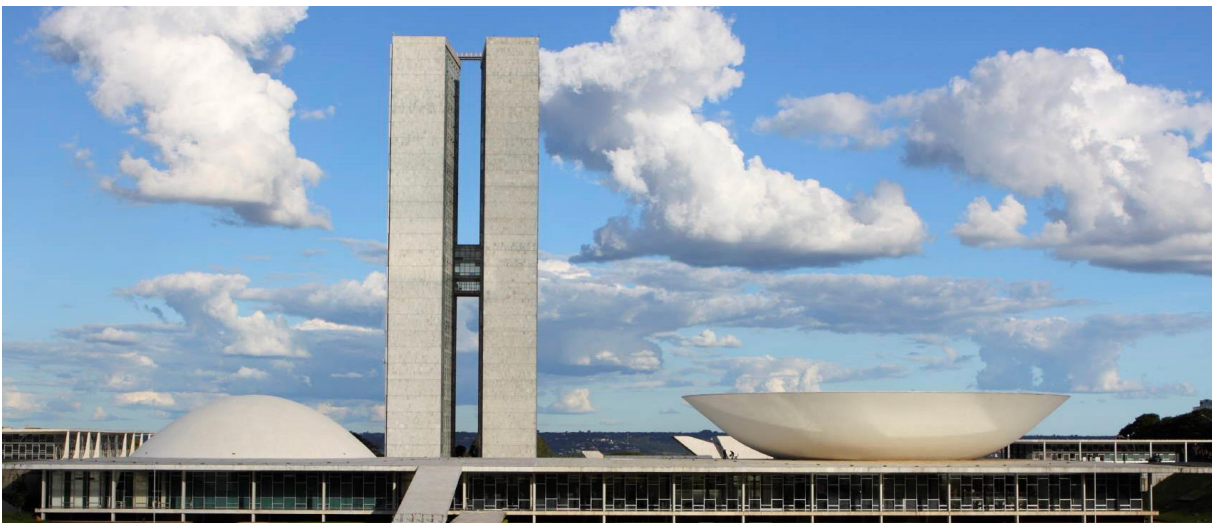


Figure 2.3 The Brasilia National Congress Complex, featuring the world’s first tall buildings linked at height. Photo from [p, 7].

So far tall buildings had been built with only commercial interests in mind, consisting primarily of offices. One of the first tall buildings to offer multi-use spaces were the twin Marina City Towers from 1964. The 180-meter-tall towers not only included office space, but also a yacht marina, shops, restaurants, car parking and 40 floors of residential apartments. These buildings would become early examples of what we now call “vertical cities”.

The development of tall buildings continued with the buildings ever increasing in height. This caused challenges for the rigid-frame buildings, as the increase in height imposed larger shear, bending and axial actions on the columns due to the larger vertical and lateral loads. The slender columns at the lower levels of a rigid-frame are worse equipped to tackle this increased stress than a reinforced concrete core, due to the rigid-frame suffering from large shear distortions, as opposed to the tube-form, which does not. See Figure 2.4.

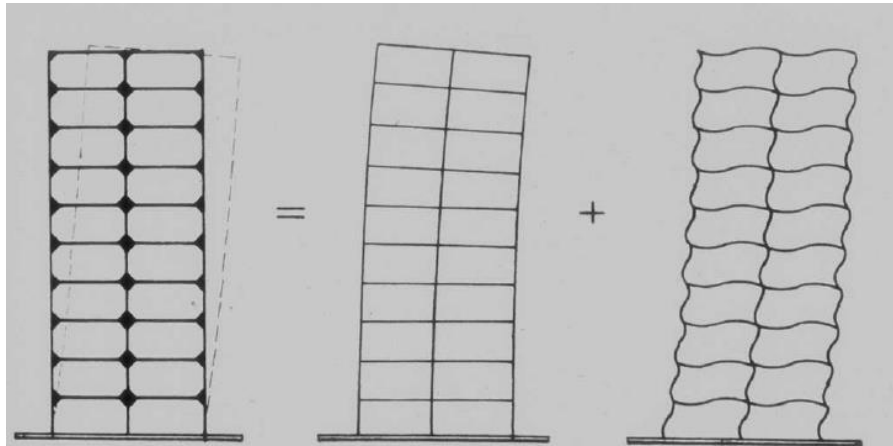


Figure 2.4 Deformations for a rigid frame (left), consisting of bending sway (middle), and shear sway (right). A rigid frame is subject to large shear deformations, which dominate the displacements and create large moment, shear and axial forces in the beams and columns. A tube form like a reinforced concrete core does not experience this shear sway, but instead deforms only in bending, which is much stronger. Figure from [p, 8].

One solution for increasing the stiffness of such rigid-frame structures was to move all the columns to the periphery of the building and space them so close together that together they behaved more like perforated walls, rather than individual columns, essentially creating a “framed tube” at the perimeter of the building. An example of this solution are the original twin towers of the World Trade Center in New York. Built in 1971, the columns on the exterior are set only 1 meters apart, with the beams being 1,3 meters deep, see Figure 2.5. Some buildings also added reinforced concrete cores in the centre of the building in addition to the framed tube along the perimeter, creating a “tube-in-tube” structure.

2. Tall buildings – development and structure



Figure 2.5 The bottom of a World Trade Center tower (left), Willis Tower (centre), and John Hancock Building (right). Note how closely spaced the columns in the World Trade Center tower area the bottom 2 floors. Photos from [p, 9], [p, 10] and [p, 11].

Another continuation of the framed tube structural form was the Willis Tower from 1973, which rose to heights greater than the World Trade Center, utilising a floor plan consisting of 9 smaller tubes bundled together in a 3x3 grid to form the whole structure. This linking of framed tubes improved the buildings effectiveness by making it behave more like an idealized tube than the individual tubes would by themselves.

The other effective option that later emerged in skyscraper design was the use of diagonals. Unlike the aforementioned IBM-building, which only used diagonal members without any vertical columns to effectively carry the gravity loads, the optimal solution was adding diagonal members to a standard column-beam frames and thus constructing a frame-type that essentially transformed the buildings into giant vertical trusses. This design is effective as it splits the functions of the frame into parts: the columns can carry the vertical loads without being weakened by the effects of the lateral loads, while the diagonals can transfer the lateral forces into the ground without also having to inefficiently take the vertical loads. In addition, the diagonals can help with distributing the vertical loads from column to column where needed.

The Hancock Building in Chicago is a prime example of this structural system, with its 100 stories almost reaching the height of the World Trade Center, the world’s tallest building at the time. Figure 2.6 shows elevation and plan views of some of the different tube systems mentioned.

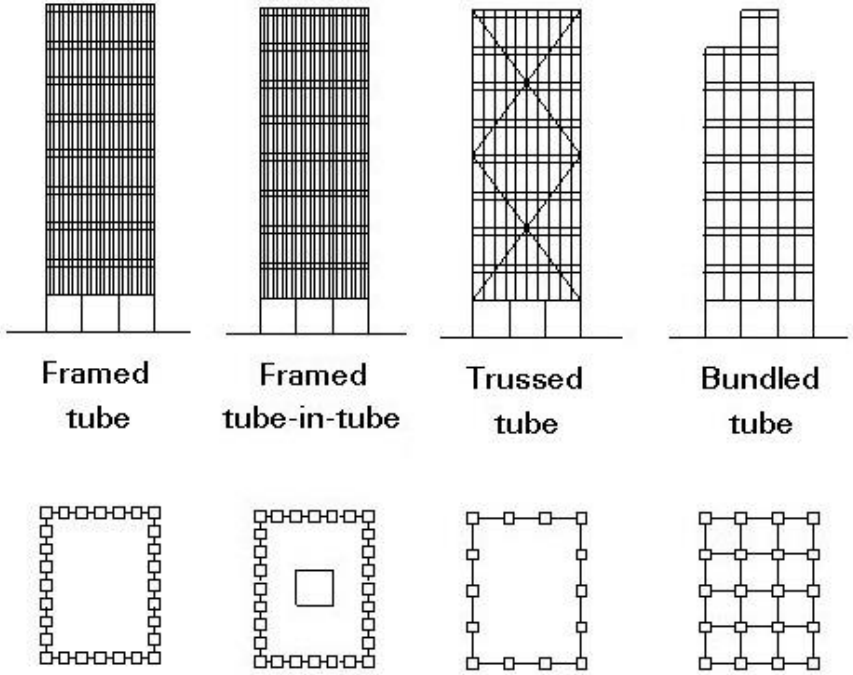


Figure 2.6 Different “tube” structural systems for tall buildings. The World Trade Center is an example of a framed tube, the John Hancock center a trussed tube, and the Willis Tower is made up of a bundled tube. Figure from [p, 12].

These structural systems became the primary ways of supporting high-rise buildings, and remained mostly the same for the rest of the century, but as buildings grew taller just for the sake of being tall, other innovations were popping up to improve the effectiveness of tall structures.

Up until this point, while concrete cores with their tube-like behaviour were very structurally efficient, the tallest buildings in the world had still been built in steel. The World Trade Center and the Hancock Building were both steel structures, however, the emergence of supertall buildings made primarily from reinforced concrete would soon begin. In 1998 the Petronas Twin Towers, one of the most famous examples of skyscrapers connected by a skybridge, was

2. Tall buildings – development and structure

built, using reinforced concrete in a tube-in-tube configuration. With their spires reaching a height of 451,9 m, they became the tallest buildings in the world, a title they held until 2004.



Figure 2.7 The Petronas Towers in Kuala Lumpur. Photo from [p, 13].

The development of skyscrapers has at present times shifted from America to Asia and the Middle-East, and structures that use different systems for stability than those mentioned above have first been used in these regions. Structures that push the technological boundaries are becoming ever taller, with the current tallest building in the world being the 800-meter-tall Burj Khalifa, which is almost twice as high as the Petronas Towers. In Saudi Arabia, the Jeddah Tower is currently under construction, and will be ca 1000 meters tall when completed.

Both the Burj Khalifa and the Jeddah Tower use the same basic concept for achieving structural stability: a triangular central reinforced concrete core, with shear walls extending from the three corners to form a Y-shape. This provides tube-like behaviour from the core, while the shear walls at the end of the corners of the Y-shape act like the flanges of a T-beam, causing more structural material to be located away from the neutral axis of the building, where it is more effective. This structural arrangement has been dubbed the “buttressed core” (Blum, 2007).



Figure 2.8 The Burj Khalifa (left), Jeddah Tower (center), and Nakheel Tower (right). Photos from [p, 14], [p, 15] and [p, 16].

Another concept that has been proposed to enable supertall buildings is using a group of conjoined towers. The Nakheel Tower is a building that was proposed to be built in Dubai. It was ultimately cancelled due to financial problems, but by using 4 towers linked together it was supposed to reach 1000 meters. The proposed 4 towers are arranged in a circle, with links going between them every 25 stories. This configuration would allow for the centre of the towers to be open space and the main structural elements to be moved further away from the neutral axis, giving a large structural depth ideal for taking the bending induced by the side loads, just like the Burj Khalifa. The advantage of using 4 linked towers is that they would be much lighter and smaller in building volume than an equivalent single tower with the same plan radius. The large gaps in the structure due to the openings between the skybridges would also greatly reduce wind loads (Moon, 2015).

An important factor when designing tall buildings is the lease depth of each floor. The lease depth is the distance between the core or shear walls to the exterior walls, and is best kept at between 8 to 15 m to allow most of the useable floor area to be near a perimeter with natural light. As lease depths increase the desirability of the space is significantly diminished (Sev and Özgen, 2009). Both the Nakheel and Jeddah Tower concepts can grow in size and

2. Tall buildings – development and structure

structural depth while keeping lease depths constant, and thus lend themselves well to being used in even taller buildings. A normal rectangular plan structure will however have to compromise on useable floor space in order to keep the lease depth reasonable as the structural depth increases, see Figure 2.9.

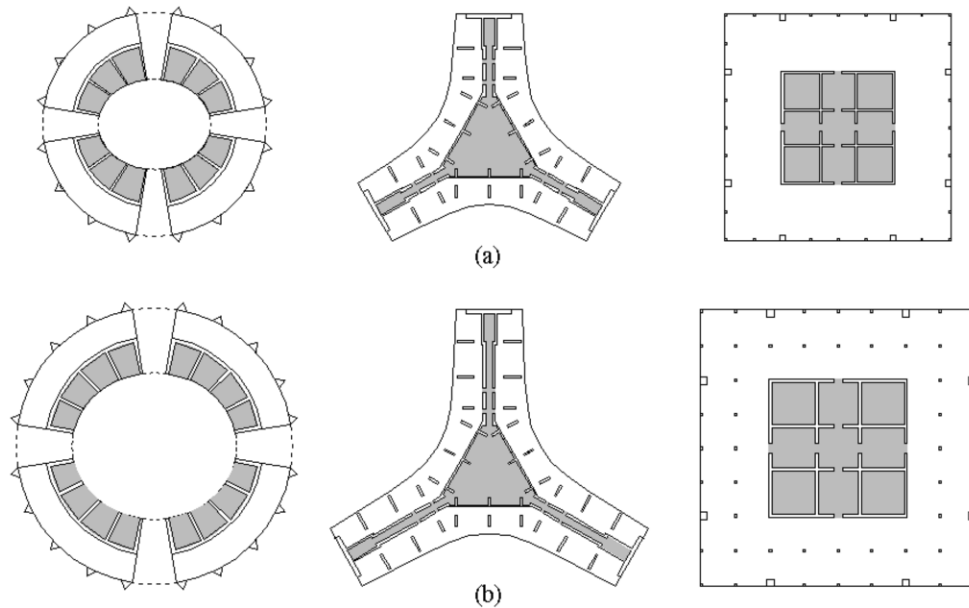


Figure 2.9 Simplified structural plans for the Nakheel (left) and Jeddah (centre) towers, compared to a standard rectangular plan structure (right). As the structural depth increases, the rectangular building has to sacrifice floor space to accommodate a larger core and lease depth, which the Nakheel and Jeddah towers do not. Figure from Moon (2015).

While the pursuit of building ever taller and taller is interesting, and is usually catalyst of technological advancements in tall building design, it is ultimately not what this thesis is about. Linking skyscrapers together with skybridges can be done regardless of if the buildings are 60 storeys tall or 160 storeys tall, and is relevant mostly for locations with a large density of tall structures, rather than places with a single megatall tower.

The building used as a basis for calculations is explained in chapter 0. But let us first consider some existing examples of tall buildings utilizing a skybridge to improve their architectural, structural, and societal function.

2.2 Existing linked skyscrapers

To gain some perspective on the possibilities offered by linking together skyscrapers, this section will present some existing projects that have implemented the use of skybridges in tall buildings with success. Some of these projects can deviate quite a lot in scope, shape and situation from the structure modelled in the following chapter, but can provide valuable lessons on the benefits and challenges that comes with connecting tall buildings at height.

2.2.1 *Linked Hybrid, Beijing.*

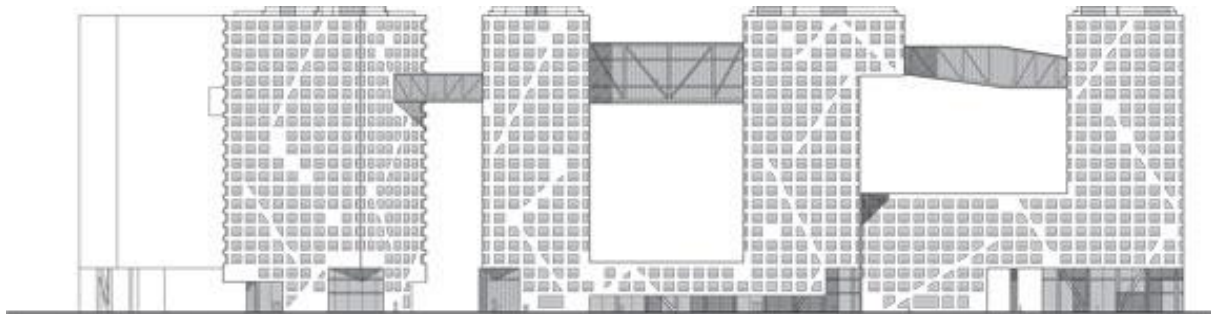


Figure 2.10 Elevation view of the Linked Hybrid complex in Beijing. Note the diagonal lines in the façade, these are structural members of reinforced concrete that help redistribute the forces throughout the rigid frame. Picture from [p, 17].

The Linked Hybrid is a building complex in Beijing consisting of 9 towers with 21 stories rising to 66 m. It was designed by Stephen Holl Architects and was completed in 2009. The towers primarily contain residential apartments, with one of the towers being a hotel. As can be seen from the figures, the towers are connected not only at ground level, but at the intermediate and upper levels as well.

The towers are carried by rigid reinforced concrete frames, with the addition of interior shear walls to ensure stability. The frame also incorporates concrete diagonals along the façade to help redistribute forces in the frame (DIVISARE, 2006), see Figure 2.10. The skybridges consist of steel trusses going the height of several stories.

What is particularly exciting about this complex is the fact that though the main functions are apartments, it also provides parks, shops, restaurants, cinemas, kindergartens and swimming pools. These secondary functions are woven into the building at not only ground level, but

2. Tall buildings – development and structure

also the intermediate and upper paths, encouraging circulation at multiple levels and embodying the spirit of the vertical city.



Figure 2.11 View of the Linked Hybrid. Photo from [p, 18].

Due to this successful use of architecture to promote a better environment for both residents of the complex as well as the public, the Linked Hybrid won the title of “Best Tall Building Worldwide” in the 2009 CTBUH Awards Program, because “Though this project is not especially tall, it points the way forward for the intensified multi-use, multi-level, connected cities of the future.” - Antony Wood, CTBUH (2009).

2.2.2 Pinnacle @ Duxton, Singapore



Figure 2.12 Pinnacle @ Duxton, Singapore. Photo from [p, 19].

The Pinnacle @ Duxton is a large public housing project in Singapore, completed in 2009. It consists of seven 51 storey apartment blocks connected continuously by skybridges and skyparks at top and mid-height of the towers. It was designed by ARC Studio Architecture, and is 156m high (Wikipedia, 2017).

It is hard to find information about its structural system, but from looking at pictures from its construction it is assumed that the towers are built with shear walls taking lateral load, and carrying flat slabs without any interior columns. The skybridges are made out of steel trusses.

2.2.3 Sky Habitat, Singapore

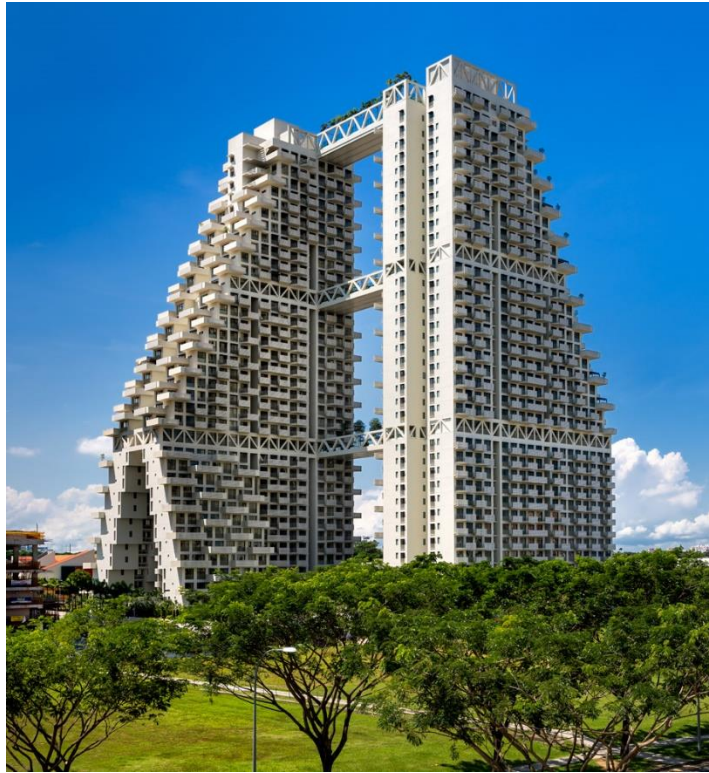


Figure 2.13 Sky Habitat, Singapore. Photo from [p, 20].

Sky Habitat is another public housing project in Singapore, a 130m high, 38 floor complex designed by Safdie Architects. The complex consists of two towers connected by skybridges at three levels. The project was finished in 2015 (CTBUH, 2017b).

The structure appears to be made of rigid reinforced concrete frames with the support of shear walls at the ends, as well as belt trusses at the link heights. The skybridges are made of steel trusses. Both the belt trusses and truss links are clearly visible on Figure 2.13.

2.2.4 Additional examples

These are only a few of the skyscrapers that exist today that utilize structural links to connect buildings at height. Some other examples for the interested reader include:

- Dancing Copper Apartments, New York. By SHoP Architects
- Umeda Sky Building, Osaka. By Hiroshi Hara
- Marina Bay Sands, Singapore. By Safdie Architects
- Golden Dream Bay, Qinhuangdao. By Safdie Architects
- Raffles City Chongqing (under construction (CTBUH, 2017a)), Chongqing. By Safdie Architects



Figure 2.14 Dancing Copper Apartments (top left), Umeda Sky Building (top right), and Marina Bay Sands (bottom). Photos from [p, 21], [p, 22] and [p, 23]

2. Tall buildings – development and structure



Figure 2.15 Golden Dream Bay in Qinhuangdao. Photo from [p, 24].



Figure 2.16 Raffles City in Chongqing. Photo from [p, 25].

3 Structural model and loading

With some background knowledge on how tall buildings function, it is time to start analysing the behaviour of a tall structure in more detail, and see how a skybridge affects the system. To do this a model and a load condition is required.

3.1 Structural model

A suitable structural model off which to base the calculations is necessary. Song and Tse (2014) wrote a paper on the behaviour of linked twin buildings subject to wind load, investigating the effect of the link on the natural frequencies of the system. The model they used for their calculations was chosen as a template, providing a realistic structural system as well as a reference to compare the model with verify that it is working correctly.

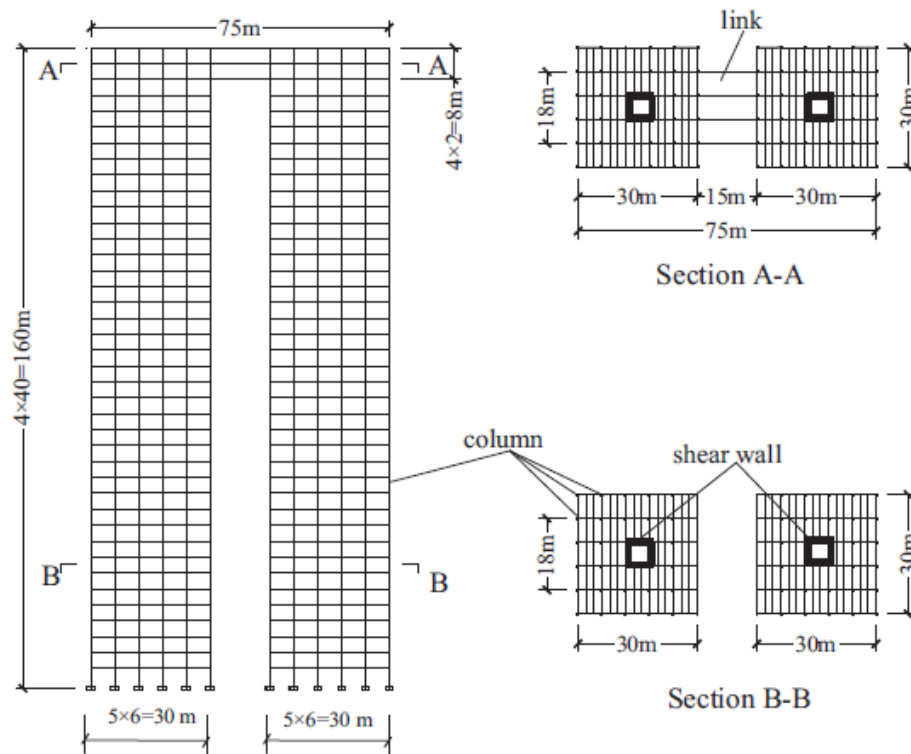


Figure 3.1. Model configuration, from Song and Tse (2014).

The model consists of two 30x30 m², 160 m tall, 40 floor reinforced concrete towers supported by a rigid frame with a central shear wall core. The base model has a link between

the buildings at the top three floors, consisting of reinforced concrete beams spanning directly between the exterior frame columns of each building, supporting a one-way slab floor. The link is modelled with fixed connections to the rigid frame of the two towers, allowing full transfer of moments. See Figure 3.1. Concrete strengths used are all C55/67.

The structural member sizes are summarized in Table 3.1. The models are analysed in the finite element method (FEM) software package Autodesk Robot Structural Analysis Professional 2017, hereby referred to as Robot, see Figure 3.2.

Table 3.1. Structural member sizes, from (Song and Tse, 2014). Units in mm.

Element	Floor number						Link
	1-4	5-10	11-15	16-26	27-33	34-40	
Column (B × W)	1400 × 1400	1000 × 1000	800 × 800	600 × 600	500 × 500	400 × 400	-
Beam (B × D)	300 × 700	300 × 700	300 × 700	300 × 700	200 × 500	200 × 500	1200 × 500
Shear wall (t)	550	450	350	250	200	150	-
Slab (t)	120	120	120	120	120	120	120

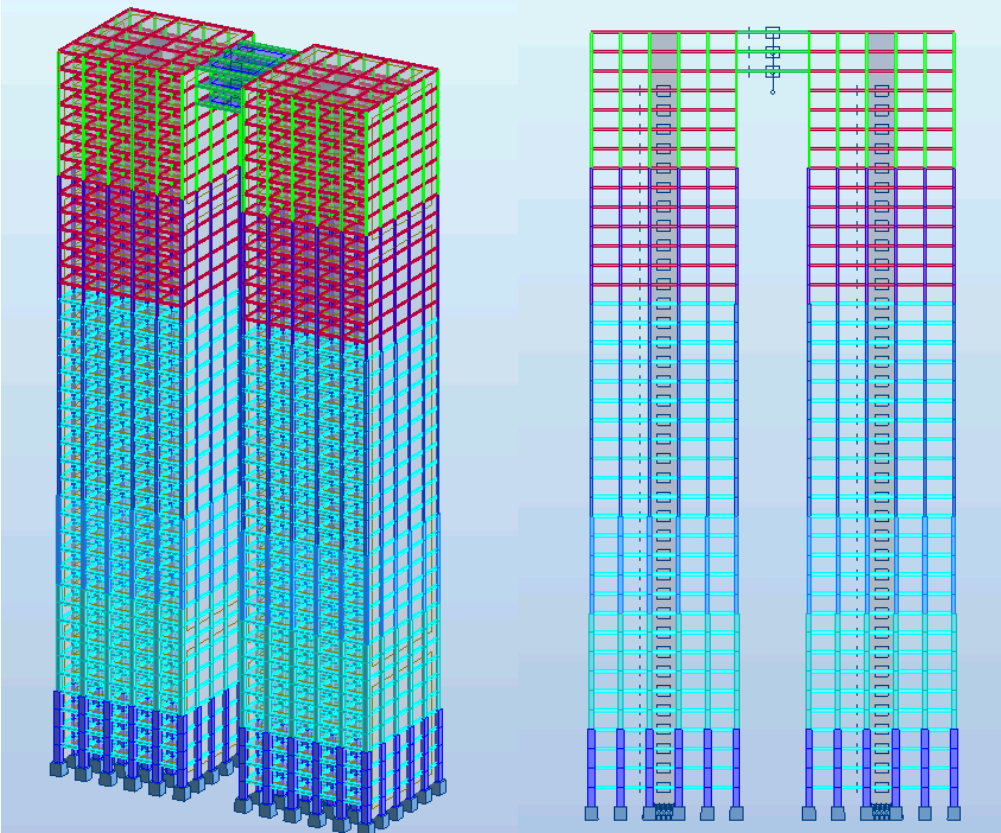


Figure 3.2. Structural model in Autodesk Robot. 3D and elevation views. The different colours correspond to the different member sizes detailed in Table 3.1.

3.2 Loading

For the relevant load condition, a quasi-static wind load was calculated according to the European Standard NS-EN 1991-1-4:2005+NA:2009, Eurocode 1: Actions on Structures, Part 1-4: General actions. Wind actions, with the corresponding Norwegian National Annex from 2009 (European Committee for Standardization, 2009), hereby simply referred to as EC1. While the load obtained is a static load, it takes into consideration the dynamic (or “non-static”) response of the structure by considering the effect of turbulence and the natural frequency of the building, hence the term “quasi-static”.

As the scope of this paper is not concerned with detailed structural design, the rules presented in EC1 will generally be adhered to, with some exceptions, in the interest of saving time and reducing the complexity of the problem. The details of the calculation shown in the following sections

Equation numbers in square brackets, e.g. [4.1], refer to the number given in EC1, while round brackets, e.g. (4.1), refer to the equations numbered in this thesis.

3.2.1 *General parameters*

First let us establish the necessary parameters:

z = height above ground level

h = building height

h' = height to top of skybridge

h_s = height of each storey

b = building width across the wind direction

d = building depth in the along-wind (x) direction

3.2.2 Wind loads

The general equation given by EC1 to obtain the equivalent static wind load on the structure is

$$F_{w,k}(z_e) = q_p(z_e) \cdot c_{pe,k} \cdot c_s c_d \quad (3.1)$$

Where

$F_{w,k}(z_e)$ is the wind load in kN/m² as a function of z_e in zone k

z_e is a reference height above ground level in meters

$q_p(z_e)$ is the peak wind pressure in kN/m² at height z_e

$c_{pe,k}$ is a pressure coefficient for external pressure in zone k

$c_s c_d$ is a structural factor accounting for the size of the building and the dynamic effects of turbulence in resonance with the building mode

This equation corresponds to equation [5.5] in EC1, but has been modified to work as a surface load rather than a point load. For simplicity, only external pressures (loads) are considered for this analysis. Internal pressures and friction forces are ignored. All necessary parameters and equations to obtain these values will be presented in the following sections, with references to the relevant paragraphs or equations in Eurocode 1. A calculation summary for the base model, with corresponding numerical values for each parameter, will then be presented.

3.2.3 Wind pressure

The wind pressure on a building is directly related to the wind speed at its location. The wind speed consists of a mean and a turbulent component. The mean wind speed $v_m(z)$ is constant with time, and varies only with height above ground, while the turbulent wind component fluctuates with time, as well as its position in the three spatial dimensions x , y and z , see Figure 3.3. The average value for the turbulent wind component over time is zero.

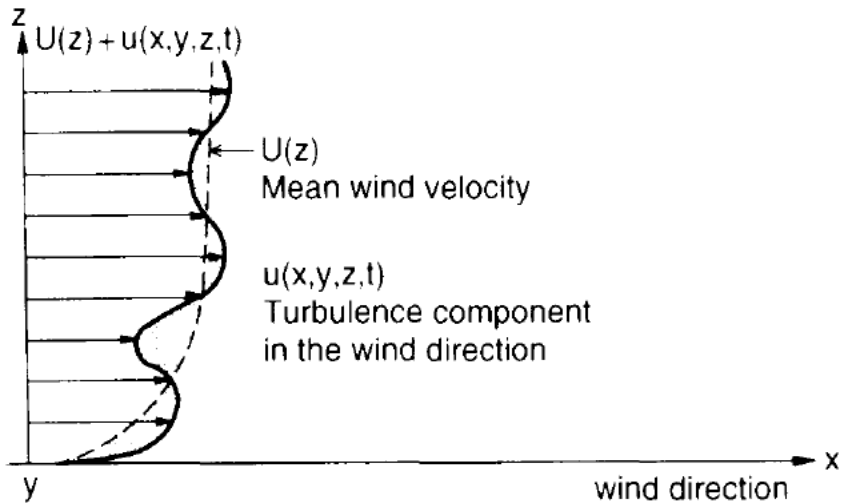


Figure 3.3. Total wind speed $U(z) + u(x, y, z, t)$, from Dyrbye and Hansen (1997). $U(z)$ in this figure denotes the mean wind velocity, which is constant in time and is only a function of height above ground. $u(x, y, z, t)$ is the turbulent wind component, which varies in both time and space, with an average value over time equal to zero.

The mean wind speed is calculated based on the location, surrounding terrain roughness and shape, of the structure.

Basic wind speed

Equation [4.1] in EC1 gives the basic wind speed in any location by

$$v_b = c_{dir} \cdot c_{season} \cdot v_{b,0}$$

Where

v_b is the basic wind speed

c_{dir} is a wind direction factor, assumed equal to 1

c_{season} is a seasonal factor, assumed equal to 1

$v_{b,0}$ is a reference velocity corresponding to the 10 minute mean wind speed 10 meters above ground level, independent of wind direction or season, assumed equal to 30 m/s

Thus

$$v_b = v_{b,0} \quad (3.2)$$

Terrain category

The hypothetical structure will be in a city with a large density of tall buildings. This is assumed to correspond to terrain category IV – “Area where at least 15% of the ground surface is occupied by buildings, with an average height greater than 15 m”, in table NA.4.1 of EC1.

This terrain category gives terrain roughness parameters $z_0 = 1$ m and $k_r = 0,24$, where z_0 is the height above ground level at which the mean wind speed is zero (Dyrbye and Hansen, 1997), and k_r is the terrain roughness factor as a function of z_0 .

Mean wind speed

The mean wind speed is found by equation [4.3] in EC1:

$$v_m(z) = c_r(z) \cdot c_o(z) \cdot v_b$$

Where

$c_r(z)$ is the roughness factor given in EC1 equation [4.4]

$c_o(z)$ is the terrain orography factor, assumed equal to 1

The roughness factor depends on the parameters given by the terrain category from the previous section by

$$c_r(z) = k_r \cdot \ln\left(\frac{z}{z_0}\right)$$

In our case, the mean wind speed equation becomes

$$v_m(z) = k_r \cdot \ln\left(\frac{z}{z_0}\right) \cdot v_{b,0} \quad (3.3)$$

Wind turbulence

The effect of the turbulent wind component is found by calculating the turbulence intensity $I_V(z)$ as a function of z , given by equation [4.7] in EC1:

$$I_V = \frac{k_t}{c_o(z) \cdot \ln\left(\frac{z}{z_0}\right)}$$

Where k_t is the turbulence factor, assumed equal to 1. As $c_o(z)$ also is equal to 1, the equation becomes

$$I_V = \frac{1}{\ln\left(\frac{z}{z_0}\right)} \quad (3.4)$$

Peak wind pressure

The peak wind pressure is then found by equation [4.8] in EC1

$$q_p(z) = [1 + 7 \cdot I_V(z)] \cdot \frac{1}{2} \rho \cdot v_m^2(z) \quad (3.5)$$

Where ρ is the air density, equal to 1,25 kg/m³ according to EC1 paragraph 4.5(1), note 2.

3.2.4 Pressure and force coefficients

The wind pressure distribution on the actual structure depends on the shape of the building and its surroundings. This is taken into account by the Eurocode through pressure coefficients and parameters that describe how the load should be distributed along the height and on the different faces of the building. Wind cover from nearby structures is assumed equal to zero.

Pressure coefficients

The Eurocode only details pressure coefficients for single free-standing structures not obstructed by other buildings of the same or greater height in the immediate vicinity, and then suggest wind tunnel tests should be used to find pressure coefficients for buildings that do not meet this requirement, which our model does not. However, wind tunnel testing is outside the scope of this thesis, so a few simplifications have been made instead to make use of the pressure coefficients in EC1 to obtain a realistic load for our structures.

For a single structure, EC1 divides the walls of the building into 5 different zones k that have different pressure coefficients $c_{pe,k}$. Zones $k = A, B$ and C correspond to different parts of the two faces of the building parallel to the wind direction, while zone D corresponds to the windward face, and zone E corresponds to the leeward face, see Figure 3.4. The pressure coefficients $c_{pe,10,k}$ for each zone are given in

Table 3.2. According to EC1 figure 7.2, for our structure $c_{pe,k} = c_{pe,10,k}$, as $A \geq 10m^2$, where A is wind loaded area for each zone.

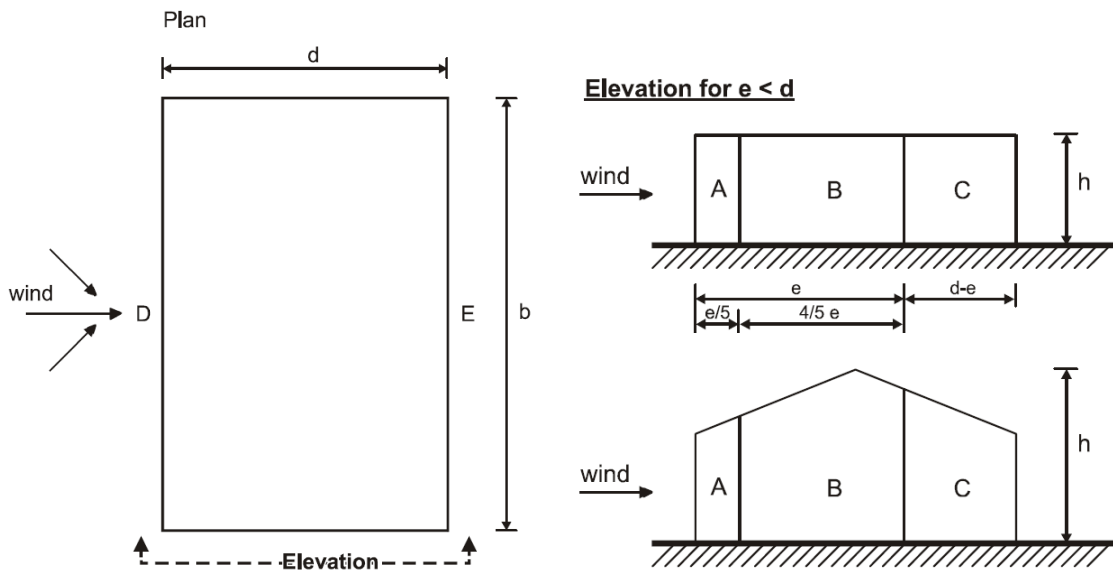


Figure 3.4 External pressure zones on a single building, taken from EC1 figure 7.5. Left shows the plan view of building, right shows the elevation view. Zone D is the windward face of the building, zone E is the leeward face, and zones A, B, C are on the sides parallel to the wind direction, with zone A being the zone nearest to the windward face. All zones except D have negative pressures, which means they are in suction.

Table 3.2 This is EC1 table 7.1, which gives external pressure coefficients for the pressure zones on vertical walls in rectangular buildings with different height to depth ratios.

Zone	A		B		C		D		E	
	$c_{pe,10}$	$c_{pe,1}$	$c_{pe,10}$	$c_{pe,1}$	$c_{pe,10}$	$c_{pe,1}$	$c_{pe,10}$	$c_{pe,1}$	$c_{pe,10}$	$c_{pe,1}$
h/d										
5	-1,2	-1,4	-0,8	-1,1	-0,5		+0,8	+1,0	-0,7	
1	-1,2	-1,4	-0,8	-1,1	-0,5		+0,8	+1,0	-0,5	
$\leq 0,25$	-1,2	-1,4	-0,8	-1,1	-0,5		+0,7	+1,0	-0,3	

3. Structural model and loading

To simplify how the wind interacts with the two buildings when moving along the x-axis, we can assume that it flows around the twin towers as if they were a single imaginary building. The depth of each tower, d_1 and d_2 , and the distance between the towers, L , would then make up the total depth of the building, such that $d = d_1 + L + d_2$. The length e in Figure 3.4 is the lesser of b or $2h$ (EC1 fig.7.5), which means that $e = b = d_1 = d_2$ for our case, see Figure 3.5.

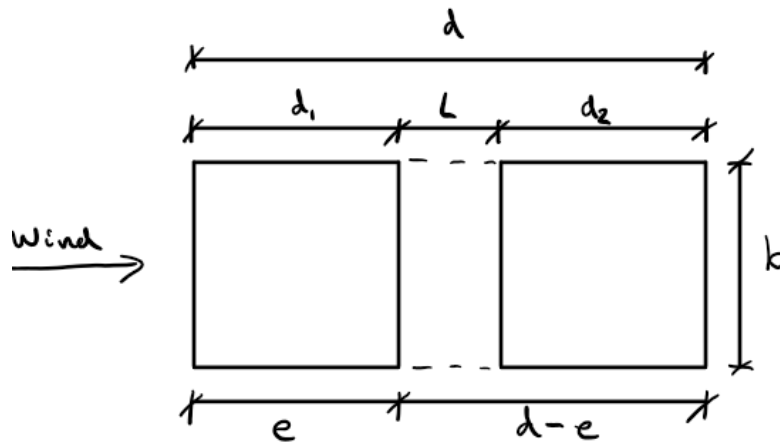


Figure 3.5 The linked building system imagined as one hypothetical structure. The length e corresponds to the measure used in Figure 3.4

The wind load distribution on the imaginary structure with its different zones and pressure coefficients according to Figure 3.4 and Table 3.2 is presented in Figure 3.6.

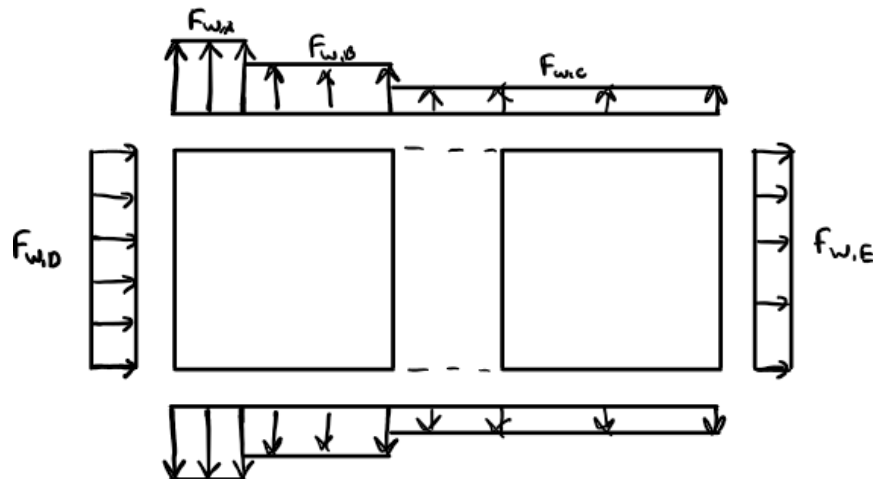


Figure 3.6. Wind load distribution on the different faces of the hypothetical single structure. The relative magnitude of each load $F_{w,k}$ is correlated to the pressure coefficients from Table 3.2.

As stated before, wind actions perpendicular to the building’s main horizontal axis (the x-axis) are not investigated in this thesis, and thus will be ignored. However, we can use the pressure zones A, B, and C to find the load on the walls that face towards each other, i.e. the faces in-between the buildings. To do this, we assume that the suction on the imaginary walls parallel to the wind direction that connects the two towers (the dotted lines in Figure 3.6) must act with the same magnitude perpendicular to all surfaces in that zone. Thus, we can assume that for our models, the in-between faces are subject to a suction force each equal to the suction force in zone C, $F_{w,c}$, see Figure 3.7.

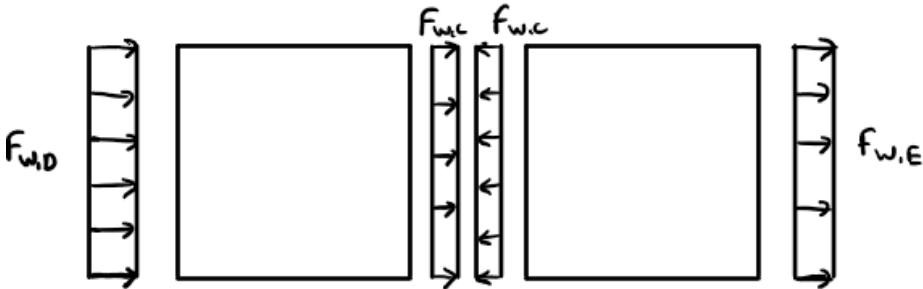


Figure 3.7 Plan view of the wind load distribution on the relevant faces of the twin towers. The area in-between the towers is assumed to be subject to a negative pressure equal to that of zone C from Figure 3.6.

This means that the pressure coefficients we are interested in, belongs to zone D, E and C, for the windward, leeward, and in-between faces, respectively.

Reference height z_e

Like the wind speed, the wind load varies with height. EC1 figure 7.4 and NA.7.2.2(1) divides the building walls into different reference heights z_e depending on the actual height h and the width b of the building, see Figure 3.8.

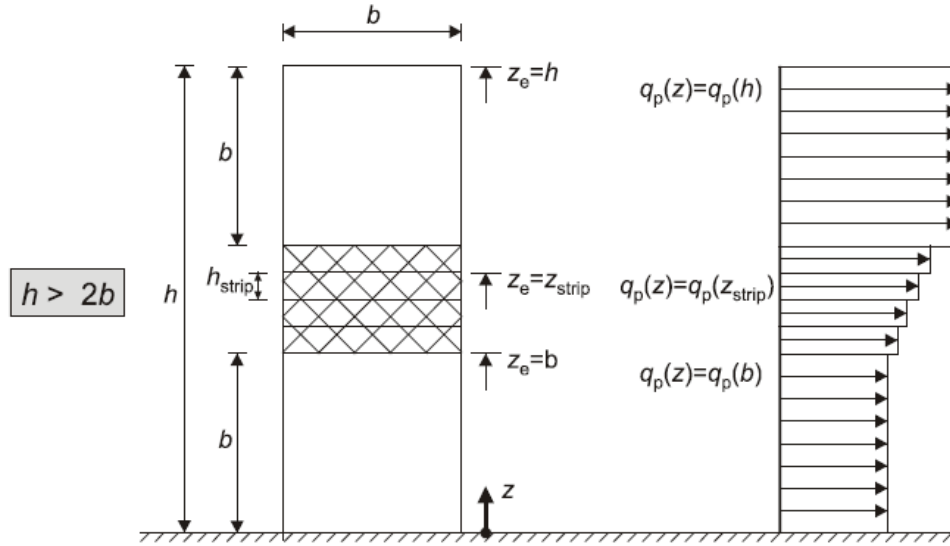


Figure 3.8 Reference height z_e along the height of the building, from EC1 figure 7.4. In the top b meters of the building, z_e is equal to h and for the bottom b meters z_e is equal to b . The intermediate heights are divided into strips, where z_e for each strip is equal to the height to the top of the strip.

Force coefficient

The force coefficient c_f for the building is necessary later in the calculation of aerodynamic damping of the structure, and is found through EC1 equation [7.9]:

$$c_f = c_{f,0} \cdot \psi_r \cdot \psi_\lambda \quad (3.6)$$

Where

$c_{f,0}$ is the basic force coefficient for a rectangular plan structure with sharp corners and without free-end flow

ψ_r is a reduction factor taking into account rounded corners, assumed equal to 1

ψ_λ is the end-effect factor for elements with free-end flow

$c_{f,0}$ depends on the building depth to width ratio d/b and is found in EC1 figure 7.23. ψ_λ depends on the effective slenderness λ of the building and its solidity ratio φ .

λ is found in EC1 table 7.16, as a function of the length of the building $l (= h - b)$, such that

$\lambda = \min(1,4 \cdot \frac{l}{b}; 70)$. φ is found by EC1 equation [7.28], $\varphi = A/A_c$, where A and A_c are

defined in EC1 figure 7.37, see Figure 3.9. A is the projected area by the beams, columns, slabs, and walls when viewing the structure in elevation, while A_c is the area of the enclosed building envelope.

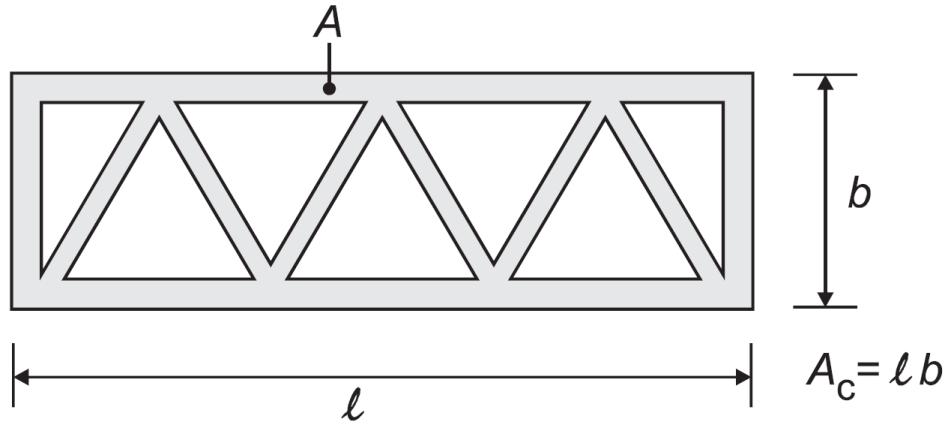


Figure 3.9. Projected area A and envelope area A_c from EC1 figure 7.37. In the context of our model the objects that make up A are the beams, columns, slabs and walls when viewing the model in elevation.

With these values the end-effect factor ψ_λ is read from EC1 figure 7.36.

3.2.5 Structural factor

The structural factor $c_s c_d$ is important as it takes into account the dynamic response of the building, a very key element in tall building design. It is given by equation [6.1] in EC1

$$c_s c_d = \frac{1 + 2 \cdot k_p \cdot I_V(z_s) \cdot \sqrt{B^2 + R^2}}{1 + 7 \cdot I_V(z_s)} \quad (3.7)$$

Where

z_s is a reference height, taken as $0,6h$ (from figure 6.1 of EC1)

k_p is a peak factor, defined as the ratio of the maximum value of the fluctuating part of the response to its standard deviation

B^2 is a background factor, accounting for correlation of the pressure distribution on the structure's surface

R^2 is a resonance response factor, accounting for turbulence in resonance with the building's natural frequency

The Eurocode proposes two methods for determining k_p , B^2 and R^2 , procedure 1 given in Annex B, and procedure 2 given in Annex C. The Eurocode recommends procedure 1. However, when Steenbergen et al. (2009) compared the two methods, it was found that results obtained from procedure 2 were closer to theoretical values. The results from procedure 1 were deemed to be unconservative and potentially unsafe, deviating with as much as up to 10% from the results obtained through procedure 2. Similarly, Dyrbye and Hansen (1997) deemed EC1 procedure 1 less accurate than procedure 2, while also being more complicated. Thus, we will be using procedure 2. The following sections detail how to obtain the required factors.

Wind turbulence

A few parameters related to wind turbulence are required to calculate the structural factor. The turbulent length scale $L(z)$ represents the average gust size, and is found by equation [B.1] in EC1.

$$L(z) = L_t \cdot \left(\frac{z}{z_t}\right)^\alpha \quad (3.8)$$

Where $z_t = 200m$, $L_t = 300m$, $\alpha = 0,67 + 0,05\ln(z_0)$. The non-dimensional spectral density function for the wind distribution over varying frequencies, $S_L(z, n)$ is given in EC1 equation [B.2]:

$$S_L(z, n) = \frac{6,8 \cdot f_L(z, n)}{(1 + 10,2 \cdot f_L(z, n))^{\frac{5}{3}}} \quad (3.9)$$

Where $f_L(z, n) = \frac{n \cdot L(z)}{v_m(z)}$ is a non-dimensional frequency given by the real natural frequency n of the structure.

Background factor

The background factor B^2 is given in EC1 equation [C.1]

$$B^2 = \frac{1}{1 + \frac{3}{2} \cdot \sqrt{\left(\frac{b}{L(z_s)}\right)^2 + \left(\frac{h}{L(z_s)}\right)^2 + \left(\frac{b}{L(z_s)} \cdot \frac{h}{L(z_s)}\right)^2}} \quad (3.10)$$

Where $L(z_s)$ is the turbulent length scale value at height z_s .

Resonance response factor

The resonance response factor R^2 is given by equation [C.2] in EC1

$$R^2 = \frac{\pi^2}{2 \cdot \delta} \cdot S_L(z_s, n_{1,x}) \cdot K_s(n_{1,x}) \quad (3.11)$$

Where δ is the total logarithmic decrement of damping for the structure and K_s is the size reduction function, given by equation [C.3] in EC1

$$K_s(n) = \frac{1}{1 + \sqrt{(G_y \cdot \phi_y)^2 + (G_z \cdot \phi_z)^2 + \left(\frac{2}{\pi} \cdot G_y \cdot \phi_y \cdot G_z \cdot \phi_z\right)^2}} \quad (3.12)$$

Where $\phi_y = \frac{c_y \cdot b \cdot n}{v_m(z_s)}$ and $\phi_z = \frac{c_z \cdot h \cdot n}{v_m(z_s)}$, and c_y, c_z are decay constants both equal to 11,5. G_y and G_z are constants that depend on the structure's mode shape and are given in table C.1 in EC1.

Total logarithmic decrement of damping is found as $\delta = \delta_s + \delta_a + \delta_d$ (equation [F.15]). δ_d depends on any damping devices in the structures, and is assumed equal to 0, and δ_s is given in EC1 table F.2.

The aerodynamic damping decrement δ_a is given by Eurocode 1 equation [F.18]:

$$\delta_a = \frac{c_f \cdot \rho \cdot b \cdot v_m(z_s)}{2 \cdot n_{1,x} \cdot m_e} \quad (3.13)$$

Where m_e is the equivalent modal mass per unit length of the building, for the mode shape $\Phi(z)$ corresponding to the first natural frequency $n_{1,x}$, given by equation [F.14] in EC1:

$$m_e = \frac{\int_0^h m(z) \cdot \Phi^2(z) dz}{\int_0^h \Phi^2(z) dz} \quad (3.14)$$

$m(z)$ = mass per vertical meter at height z of the structure. To calculate these integrals the values for $m(z)$ and $\Phi(z)$ are extracted at every storey, i.e. at h_s intervals in the z -direction for every N number of storeys, from the FEM-model in Robot. The integrals are then approximated using the trapezoidal method:

$$\int_0^h f(z) dz \approx \frac{h_s}{2} \sum_{i=1}^N (f(z_{i+1}) + f(z_i)) = \frac{h_s}{2} \cdot (f(z_1) + 2f(z_2) + \dots + 2f(z_N) + f(z_{N+1}))$$

Where i represents each storey such that $z_{i=1} = 0, z_2 = h_s, z_{i=N} = (h - h_s)$ and $z_{i=N+1} = h$, and $f(z)$ is an arbitrary function of z , such that $f(z) = m(z) \cdot \Phi^2(z)$ or $f(z) = \Phi^2(z)$, depending on the integral.

Peak factor

The peak factor k_p is given by equation [B.4] in EC1

$$k_p = \sqrt{2 \cdot \ln(v \cdot T)} + \frac{0,6}{\sqrt{2 \cdot \ln(v \cdot T)}} \geq 3 \quad (3.15)$$

Where $T = 600s$ (10 minutes) and v is the up-crossing frequency given by equation [B.5]:

$$v = n_{1,x} \sqrt{\frac{R^2}{B^2 + R^2}} \geq 0,08 \text{ Hz} \quad (3.16)$$

3.2.6 Design wind load

Thus, with all the obtained parameters the design wind load for each zone is finally calculated using equation (4.1) as given earlier:

$$F_{w,k}(z_e) = q_p(z_e) \cdot c_{pe,k} \cdot c_s c_d$$

3.3 Building acceleration

The maximum acceleration of the building can also be found using the method given in the annexes of EC1. Like for the structural factor $c_s c_d$, procedure 2 has been used, i.e. Annex C. According to EC1 C.4(3) the acceleration at height z is found through

$$a(z) = k_{p,a} \cdot \sigma_{a,x}(z)$$

Where $k_{p,a}$ is the peak factor k_p , but with $v = n_{1,x}$, i.e.:

$$k_{p,a} = \sqrt{2 \cdot \ln(n_{1,x} \cdot T)} + \frac{0,6}{\sqrt{2 \cdot \ln(n_{1,x} \cdot T)}} \quad (3.17)$$

and $\sigma_{a,x}$ is the standard deviation of the acceleration due to wind as given in equation [C.4] in EC1:

$$\sigma_{a,x}(y, z) = c_f \cdot \rho \cdot I_V(z_s) \cdot v_m^2(z_s) \cdot R \cdot \frac{K_y \cdot K_z \cdot \Phi(y, z)}{\mu_{ref} \cdot \Phi_{max}}$$

Where K_y and $K_z = 1, 3/2$ or $5/3$ depending on the mode shapes in the transverse horizontal (y) and vertical (z) directions, respectively, and $\mu_{ref} = m_e/b$ (EC1 section F.5). When assuming the mode shape $\Phi(y, z)$ is constant at every height z in the y-direction,

$$\Phi(y, z) = \Phi(z) \rightarrow K_y = 1$$

and considering only the acceleration at the top of the building

$$\Phi(z = h) = \Phi(h) = \Phi_{max}$$

equation [C.4] then becomes:

$$\sigma_{a,x}(h) = c_f \cdot \rho \cdot I_V(z_s) \cdot v_m^2(z_s) \cdot R \cdot \frac{K_z}{\mu_{ref}} \quad (3.18)$$

Combining equations (4.17) and (4.18), the maximum acceleration is found by

$$a(h) = a_{max} = k_{p,a} \cdot \sigma_{a,x}(h) \quad (3.19)$$

3.4 Base model load calculation

A summary of the calculation carried out on the base model described in section 0 is presented in Table 3.3. The mode shape and mass distribution for the base model is given in appendix A. From this we obtain the wind load profile given in Figure 3.10 (left). The load on the model has been averaged for the intermediate heights, where $z_e = z_{strip}$, to provide the simplified wind profile shown in Figure 3.10 (right). These load values are tabulated in Table 3.4. Figure 3.11 shows the load applied to the Robot model.

Table 3.3 Results of wind loading and acceleration calculations for the base model.

First natural frequency $n_{1,x}$ (Hz)	0,24	Non-dimensional frequency $f_L(z_s, n_{1,x})$	1,340
Height h (m)	160	Spectral density function $S_L(z_s, n_{1,x})$	0,1037
Width b (m)	30	Mean wind speed $v_m(z_s)$ (m/s)	32,9
Reference wind speed v_b (m/s)	30	ϕ_y	2,52
Roughness length z_0 (m)	1	ϕ_z	13,44
Terrain factor k_r	0,24	Shape factor G_y (assuming constant)	1/2
Depth to width ratio d/b	2,5	Shape factor G_z (assuming parabolic)	5/18
Basic force factor $c_{f,0}$	1,5	Size reduction factor $K_s(n_{1,x})$	0,168
Slenderness length l (m)	130	Structural damping δ_s	0,1
Slenderness ratio λ	6,067	Modal mass per unit length m_e (kg/m) ¹	597195
Projected area A (m ²)	2028	Aerodynamic damping δ_a	0,00580
Envelope area A_c (m ²)	3900	Total damping δ	0,10580
Solidity ratio ϕ	0,52	Resonance response factor R^2	0,813
End-effect factor ψ_λ	0,9	Up-crossing frequency ν (Hz)	0,194
Force factor $c_{f,0}$	1,35	Peak factor k_p	3,280
Reference height z_s (m)	96	Structural factor $c_s c_d$	1,026
Turbulence intensity $I_V(z_s)$	0,219	Acceleration peak factor $k_{p,a}$	3,343
Turbulent length scale $L(z_s)$ (m)	183,5	Standard deviation $\sigma_{a,x}(h)$ (m/s ²)	0,00092
Background factor B^2	0,426	Acceleration a_{max} (m/s ²) ²	0,00307

¹ This value is wrong by a factor of 4 due to a calculation error, see the explanation in section 4.9. However, the difference this has on load magnitude is negligible, the incorrect value overestimates the load by about 3%. The acceleration values quoted later in section 4, have been calculated based on the correct values

² This value is wrong, see previous note. The correct acceleration is given in Table 4.3.

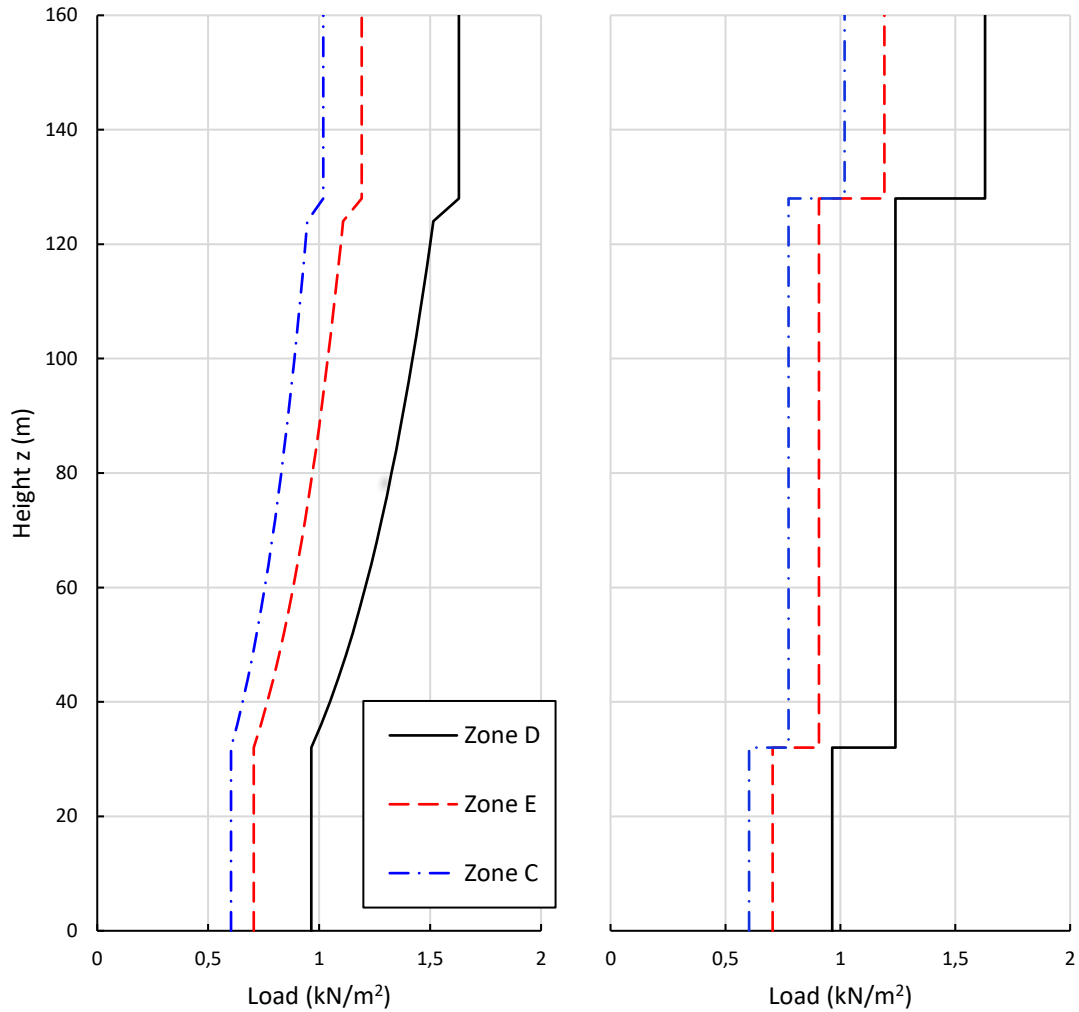


Figure 3.10 Wind load magnitudes on the structure for the different pressure zones. To the left is the profile with values for each strip, to the right is the profile with averaged values. Zone D is a positive pressure, that pushes on the wall. Zones E and C are negative pressures, that pull on their respective surfaces.

Table 3.4 Wind load values for the different faces and heights of the building.

Wind loads $F_{w,k}$ (kN/m ²)			
Building face	Windward	Leeward	In-between
Zone	D	E	C
Bottom (z = 0 to 32m)	0,964	-0,705	-0,602
Intermediate (z = 32 to 128m)	1,239	-0,906	-0,774
Top (z = 128 to 160m)	1,629	-1,191	-1,018

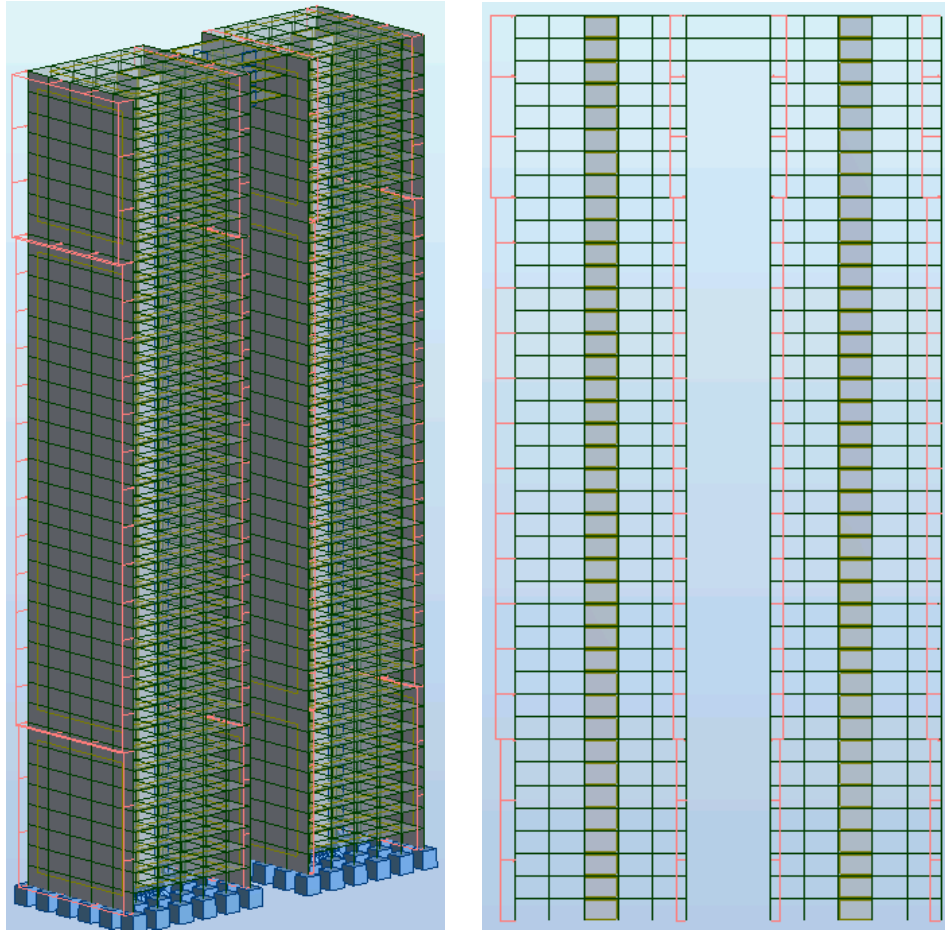


Figure 3.11 Calculated wind loads applied to the base model. Left: 3D view, right: elevation view. Due to the scale of the model relative to the load, the orange lines and arrows that symbolize the loads are difficult to see.

It should be mentioned that the modal mass m_e necessarily depends on the link mass and location. This effect had to be ignored however, due to modelling errors that occurred while creating the models. The details of this are explained in section 4.9.2. The modal mass used in the calculations is based on the mass distribution for the towers with no link.

3.5 Loads applied to other models

The loads obtained for the base model are based on the dynamic characteristics of that specific structure, and as such will not be equal to the load calculated for another model with a different mode shape or natural frequency. However, for the rest of this thesis the load for the base model is the one used on all other models to obtain their load effects. Doing this

misrepresents the true dynamic response magnitudes of structures with a smaller or greater design loads than that of the base model, but it was done for three reasons:

1. The dynamic load for each model was initially calculated for most structures and was found to deviate in magnitude by only a small percentage from the base model load.
2. It greatly speeds up model generation, making it possible to create many similar permutations of a model without having to apply the corresponding load magnitudes in Robot, which is a relatively time-consuming process.
3. It gives a more direct comparison of each structure's response to a static load, which can also of interest.

Each model's real load will be compared directly to the base model load considering the models' structural behaviour in chapter 4. Because of this, it is a good idea to understand how we expect the load to change with the structures.

3.5.1 Discussion of wind load sensitivity

Therefore, we need to identify the parameters that will have the greatest impact on the load magnitude, taking into consideration how relevant they are to the structural characteristics the skybridges can potentially alter. The towers will not change in size, and we can assume that the terrain and location parameters will remain constant, which leaves only the natural frequencies and mode shapes as relevant variables.

The results of a quick parametric study comparing load magnitude, normalized to the base model, with different mode shapes and natural frequencies are shown in Figure 3.13 and Figure 3.14, respectively. The mode shapes are based on the function $\Phi(z) = \left(\frac{z}{h}\right)^\zeta$, with ζ (zeta) ranging from 0,5 to 2,5. These shapes are shown in Figure 3.12, along with the mode shape for the base model, which is very close to the line $\zeta = 1,5$. For this study it was assumed for simplicity that the mode shape and natural frequency are independent, which is obviously false. However, Figure 3.13 shows that the mode shape alone has a negligible effect (<0,1%) on the load magnitude, and can safely be ignored, the natural frequency for a corresponding

shape is what has an impact. We can see from Figure 3.14 that the load magnitude decreases as the natural frequency of the building increases. This is explained by the energy of the turbulent wind component being significant for large wind eddies which occur at lower frequencies (Dyrbye and Hansen, 1997). As the frequency of the building increases, the effect of these eddies on the structure decreases.

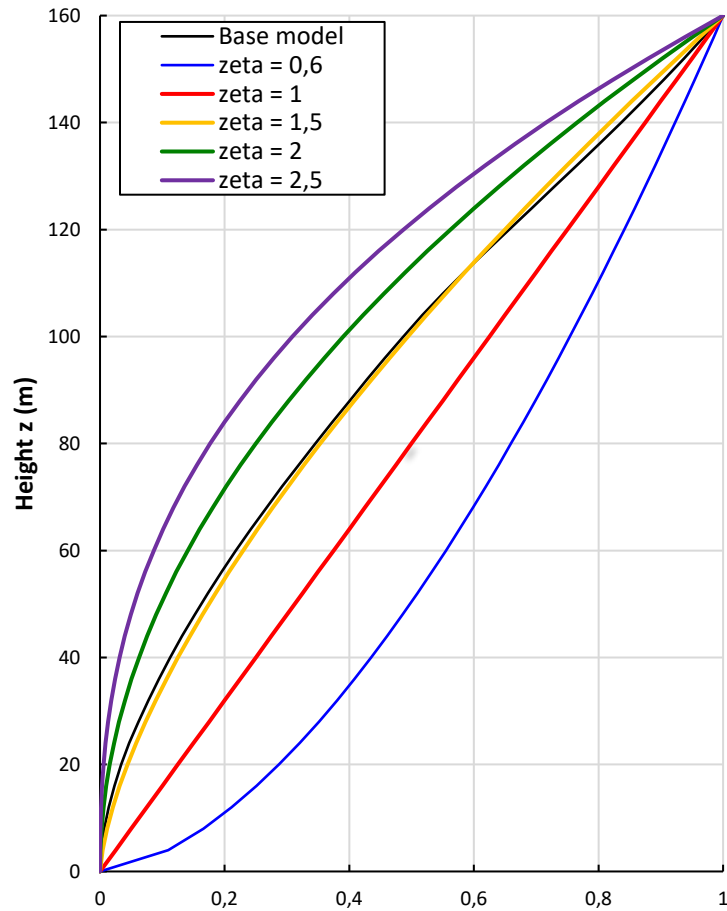


Figure 3.12 Mode shapes used for the parametric study on the mode shape's effect on wind load magnitude. The shapes follow the function $\Phi(z) = \left(\frac{z}{h}\right)^\zeta$, and is suggested by EC1 section F.3. $\zeta = 0,6$ and $1,5$ correspond to a rigid frame and a central concrete core cantilevering from the ground, respectively.

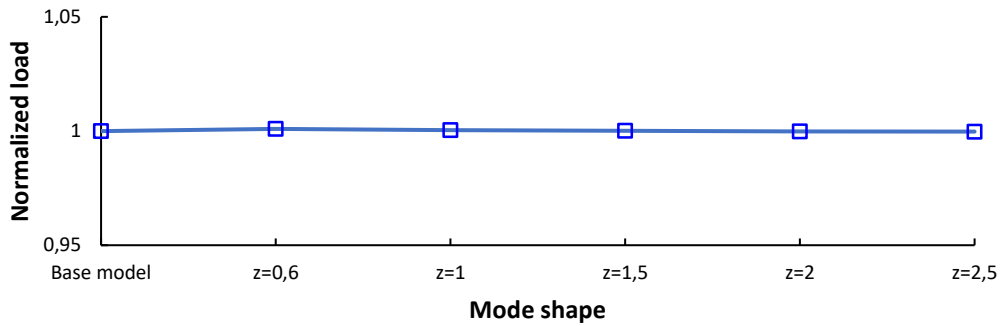


Figure 3.13 Load magnitude normalized to the base model as a function of the mode shapes shown in Figure 3.12. The max and min values are 1,00094 for zeta = 0,16 and 0,99975 for zeta = 2,5, respectively. This is less than a 0,1% deviation from the base model, and the effect can thus be ignored. (z is short for zeta on the x-axis)

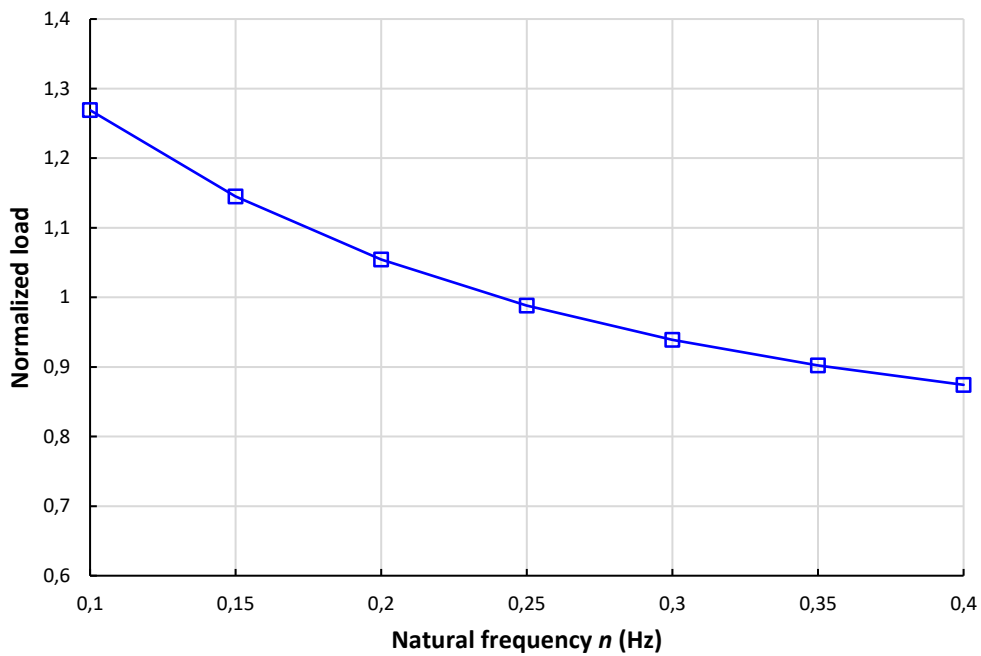


Figure 3.14 Load magnitude normalized to the base model as a function of the natural frequency of the building. Increasing the natural frequency of the building increases the load. The load is 1,27 times greater than the normal load for $n = 0,1$ Hz, and equal to 0,87 times the normal load for $n = 0,4$ Hz. For $n = 0,25$ Hz the load is very close to 1, because the natural frequency of the base model is equal to 0,24 Hz.

3.6 Verification of model

3.6.1 Dynamic behaviour

The natural frequency for the different vibration modes of the structure were compared to the data obtained by Song and Tse (2014), see Table 3.5. The agreement is very high, with all modes having practically identical natural frequencies to those found by Song and Tse, which means that the dynamic behaviour of the model can be assumed to be correct.

Table 3.5. Natural frequencies for the base model calculated by Robot, compared to the FEM results given by Song and Tse (2014).

Mode	Robot model	Song & Tse	
	Hz	Hz	% difference
1	0,24	0,239	-0,42
2	0,24	0,239	-0,42
3	0,30	0,300	0,00
4	0,56	0,562	0,36
5	0,61	0,597	-2,18
6	0,64	0,644	0,62
7	0,64	0,644	0,62
8	0,72	0,706	-1,98
9	0,81	0,814	0,49

3.6.2 Approximate methods check

In addition to checking the modes, the displacement of the model was also checked to make sure the results were within the right order of magnitude. The top displacement for the base model is equal to 155mm, as will be shown later in section 4.4.

A very simplified calculation was carried out, assuming the load on tower 1 to be constant of 2,1 kN/m², or 63 kN/m. The end displacement for a uniformly loaded cantilever is equal to $\frac{qL^4}{8EI}$, where q is the line load in kN/m. E for C55/67 concrete is equal to 33 GPa, and the length is 160m. The second moment of area, I, was assumed to be that of a “mega-beam”, consisting of the columns of the frame, and ignoring the core. The columns were assumed constant with height, with dimensions of 75cm².

Thus, the second moment of area can be found by $I \approx \sum Ah^2$, where A is the cross-sectional area of the columns and h is the distance of each column from the neutral axis, assumed to be at the centre of the building. It follows that

$A = 0,75^2 = 0,5625\text{m}^2$, and $h = 3, 9$ and 15m , depending on the column row, which all have 6 columns. I is then calculated as

$$I = 6 \cdot 0,5625(3^2 + 9^2 + 15^2) \cdot 2 = 2116\text{m}^4$$

Which gives a total displacement for tower 1 of 588mm. Assuming this is halved by linking the towers together, then the displacement is 294mm. By adding the core to the calculation this value would be even smaller. This means that the base model's displacement of 155mm is within an order of magnitude that is reasonable.

The towers displacement is also within the limit of $L/500 = 160\text{m}/500 = 320\text{mm}$, which is commonly used for checking deflection of structures, suggesting that the structural system gives an adequate stiffness for such a tall building.

Thus, we can conclude that the model has the correct dynamic behaviour, the results from the analyses are within a reasonable range, and the structure of the model is adequate.

4 Structural behaviour

Having now obtained a relevant load condition and verified the base computer model, we are ready to start analysing the computer models. But before doing this, let us review the behaviour of some simple portal frames.

4.1 Portal frames

Doing this accomplishes two goals:

- It lets us predict the behaviour of the towers on a macro scale, as the linked building system itself can be regarded as one simple portal frame, with the towers acting as giant columns, and the skybridge acting as the connecting beam.
- It will also help us understand the behaviour of the towers on a micro scale, as the rigid frame is essentially a giant assembly of many portal frames. By understanding the portal frame as a standalone structural element, we can better understand the behaviour of the rigid frame as a whole.

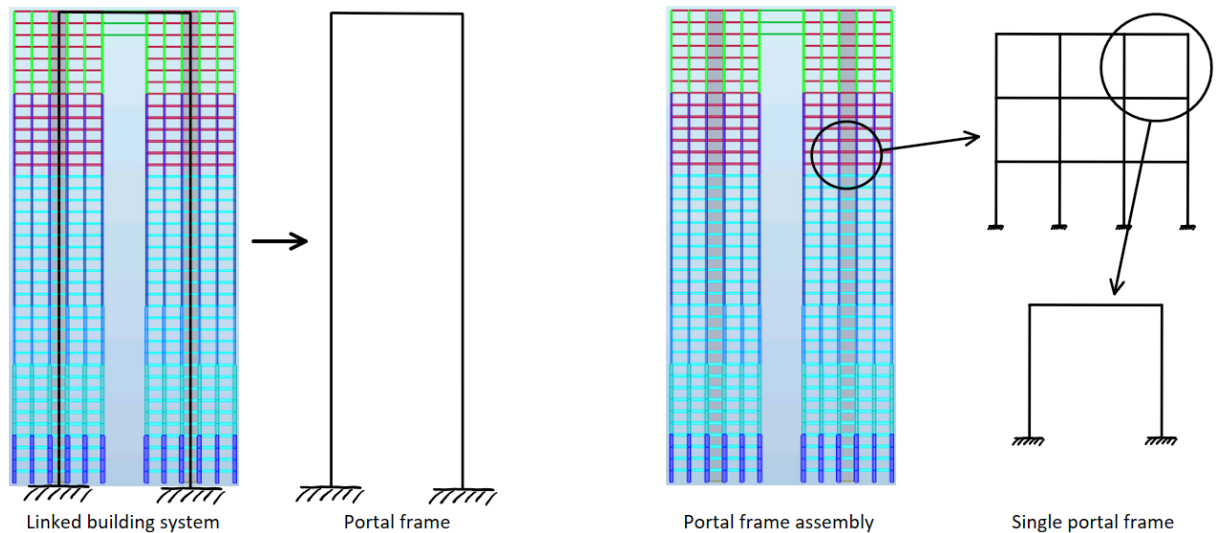


Figure 4.1 Portal frame behaviour for the linked building system. The figure to the left shows how the linked building system can be idealized into a simple portal frame with fixed supports. The figure to the right shows how the rigid frame in the towers are made up from a repetition of single portal frames in the x , y and z -directions.

The portal frames shown in Figure 4.1 are statically indeterminate. Statically indeterminate structures distribute their moments and forces, and consequently stresses, depending on the

relative stiffness of the structural members making up the system. Stiffer members will attract more stresses than those that are more flexible. See appendix B for an explanation of this. The main takeaway is that for laterally loaded portal frames with different relative stiffnesses, the difference in reaction forces, moment distribution and deformed shapes can be quite significant. See Figure 4.2.

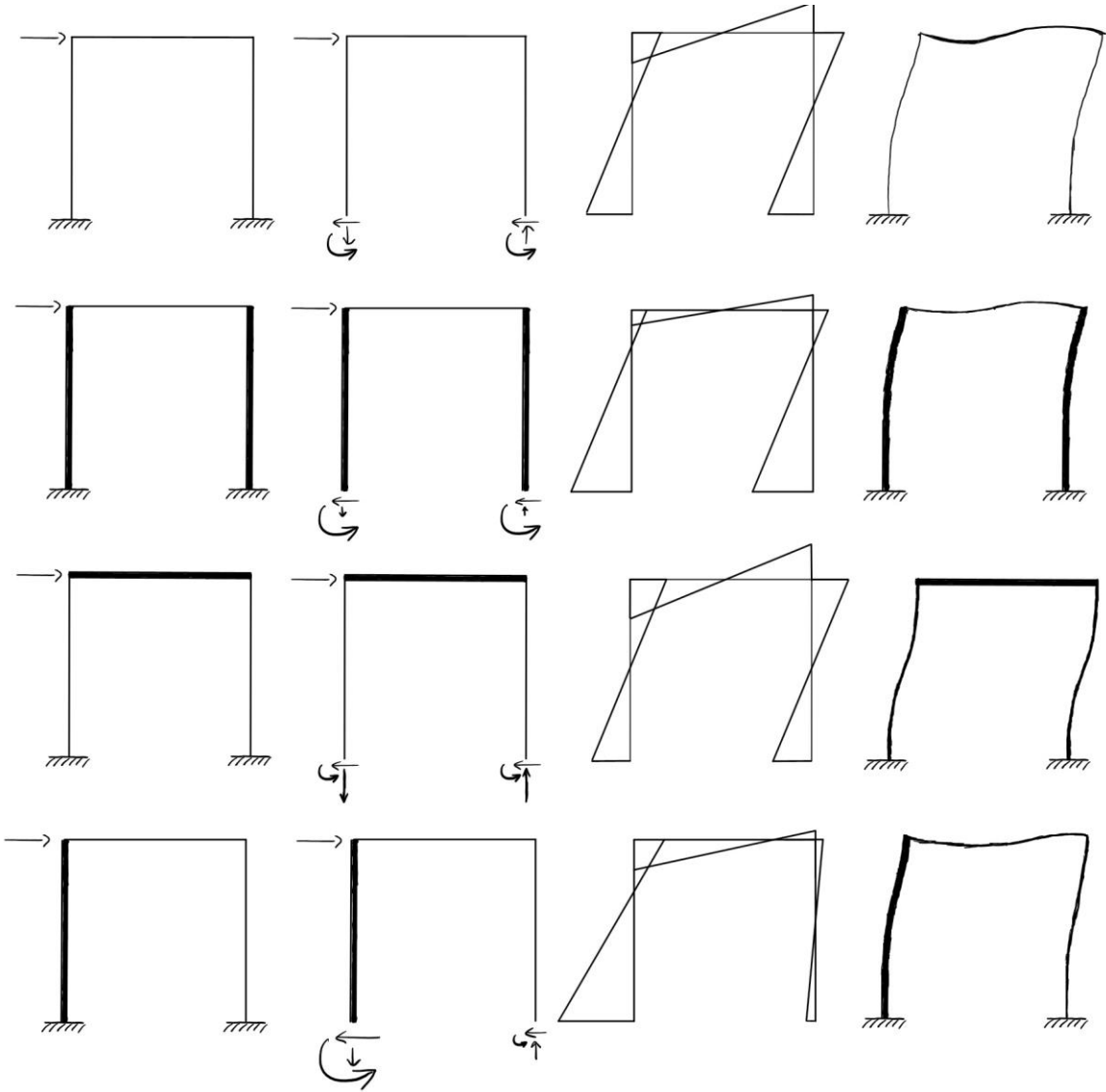


Figure 4.2 Portal frames with varying relative beam and column stiffnesses, and their corresponding support reactions, bending moment diagrams and deformed shapes, respectively. Top row: all structural members have equal stiffness. Second row: columns significantly stiffer than beams. Third row: beams stiffer than columns. Bottom row: left column stiffer than the beam and other column.

The main effects seen from this figure is that:

- Increasing column stiffness will increase the base moment of the column and reduce moments in the beam. It will also reduce the axial forces in the columns.
- Increasing beam stiffness will decrease the base moment of the column and increase moments in the beam. It will also increase the axial forces in the columns.
- The axial force in one column must always be equal and opposite to the axial force in the other column.

We obviously also understand that increasing the stiffness of the frame will reduce its deformations. It is important to note that with a stiff beam, the rotation at the column tops can be reduced significantly. This is important, as if we were to add more frames on top of the existing portal frame, then the base rotation at the column of those additional frames will depend on the beam's stiffness.

4.2 Single tower

With the work presented so far, we can begin to investigate the influence a skybridge has on the structural behaviour of tall buildings. To do this, several permutations of the base model will be considered, varying link structural type, height, and number.

The effect these bridges have on the structural behaviour is investigated by comparing displacements and the distribution of internal forces in the buildings. But to understand the structural effect of the skybridges, we first need to understand how the internal forces are distributed through the buildings when they stand as free towers, which is not immediately straightforward.

The towers consist of structural members that increase in size the lower down they are in the building, as a necessity to carry the increased vertical loads from the floors above. Additionally, the structural stability is achieved through both rigid-frame action, as well as the support of the reinforced concrete core. These traits cause a distribution of internal forces in the building which might not be immediately obvious to even a trained structural engineer, and if they are not accounted for, can make it difficult to identify which structural behaviours are a cause of the skybridges. To clarify this, the behaviour of a single tower that is part of the linked building system is shown first.

The applied actions on each tower is given below. Let us name the towers of the linked building system as towers 1 and 2, corresponding to the left and right towers in the system, respectively. The load on tower 1 must then be that of zone D + zone C, while the load on tower 2 is equal to zone E – zone C. These loads are shown in Table 4.1.

Table 4.1 Wind loads on the two towers of the linked building system. The load on tower 1 is over 10 times as large as the load on tower 2, because the loads on each face of tower 2 almost cancel each other out, while for tower 1 they add to each other.

Height	Wind loads (kN/m ²)			Tower 1	Tower 2
	Zone D	Zone E	Zone C		
Bottom (z = 0 to 32m)	0,96	0,70	0,60	1,56	0,10
Intermediate (z = 32 to 128m)	1,23	0,90	0,77	2,00	0,13
Top (z = 128 to 160m)	1,62	1,18	1,01	2,63	0,17

The overturning moments and total shear force applied to each tower when standing individually are then calculated as one would for a simple cantilever, the results are shown in Table 4.2. Tower 2 is subjected to only 6,5% of the actions on tower 1.

Table 4.2 Total overturning moment and shear force applied to the towers due to the loading given in Table 4.1

	Tower 1	Tower 2
Moment (kNm)	848333	54989
Shear (kN)	9782	634

Now, the behaviour of a single tower subject to the wind load of tower 1 in the linked building system is shown in Figure 4.3. The deformed shape of the structure, the bending moment, axial force and stress diagram for the frame, and the bending moment and shear force diagrams for the central core are given. From this figure we note that:

- The deformed shape is approximately linear with height above the bottom 10 floors, with a max deflection at the top of 297mm.
- The bending moments at the bottom 4 floors of the frame vary with height. Above this, the bending moments in the frame remain constant, with discrete jumps in magnitude occurring where the column sizes change. This is seen more clearly in Figure 4.4. The max moment in a single column at the base is 1260 kNm.
- The axial forces in the columns increase towards the edges of the building, with the max axial force being ± 2986 kN. The columns on the right side are in compression, on the left in tension.
- The maximum stress in the frame occurs around the middle of the building, with a max normal stress of ± 23 MPa.
- The bending moment in the core has roughly the shape of a cantilever subject to a uniformly distributed load, propped up by a vertical support at the end. However, due to the interaction with the frame, it experiences a local peak in moment around height $z = 104$ m, where the frame dimensions reduce significantly. From $z = 104$ m and upwards, the moment diagram for the core is that of a mini-propped cantilever. The

maximum moment at the base is 180617 kNm, about 20% of the total applied moment.

- The reduction in beam section at height $z = 104\text{m}$ is very significant with regards to the frame's stiffness, more so than the incremental reductions in column size along the height.
- The shear force sent to the core decreases linearly with height, but with some jumps where the frame changes in dimension and thus stiffness, like the moment diagram. The max shear force is 6749 kN, 69% of the total shear force.
- There is no net axial force in the tower cores, as they are both located at the neutral axis of each tower

4. Structural behaviour

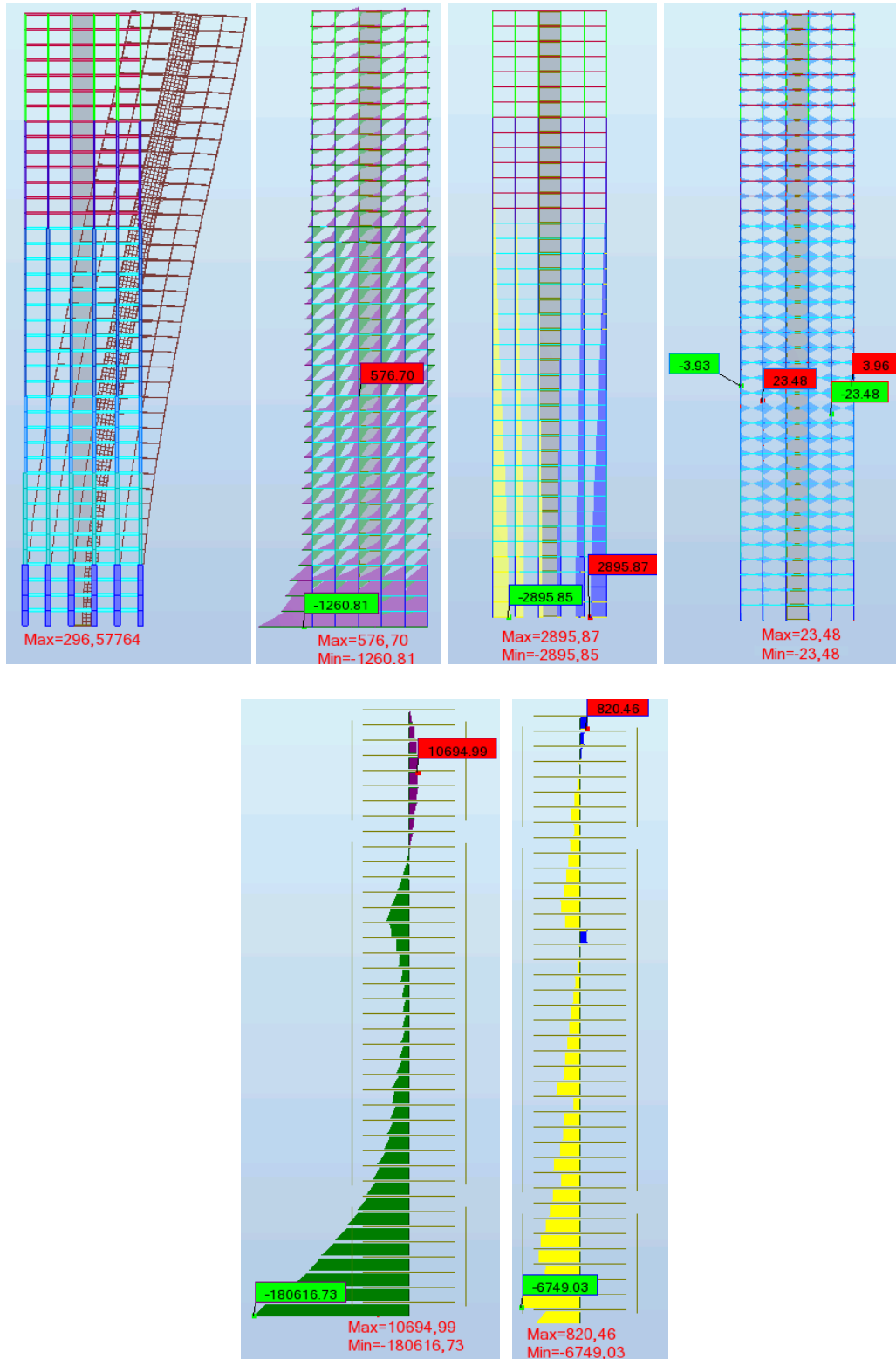


Figure 4.3 Deformed shape and bending moment, axial force and stress diagrams for the frame, with corresponding bending moment and shear force diagram for the central core, respectively, for a single tower subject to the same wind load as tower 1 in the linked building system. Units in mm, kNm, kN and MPa.

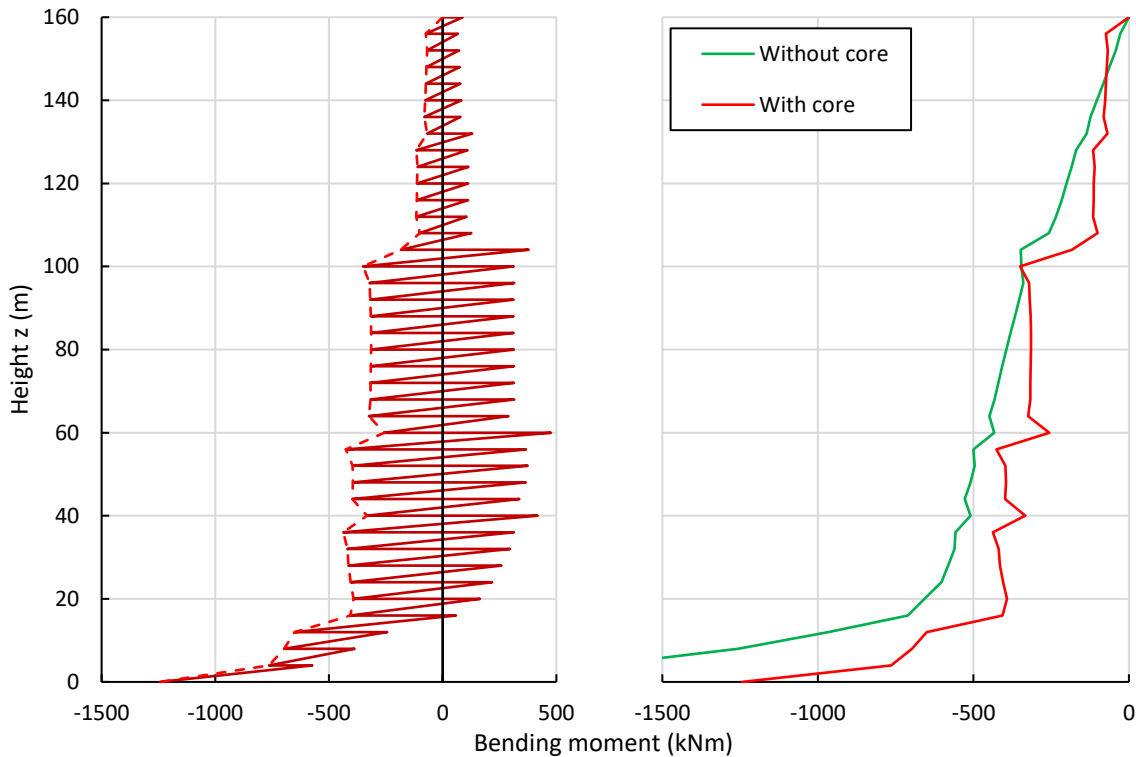


Figure 4.4 Bending moment diagram for a central column going the full height of the building (left). The base column moments (the dashed line) are compared to the values for the same model without a central core. We can see that with the core the moments in the column for segments of heights remain more or less constant, with jumps in moment magnitude corresponding to where the columns change in size. Without the core this is not the case, the moments increase more or less linearly between the jumps, because there is no core to take up the excess stresses.

This is as explained earlier the load effects for the tower 1 when it deforms like a freestanding cantilever. Tower 2 is subject to the same shape of loading, but a considerably smaller magnitude, so it is reasonable to assume the load effects will be distributed the same way, only with smaller values.

When linking the towers together to form the linked building system, they will no longer deform as pure cantilevers. The link will try to restrain the top of tower 1, pushing it to the left and making its behaviour more like a propped cantilever, which will shift the moment distribution to the right, both for the core and the frame columns. On tower 2 the link will act as an additional point load to the right, shifting its moment diagram to the left. See Figure 4.5.

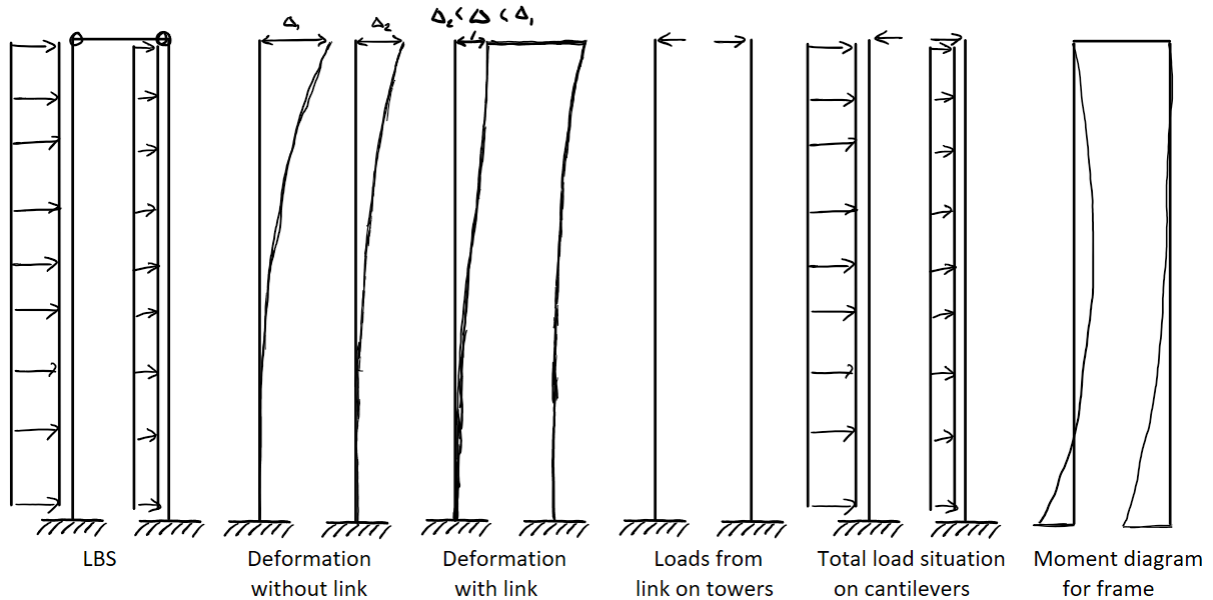


Figure 4.5 Change in behaviour of the towers due to the structural link. Because the joint displacement Δ of the LBS is smaller than Δ_1 but larger than Δ_2 , the displacements of towers 1 and 2 if they were to sway as lone cantilevers, respectively, the link must act as a point load to the left on tower 1 and to the right on tower 2. Thus, the total moment distribution in the towers must have a shape similar to that shown in the far right figure.

With this, we can begin to consider how the links change the behaviour of the system, and how it might deviate from our expectations.

4.3 Structural links

Three different link types have been analysed, the simple link used in the base model, and two stiffer links, named the truss and V-leg links.

The simple and V-leg link consist of 2-storey walkways carried by 1200x500mm² reinforced concrete beams, which are fixed to the rigid frame of the two towers. The truss frame instead uses square 300mm wide by 10 mm thick hollow sections made from S355 steel arranged in a truss to carry the walkways. The floor plates for all links are 120mm thick concrete slabs.

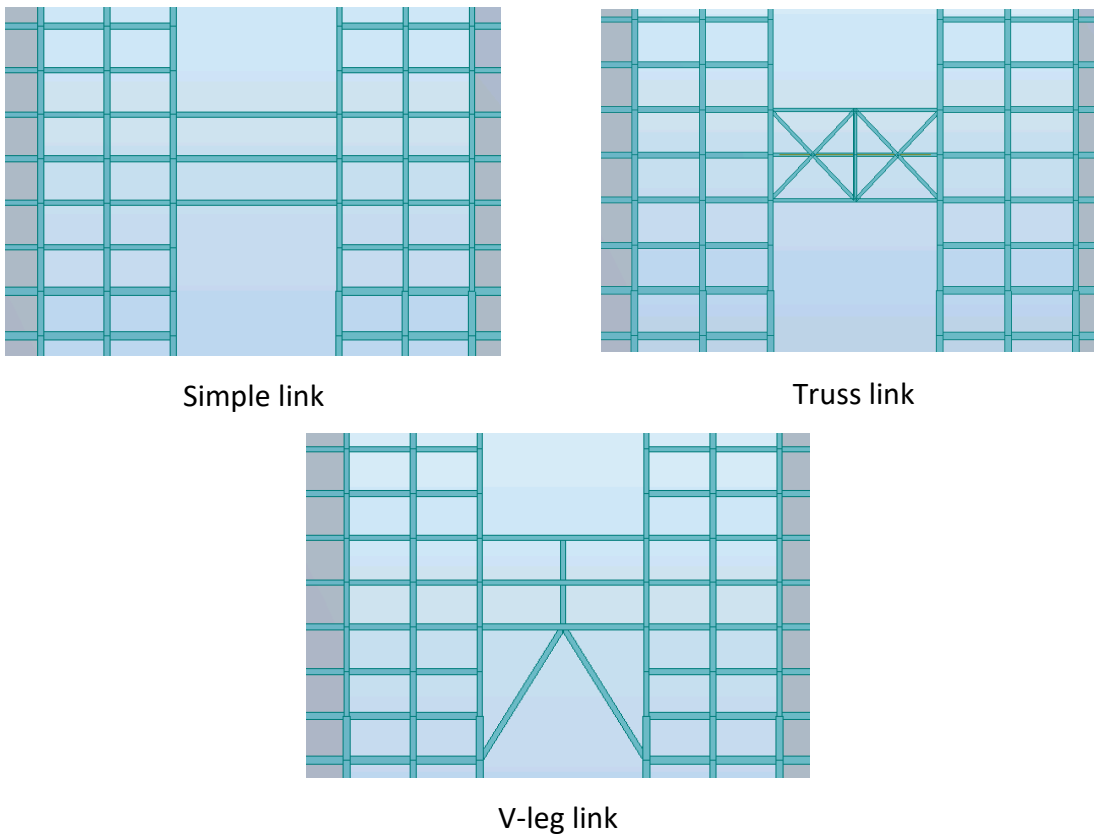


Figure 4.6 Different structural link types evaluated in the linked building system. All links have 120mm thick concrete floor plates. The truss link uses square 300mm wide by 10mm thick hollow sections for the horizontal and diagonal members, with a HEB300 profile as a vertical column, all from S355 steel. The V-leg link has 50x50cm² diagonal columns, supporting the vertical 40x40cm² central column.

The V-leg link type supports the link at its mid-span by 50x50cm² diagonal columns rising up from each tower, three storeys below the bottom of the link, which supports a central vertical 40x40cm² column.

4. Structural behaviour

These link types cause the linked building system's frame analogy to correspond to a pinned beam frame, a fixed beam frame and a fixed, stiffer beam frame, which correspond to the simple, truss, and V-leg links, respectively. This is because while all the links are fixed to the frame of the towers, the stiffness of the simple link compared to the tower is so low that it can be assumed to be negligible, and thus pinned.

The different links were connected to the towers at three different heights, $h'=160\text{m}$, $h'=120\text{m}$, and $h'=80\text{m}$. Let us start by evaluating the links connected at height $h'=160\text{m}$.

Note: when modelling the floors of the model, all slabs are modelled as "rigid diaphragms", including the slabs for the structural links. This is to make the modal analysis quicker. Because of this, there will be no transfer of axial forces through the beams in the links, which explains why all the beams are shown with zero axial force.

4.4 Links at $h'=160\text{m}$

The three models considered in this section are shown in Figure 4.7.

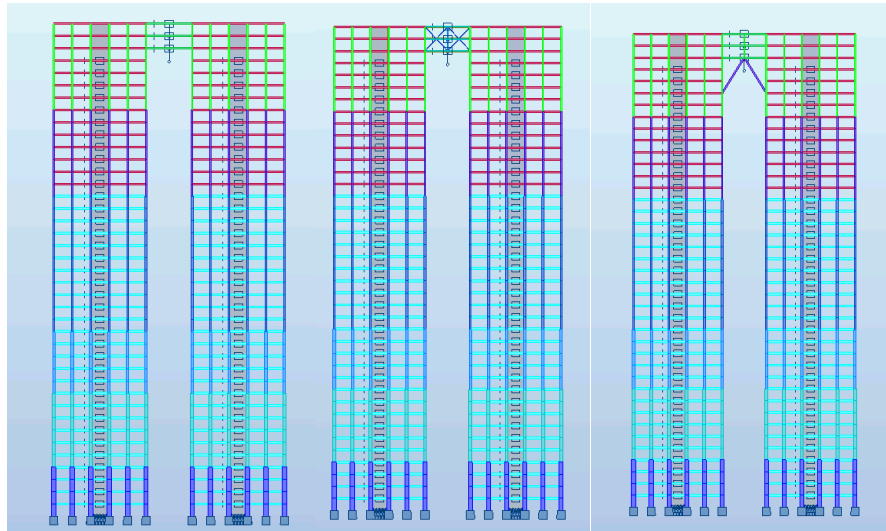


Figure 4.7 Structural models with links at $h'=160\text{m}$, showing the simple, truss, and V-leg links, respectively.

The behaviour of these models compared to the standalone towers are of interest here, and how this changes depending on the different link types. But first let us investigate how their loading differs from that of the base model.

4.4.1 Dynamic characteristics and loading

The natural frequencies and mode shapes for the models with the different link types are shown in Table 4.3 and Figure 4.8, respectively. Table 4.3 also gives the difference in applied load for the buildings compared to the base model, which had a natural frequency of $n_{1,x} = 0,24 \text{ Hz}$. The change is not significant, with a reduction of maximum 2,29% for the models. The thing to note here is that the load effects presented later on should be slightly lower for the truss, V-leg and cable models than the resented values because their load is smaller.

4. Structural behaviour

Table 4.3 Natural frequencies and loads for the four models with links at $h'=160\text{m}$. The simple link with $h'=160\text{m}$ is the base model. The other models are slightly stiffer, with higher natural frequencies and thus less load. This discrepancy is small, with only a maximum 2,29% reduction.

h'=160m Link type	Natural frequency $n_{1,x}$ (Hz)	Load $F_{w,D}$ (kN/m ²)	Load diff. from base model (%)	Peak acceleration a_{\max} (m/s ²)
Simple	0,24	1,630	0,00	0,01137
Truss	0,25	1,610	-1,20	0,01140
V-leg	0,26	1,592	-2,29	0,01100

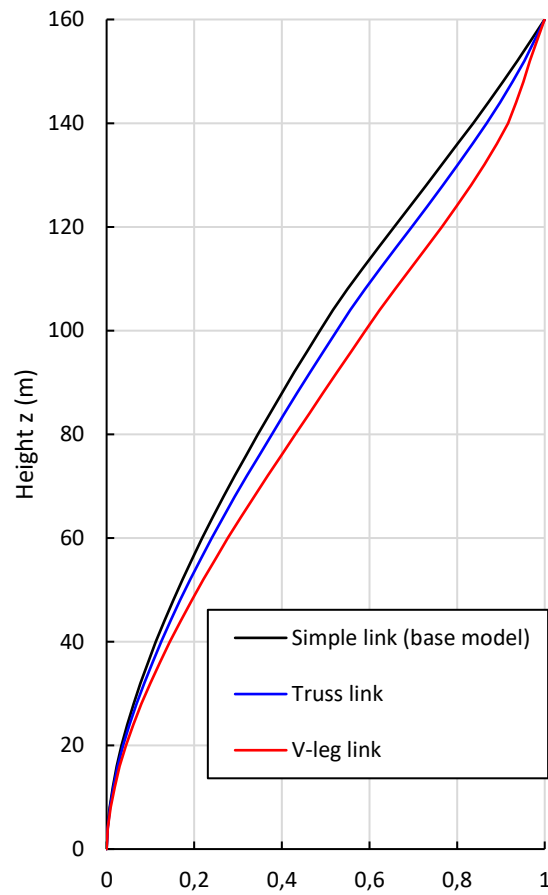


Figure 4.8 Mode shapes for the three models with links at $h'=160\text{m}$. Only the V-leg link changes the mode shapes in any substantial way. All links increase modal displacement at the lower parts of the building.

4.4.2 Simple link

The structural diagrams for the simple link at $h'=160\text{m}$ model are shown in Figure 4.9 and Figure 4.10. From these figures, we observe that:

- The deformed shape is like we expected from Figure 4.5. The max displacement at the top is 155 mm, approximately half of the displacement of the single tower (296mm).
- The moment distribution for the frames of the two towers are relatively similar, with the moments in the lower part of tower 1 being greater than tower 2, and the moments in the top part of tower 2 being greater than tower 1. The max bending moment in the beams of the link is 149 kNm. The max bending moment at the base is 958 kNm, approximately a 300 kNm reduction from the single tower.
- The axial forces for the two towers are distributed similarly, with tower 1 taking the largest axial forces, 1773 kN, compared to 1258 kN max in tower 2.
- The max stresses are still located around the middle parts of both towers. The largest stresses occur in tower 1, but have been reduced to max ± 16 MPa.
- The moment in the core has been shifted like we expected, with moments more to the right for tower 1, and to the left for tower 2. Otherwise the moment diagram shape for the two cores are similar. The base moment is now 134596 kNm for tower 1, reduced from 180617 kNm for the single tower. The base moment for tower 2 is 57560 kNm. The max moment at the link location for tower 2 is 24490 kNm.
- The shear force going to the core is very large at the top for tower 2, with 3369 kN as the max. The shear force distribution in both cores is as one would expect from Figure 4.5. Tower 1 has much larger shear forces at the base than tower 2, with max 5296 kN for tower 1, and 1889 kN for tower 2.

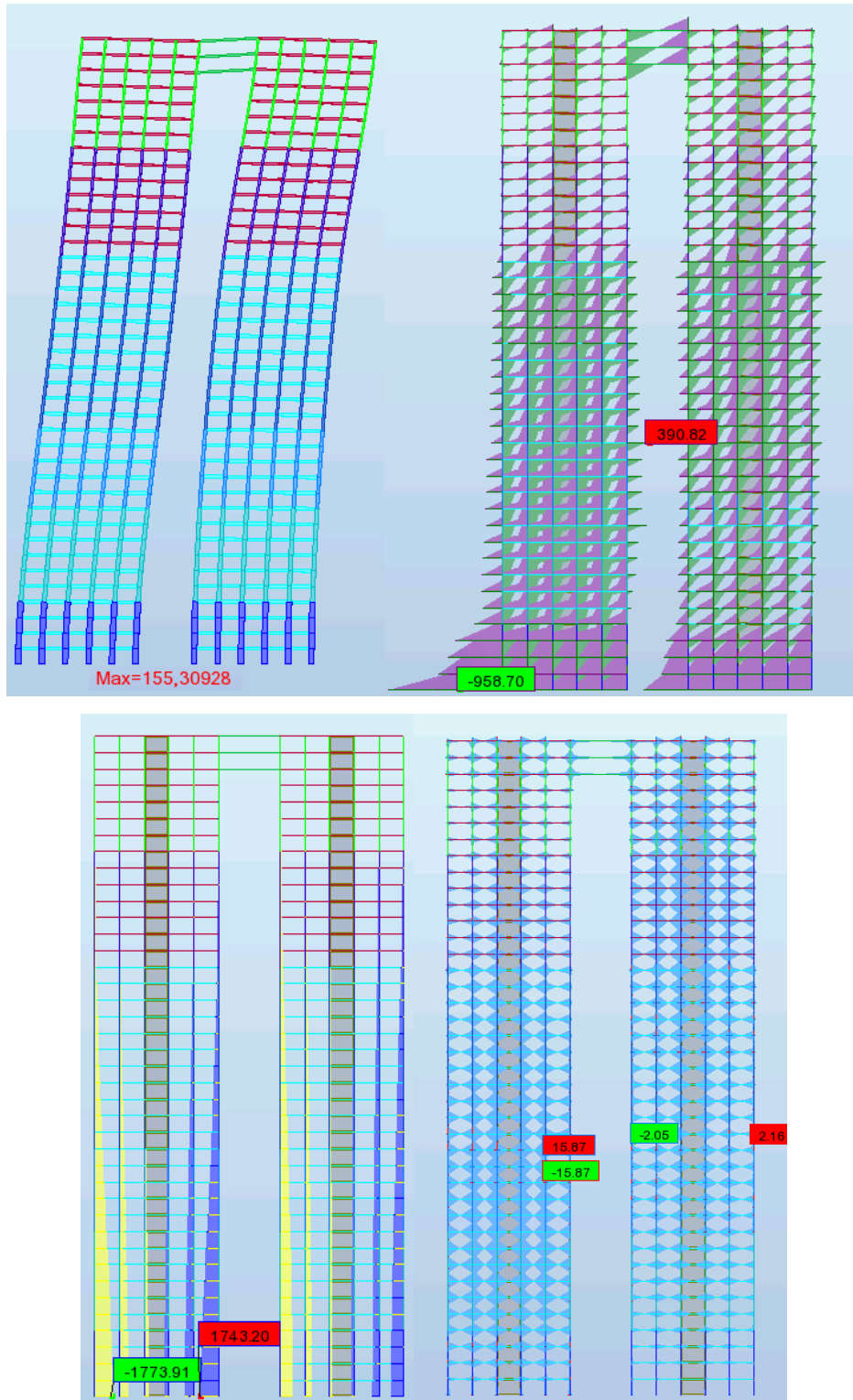


Figure 4.9 Deformed shape, bending moment, axial force and stress diagram for the frame of the simple link at $h'=160m$ model, respectively. Units in mm, kNm, kN and MPa.

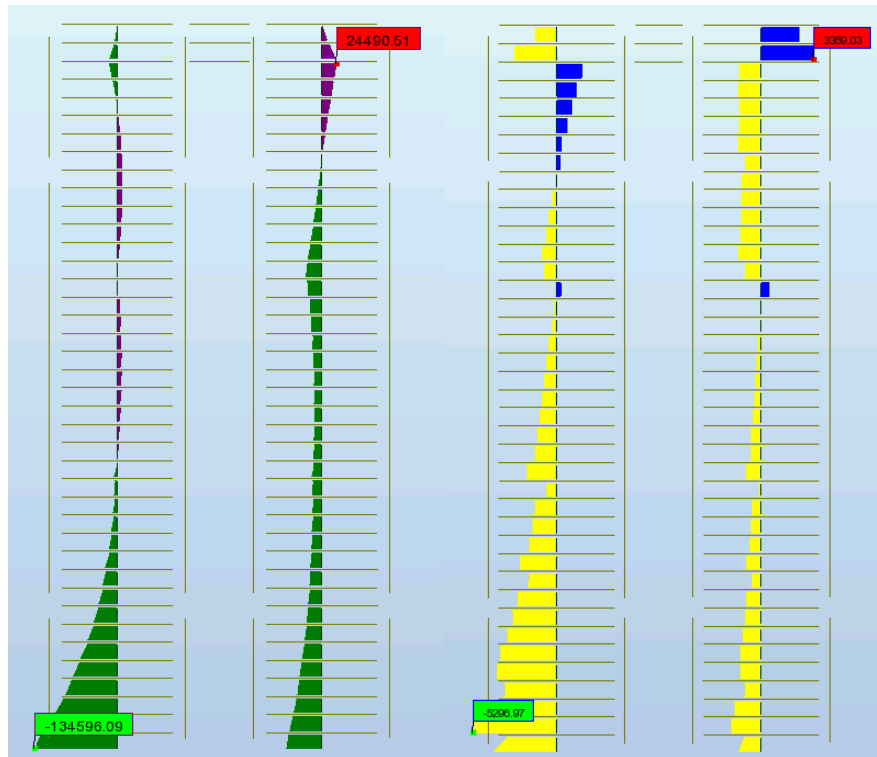


Figure 4.10 Bending moment and shear force diagram for the core of the simple link at $h'=160\text{m}$ model, respectively. Units in kNm and kN.

4.4.3 Truss link

The structural diagrams for the truss link at $h'=160\text{m}$ model are shown in figures Figure 4.11 and Figure 4.12. From these figures, we observe that:

- The deformed shape is similar to the simple link's, but with the top floors being more level. The maximum displacement is 135mm.
- The moment distribution in the frame is similar to the simple link's.
- The axial forces near the bottom are distributed as expected. The columns at the in-between faces, switch axial force direction about halfway up the building and proceed to go into tension on the left side, and compression on the right, in order to match the axial forces in the diagonals of the truss link. See also Figure 4.13. The columns below the link reach 467 kN, the diagonals in the link are subject to 390 kN.

4. Structural behaviour

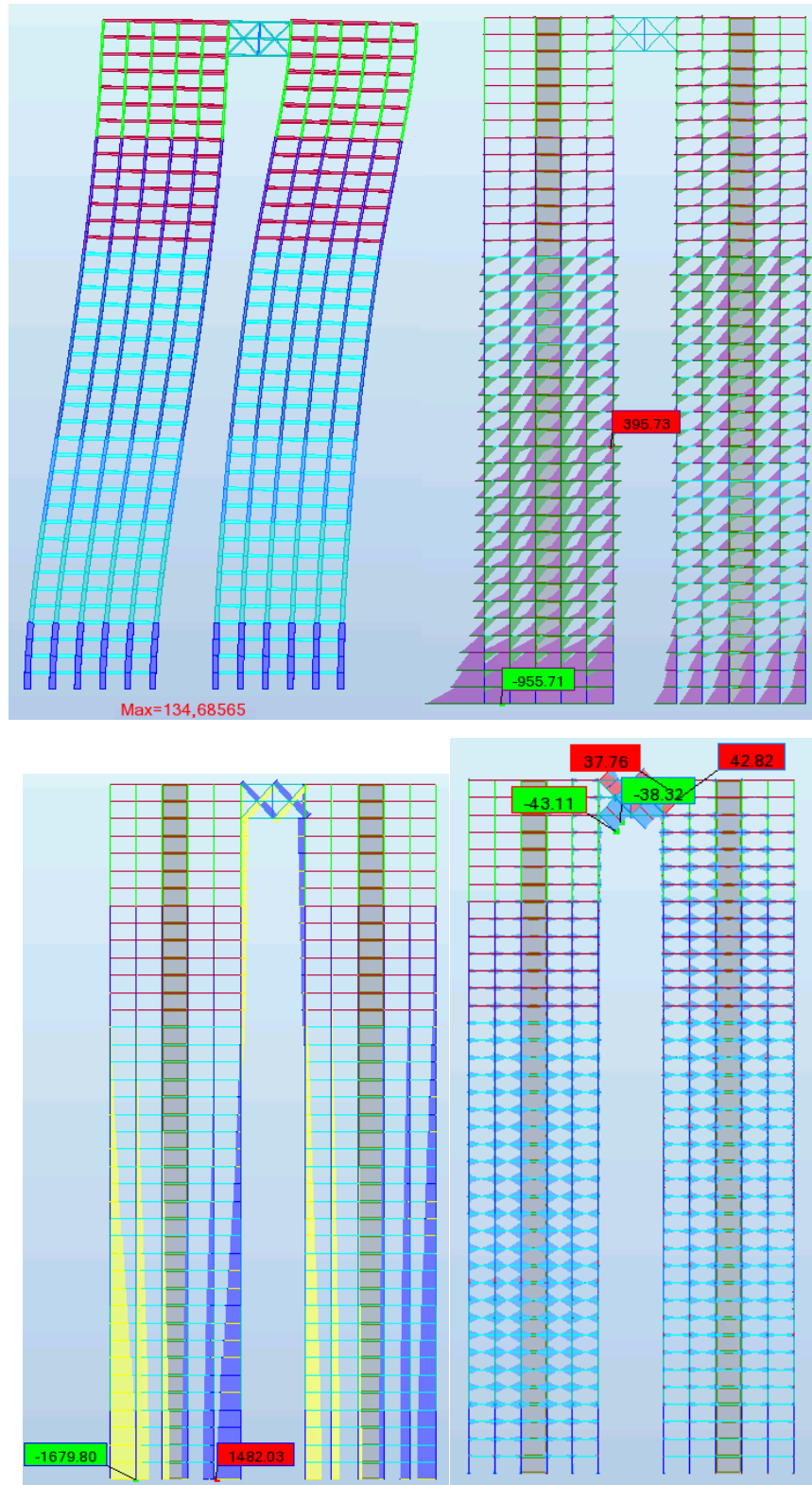


Figure 4.11 Deformed shape, bending moment, axial force and stress diagram for the frame of the truss link at $h'=160\text{m}$ model, respectively. Units in mm, kNm, kN and MPa.

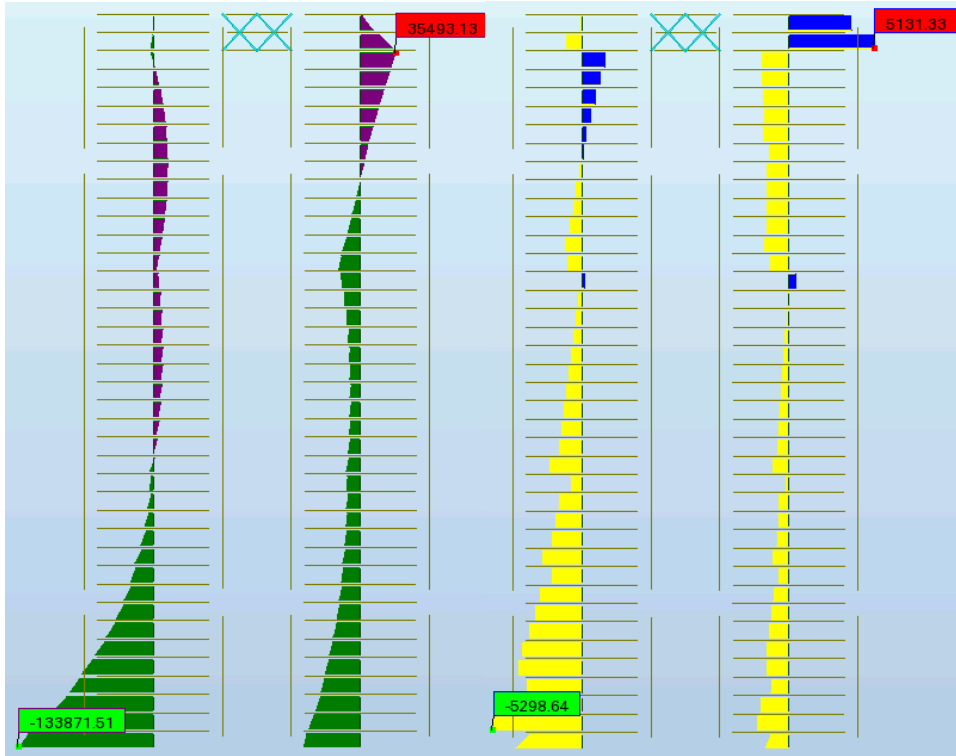


Figure 4.12 Bending moment and shear force diagram for the core of the truss link at $h'=160\text{m}$ model, respectively. Units in kNm and kN.

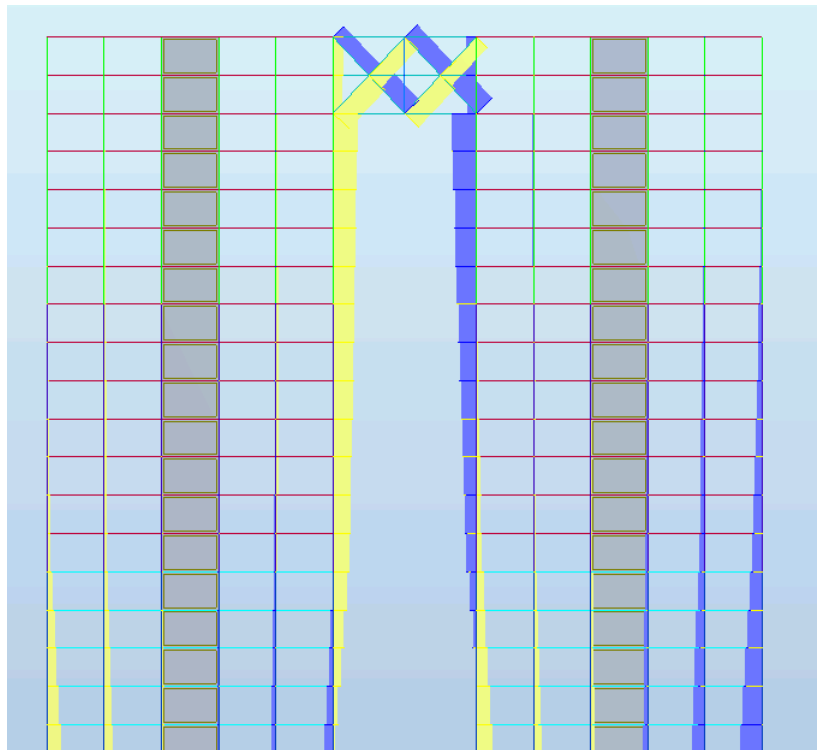


Figure 4.13 Axial force distribution for the top part of the building. The columns on the in-between faces change axial direction to resist the axial forces created in the diagonals of the truss link.

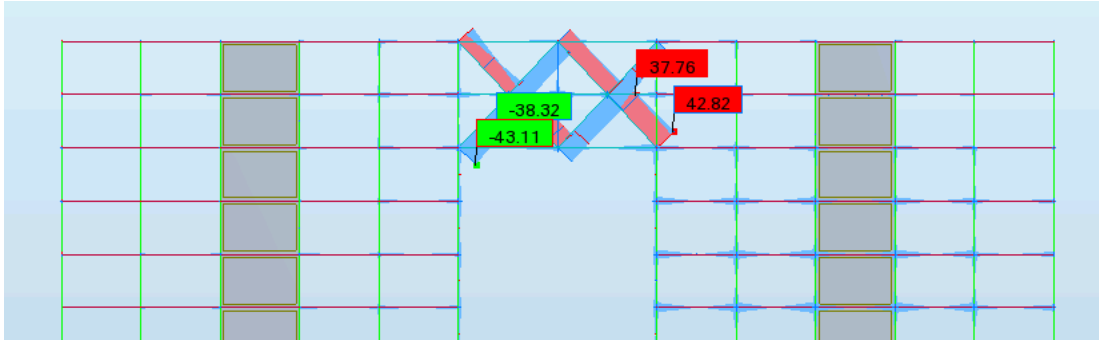


Figure 4.14 Stresses for the truss link at $h'=160\text{m}$ zoomed in on the link.

- The stresses are similarly distributed as for the simple link. Max stress at the middle of the tower 1 is around 15 MPa. The stresses in the truss are shown in Figure 4.14, with max values of 43 MPa. These members are made of steel so they are expected to endure higher stresses than the concrete members.
- Bending moments in the cores at the base of the building are like the simple link's. The bending near the link in tower 2 is 35493 kNm. We see the same in the shape of the moment diagram, with larger magnitudes of moment near the link for both cores of the truss model. This must be because the truss link is much stiffer than the simple link, and attracts more moment to itself that must be matched by the cores, like was explained in the portal frame section.
- Interestingly the link causes a larger shear force at the top of tower 2, of 5131 kN, almost a 2000 kN, or 40% increase from the simple link. Correspondingly the shear at the top of tower 1 is reduced. Shear at the bottom is unaffected.

4.4.4 V-leg link

The structural diagrams for the V-leg link at $h'=160\text{m}$ model are shown in figures Figure 4.15 and Figure 4.16. From these figures, we observe that:

- The max displacement is 125mm.
- The bending moment in the beams of the link is dominated by the upward thrust of the diagonal columns. Max moment at mid-span is around 98 kNm for the link beams.
- Like for the truss links, the columns on the in-between faces change axial force direction to absorb the axial forces from the diagonals. Max axial force in the diagonals is around 991 kN.
- The bending moment and shear force in the cores are influenced over a greater height due to the V-leg link affecting have a larger structural depth, by going 3 storeys down from the bottom of the link. Especially the moment diagram for tower 2 shows larger moment magnitude over more storeys than the two previous models. The moment is only 24019 kNm in the top part of tower 2. The max shear force at the top is reduced also, with the max being in tower 1 with 3000 kN.
- Other effects of the link, i.e. deformation shape, bending moments, axial forces and stresses in the frame, moment and shear in the core near the base of the building, are similar to that of the previous models with $h'=160\text{m}$, as expected.

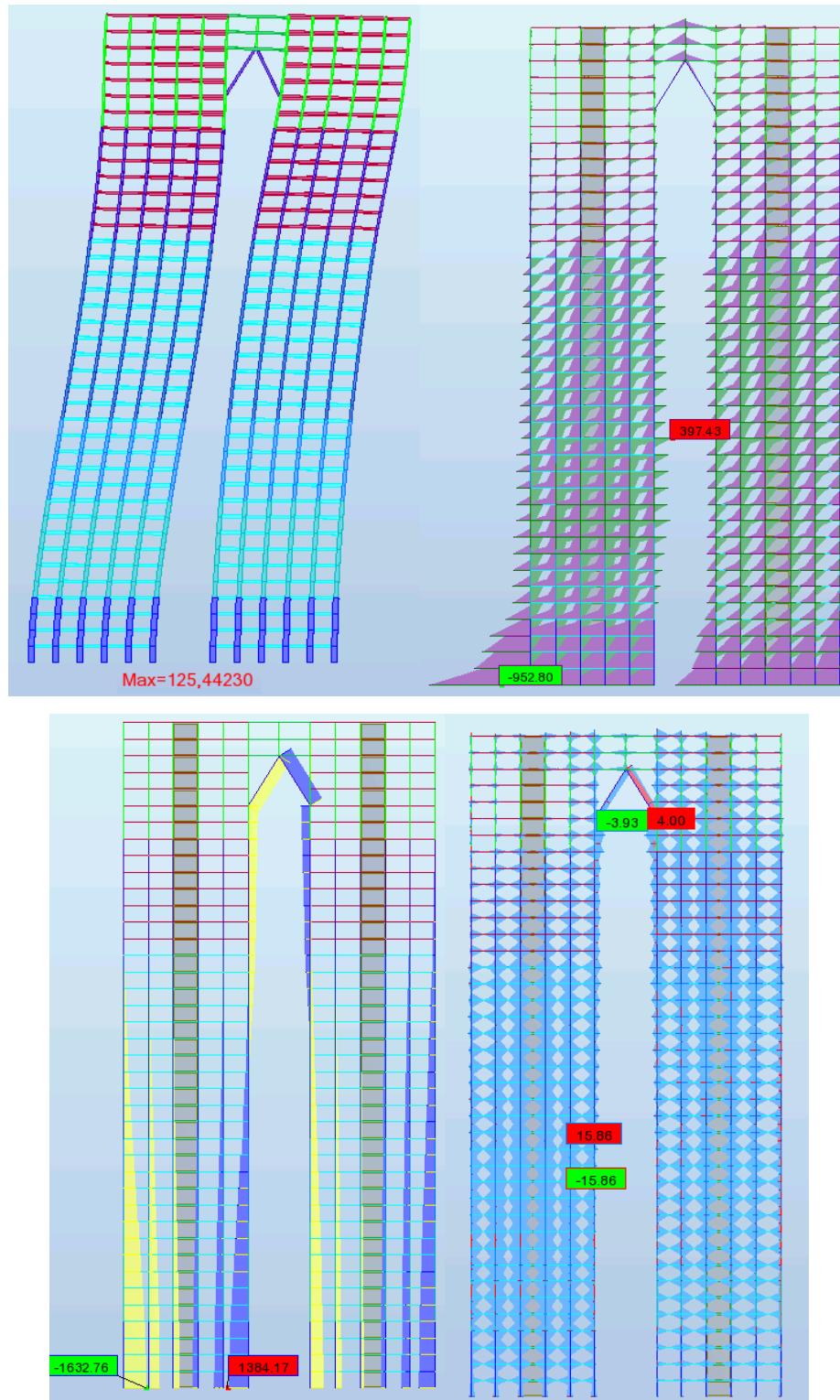


Figure 4.15 Deformed shape, bending moment, axial force and stress diagram for the frame of the V-leg link at $h'=160m$ model, respectively. Units in mm, kNm, kN and MPa.

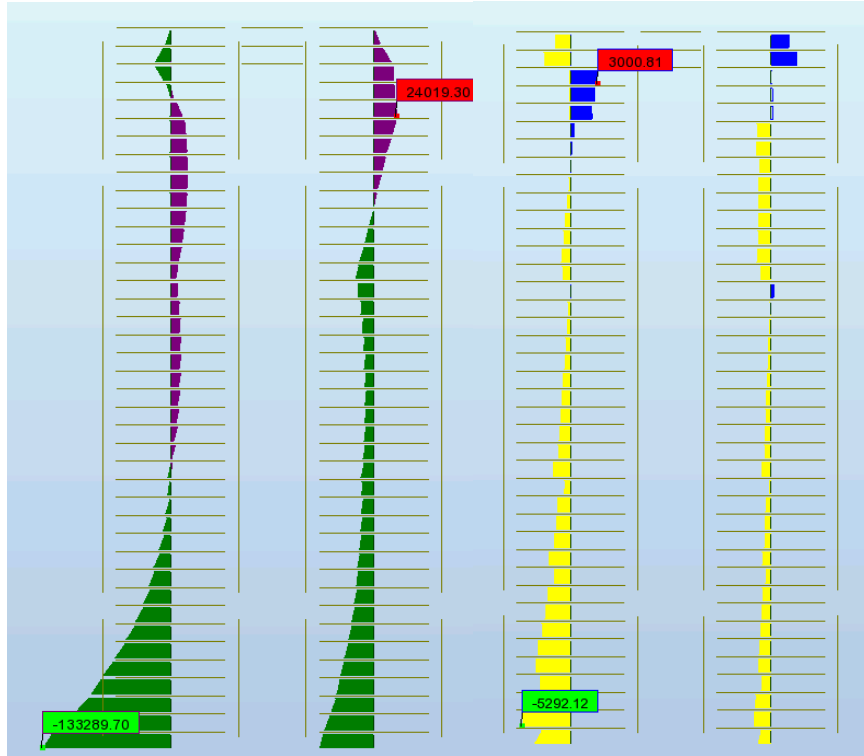


Figure 4.16 Bending moment and shear force diagram for the core of the V-leg link at $h'=160\text{m}$ model, respectively. Units in kNm and kN.

4.4.5 Summary

Figure 4.17 compares directly the displacements and bending moments in the cores of towers 1 and 2 for the links at height $h'=160\text{m}$. The V-leg link reduces displacements the most, due to producing the stiffest “beam” that connects the two “columns” (towers). This is as expected. The bending moments at the base are practically unaltered.

We see clearly that the truss link causes a significant increase in core bending moment in the top of tower 2 compared to the other links, with 35493 kNm for the truss, compared to 24490 kNm and 24019 kNm for the simple and V-leg links, respectively. This is over a 10000 kNm increase, or roughly 40%.

Figure 4.18 shows the moment diagrams for the three models. The V-leg link does show smaller moments in the frame at the top of towers 1 and 2 compared to the other models, especially compared to the simple link.

4. Structural behaviour

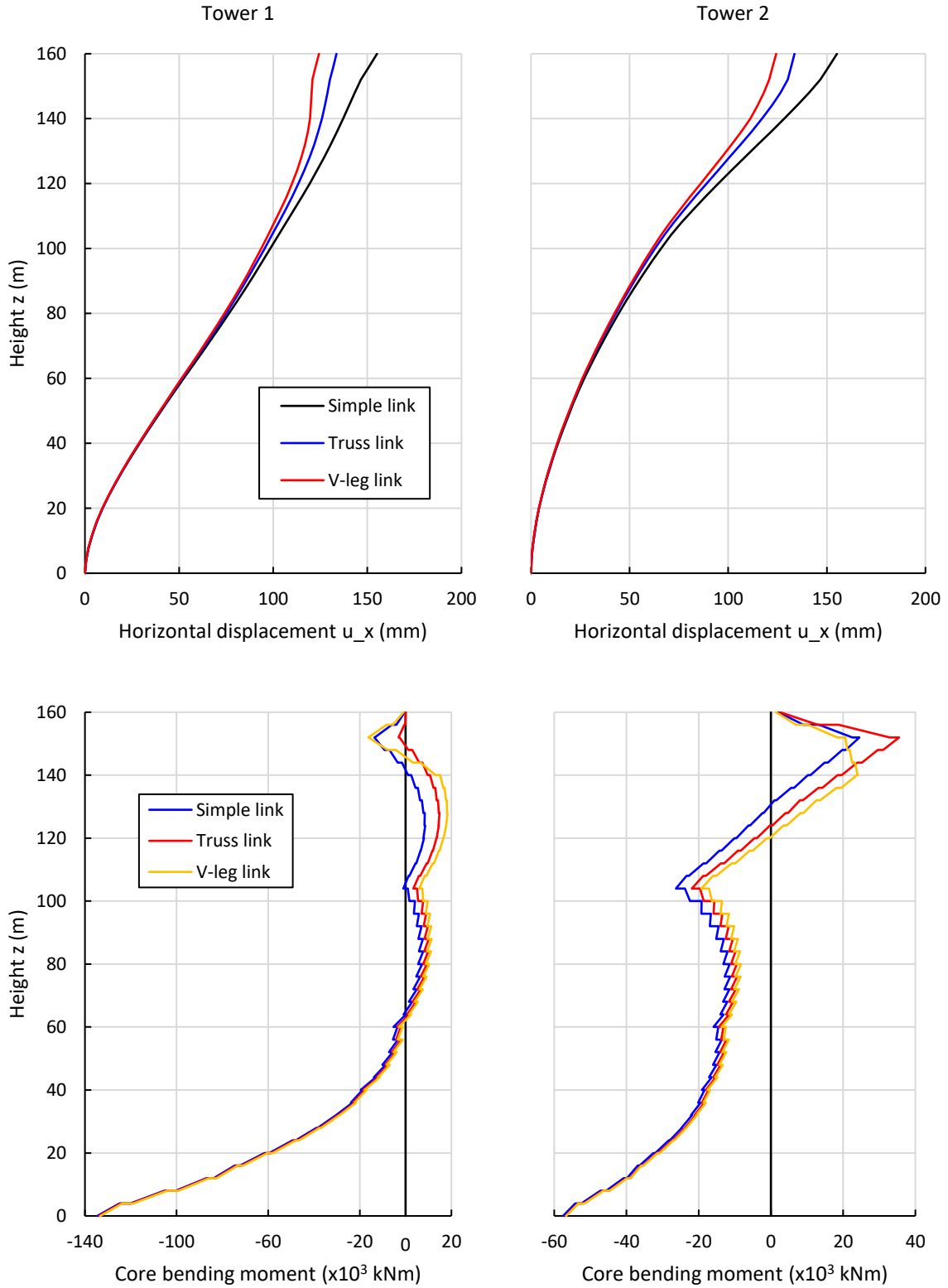


Figure 4.17 Displacements and bending moments in the cores for towers 1 and 2 for the links at $h'=160m$.

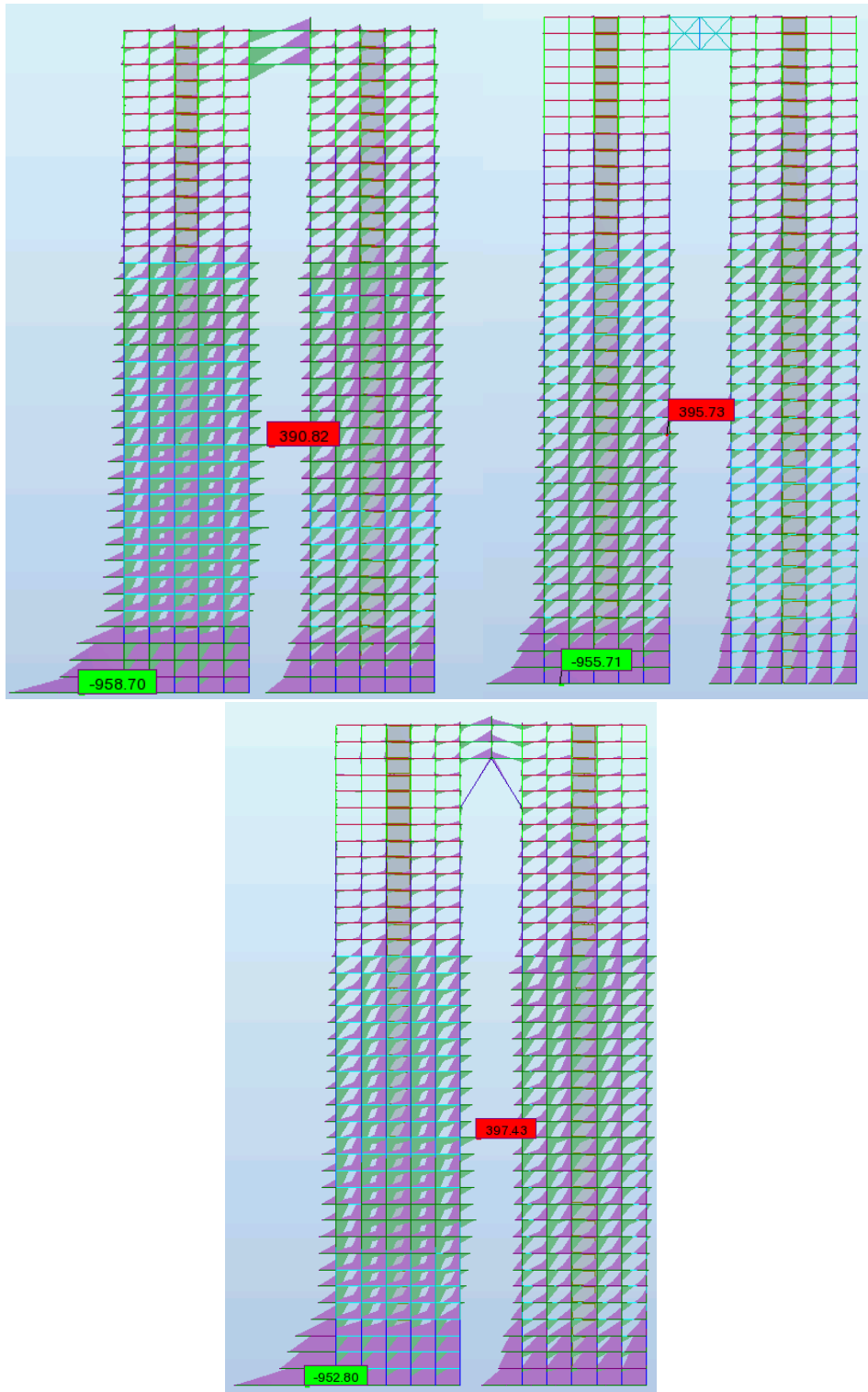


Figure 4.18 Bending moment diagrams for the rigid frames of the three different link types at $h' = 160\text{m}$. Note that the scale for each figure is not the same. In general the distribution is similar for all the three models.

4.5 Links at $h'=120\text{m}$

The next models to consider are those with the structural link located with $h'=120\text{m}$. The three models are shown in Figure 4.19.

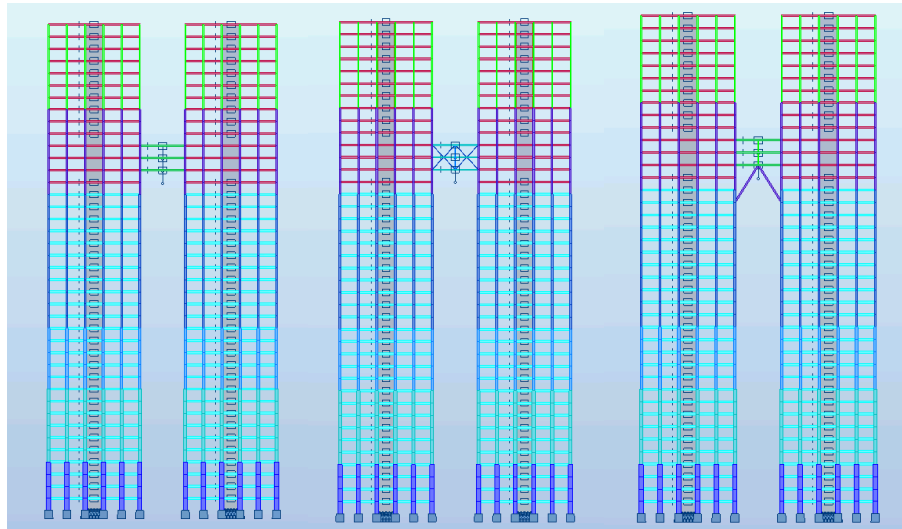


Figure 4.19 Structural models with links at $h'=120\text{m}$, showing the simple, truss, and V-leg links, respectively.

4.5.1 Dynamic characteristics and loading

The natural frequencies and “real” loads for the models are shown in Table 4.4. The load on the V-leg model should have been reduced by 3,32% to be most accurate, but this is not a large discrepancy.

Table 4.4 Natural frequencies and loads for the three models with links at $h'=120\text{m}$. The discrepancies from the base model are small, with only a maximum 3,32% load reduction.

Link type	$h'=120\text{m}$ Natural frequency $n_{1,x}$ (Hz)	Load $F_{w,D}$ (kN/m^2)	Load diff. from base model (%)	Peak acceleration a_{\max} (m/s^2)
Simple	0,24	1,629	-0,04	0,01175
Truss	0,25	1,610	-1,20	0,01137
V-leg	0,27	1,576	-3,32	0,01064

4.5.2 Simple link

The structural diagrams for the simple link at $h'=120\text{m}$ model are shown in Figure 4.20 and Figure 4.21. From these figures, we observe that:

- The max displacement at the top of tower 1 is equal to 166mm, while the at the top of tower 2 it is slightly less, 142mm. The link is skewed due to its low stiffness.
- Bending moment diagram in the frame is largely unaltered for both towers, with more bending in general for tower 1, especially above the link. Base moment is 831 kNm. Moment in the beams of the link are around 240 kNm.
- Max axial force in columns at 1600 kN, for link at 160m it was around 1770 kN, a 10% reduction.
- Max stresses now in tower 2 near the link, but low at ± 13 MPa.
- Bending moment diagram for core as expected when the point load from the link now being moved down to around 110-120m. This almost coincides with the location of the frame softening, increasing the moment peak that occurs at $z = 104\text{m}$ for the single tower. In general more moment higher up for the core in tower 1, with less moment near the base, where the max moment is 115933 kNm, compared to 134596 kNm for when the link was at the top. This is a 14% reduction. Max moment near the link is 20860 kNm for tower 1 and 17143 kNm for tower 2. Base moment for tower 2 is 76093 kNm, up from 57560 kNm for when the link was at $h'=160\text{m}$, a 32% increase.
- Shear force diagram as expected. Tower 2 above the link has shear acting to the left.

4. Structural behaviour

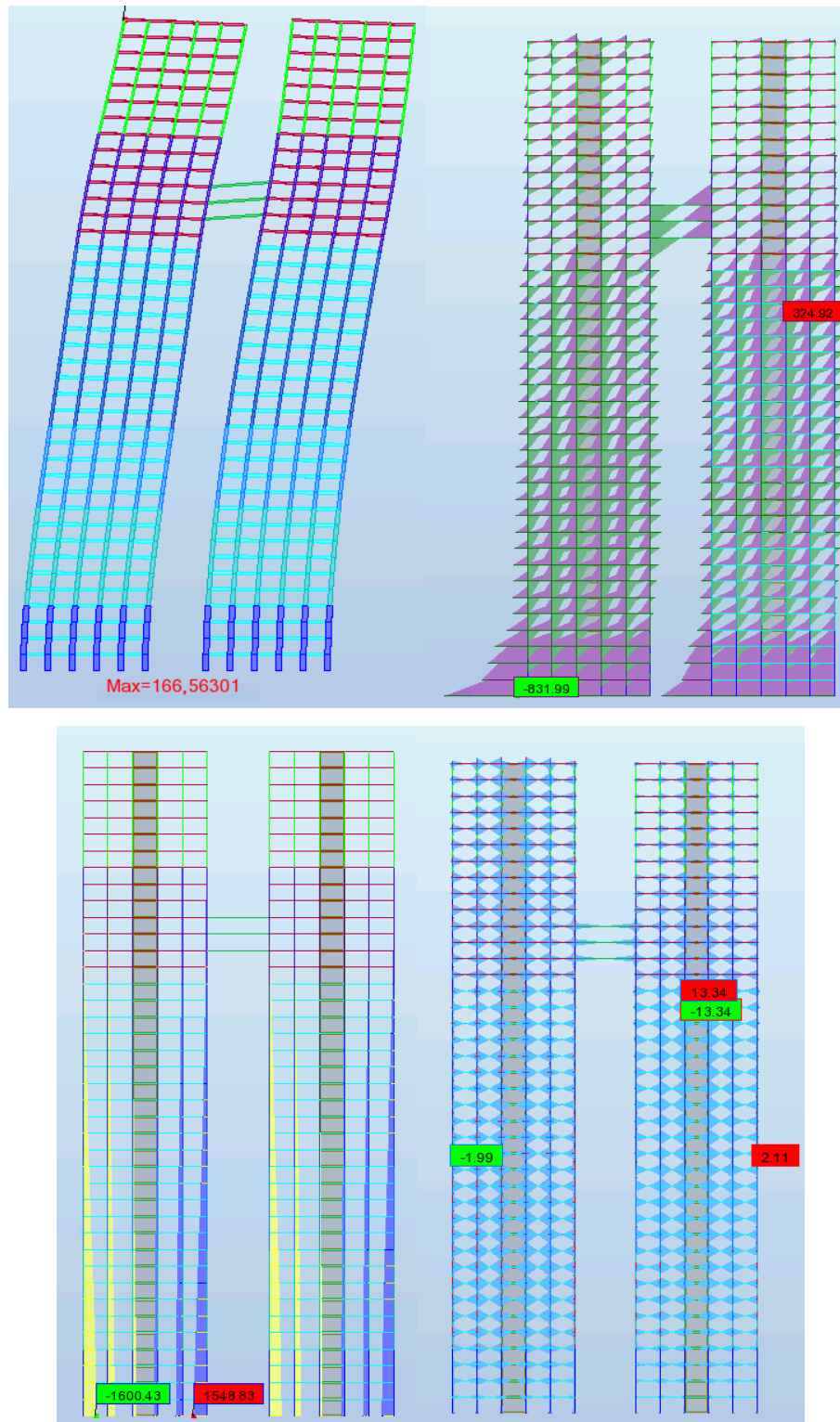


Figure 4.20 Deformed shape, bending moment, axial force and stress diagram for the frame of the simple link at $h'=120\text{m}$ model, respectively. Units in mm, kNm, kN and MPa.

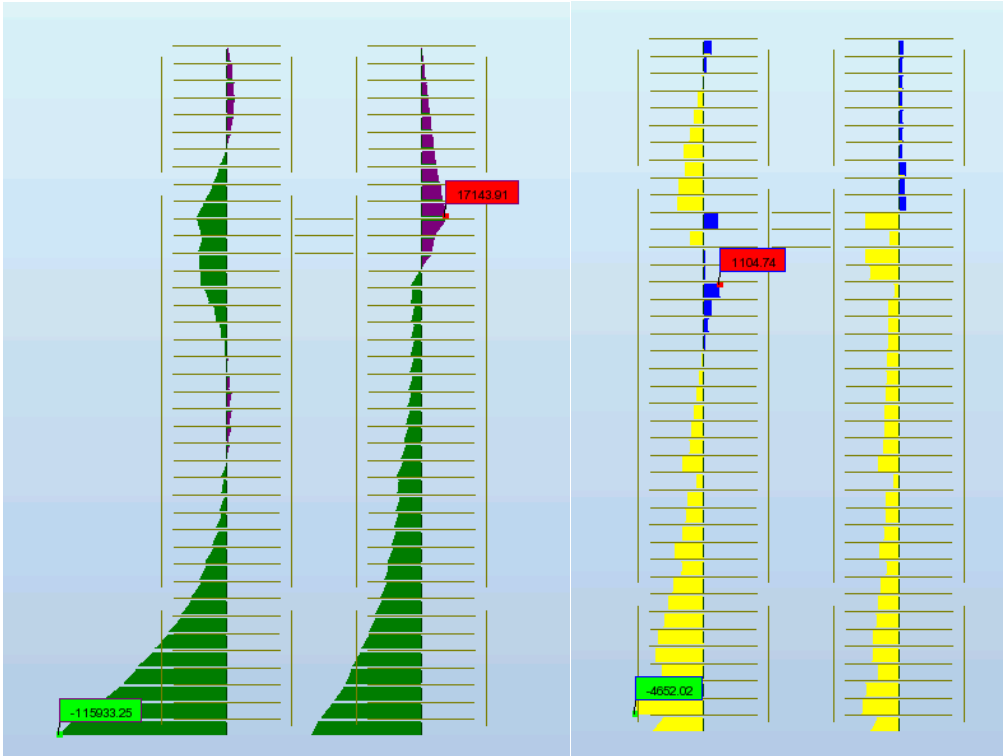


Figure 4.21 Bending moment and shear force diagram for the core of the simple link at $h'=120\text{m}$ model, respectively. Units in kNm and kN.

4.5.3 Truss link

The structural diagrams for the truss link at $h'=120\text{m}$ model are shown in figures Figure 4.22 and Figure 4.23. From these figures, we observe that:

- The max displacement is 136mm for tower 1 and 112mm for tower 2. This means that the top of tower 1 displaces approximately as much as when the truss link is located at $h'=160\text{m}$, which is unexpected. It means that the stiff truss link manages to straighten up the top of tower 1 much more than the simple link. The link also stays level.
- The truss attracts additional axial forces in the columns on the in-between faces not only under the link, but also above. See Figure 4.24. The forces in the diagonals of the truss is around 720 kN.
- The increase in diagonal axial force is also seen in the stresses, reaching 71 MPa.

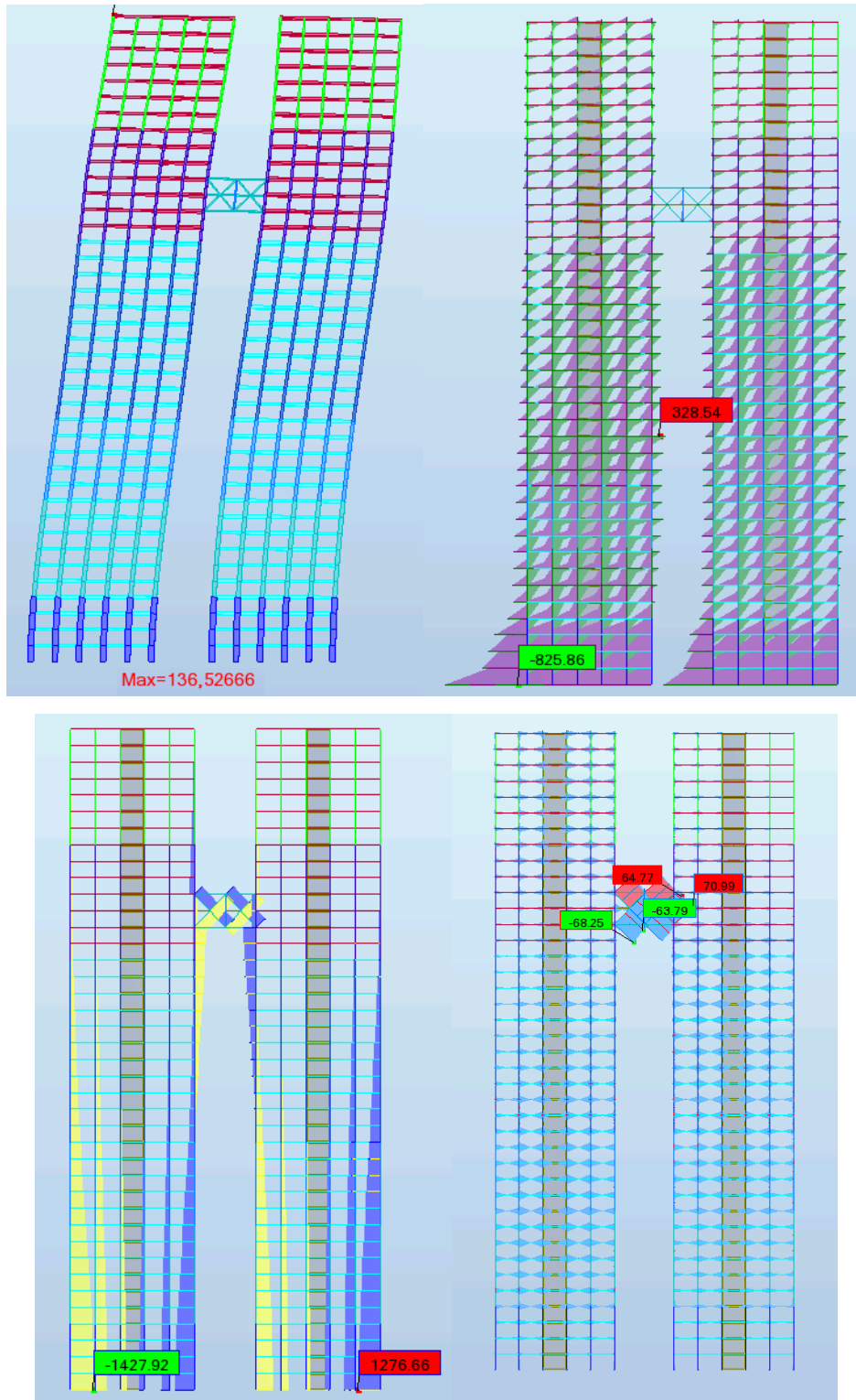


Figure 4.22 Deformed shape, bending moment, axial force and stress diagram for the frame of the truss link at $h' = 120\text{m}$ model, respectively. Units in mm, kNm, kN and MPa.

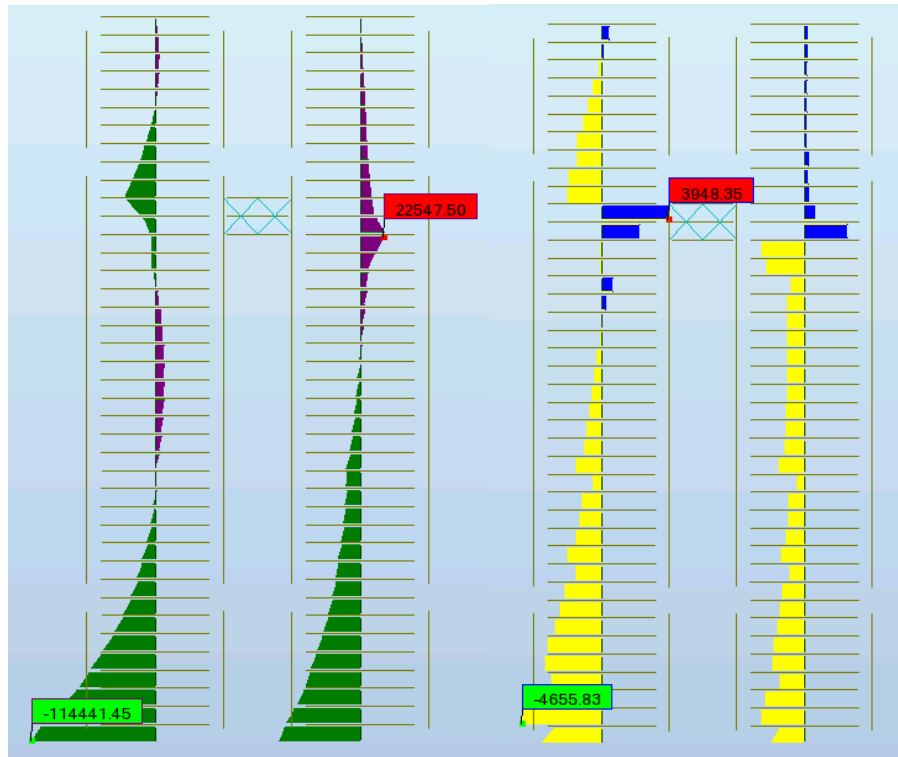


Figure 4.23 Bending moment and shear force diagram for the core of the truss link at $h'=120\text{m}$ model, respectively. Units in kNm and kN.

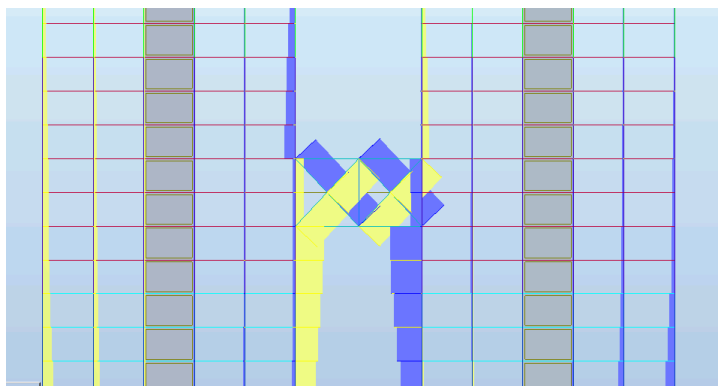


Figure 4.24 Axial force distribution in the frame around the truss link. Note the compression (blue) in the columns above the link on the left side, and the tension (yellow) in the columns above the link on the right side.

- The bending moment diagram for the cores is quite different from the simple link around the link location, with sharper peaks. Max moment here is 28051 kNm for tower 1, and 22547 kNm for tower 2. Moments at the base are same magnitude as for the simple link.
- Shear forces are correspondingly more concentrated than for the simple link, with max shear near the link at 3948 kN, compared to 1105 kN for the simple link.

4.5.4 V-leg link

The structural diagrams for the truss link at $h'=120\text{m}$ model are shown in figures Figure 4.25 and Figure 4.26. From these figures, we observe that:

- The max displacement of tower 1 is 130mm, for tower 2 it is 106mm. The V-leg link thus straightens up the building even more than the truss, as expected. Though the effect is not very large. The link remains more or less level.
- The largest axial force in the structure is now in the diagonal columns, which carry 1668 kN. The columns at the base carry about 1300 kN.
- Max stresses at 13 MPa.
- Bending moment in the cores near the link is more spread out compared to the truss link, but the peaks in tower 1 are just as large, with a max moment of 28175 kNm. Max moment in tower 2 near the link is 14618 kNm. See also Figure 4.27.

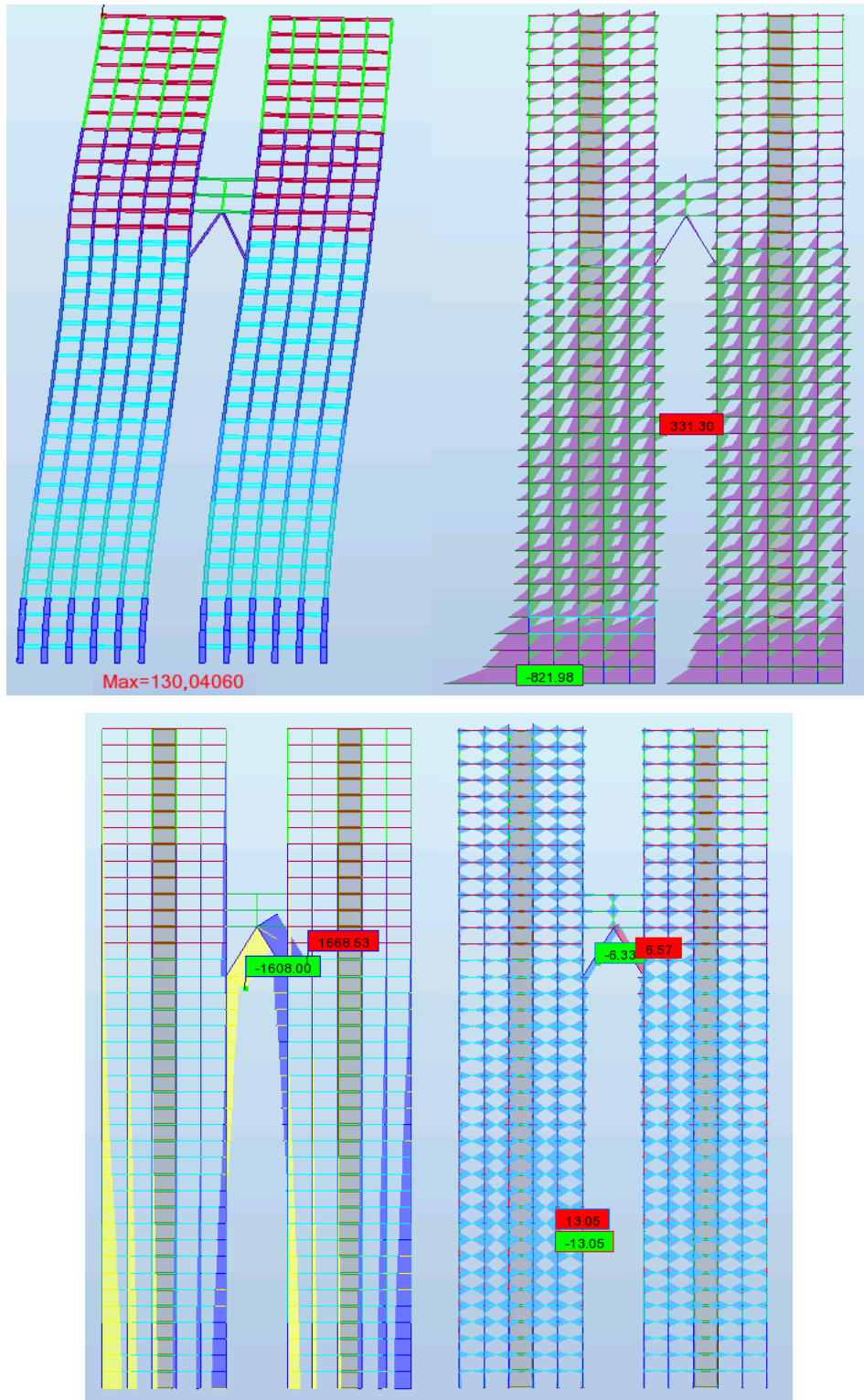


Figure 4.25 Deformed shape, bending moment, axial force and stress diagram for the frame of the V-leg link at $h' = 160\text{m}$ model, respectively. Units in mm, kNm, kN and MPa.

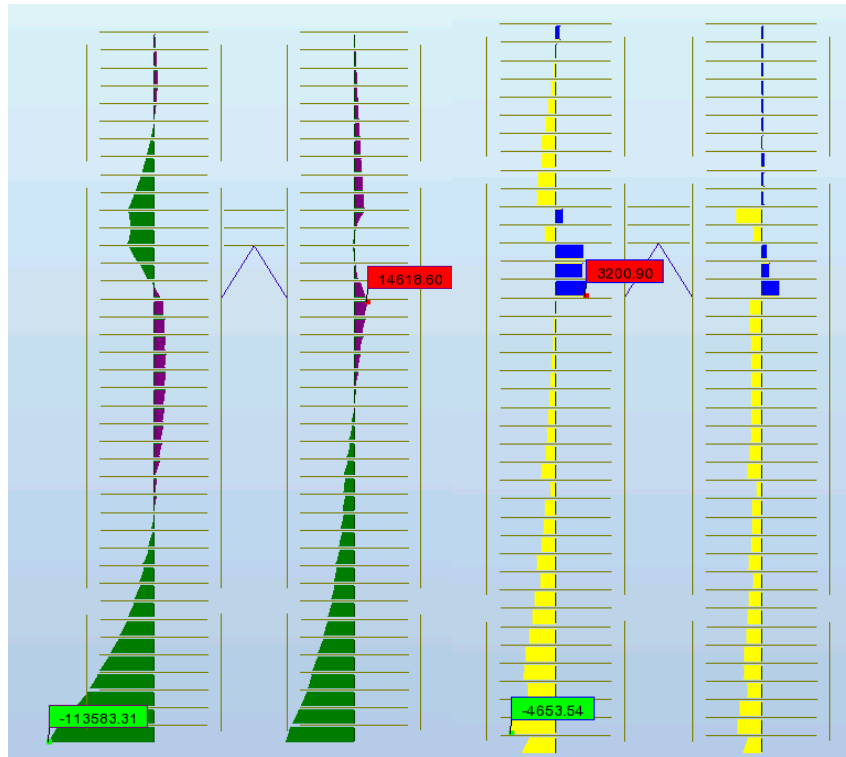


Figure 4.26 Bending moment and shear force diagram for the core of the V-leg link at $h'=160\text{m}$ model, respectively. Units in kNm and kN .

4.5.5 Summary

Figure 4.27 shows the displacements and the bending moment diagrams for the cores of the two towers compared directly. When the link is no longer at the top, the lack of stiffness from the simple link causes both towers to sway a lot more above the link location. The shape of the truss and V-leg models are very similar, with the V-leg model giving slightly sharper curvature for tower 1 near the link.

The V-leg link's effect on the core bending moment is seen at two points, at the top of the link and at the diagonal column base. Because of this it causes two peaks in the moment diagrams. The truss link causes sharper changes in moment magnitude because the peak is concentrated about only one height.

Figure 4.28 shows the moment diagrams for the frames of the three models. The frame seems largely unaffected by link type, unlike the central core.

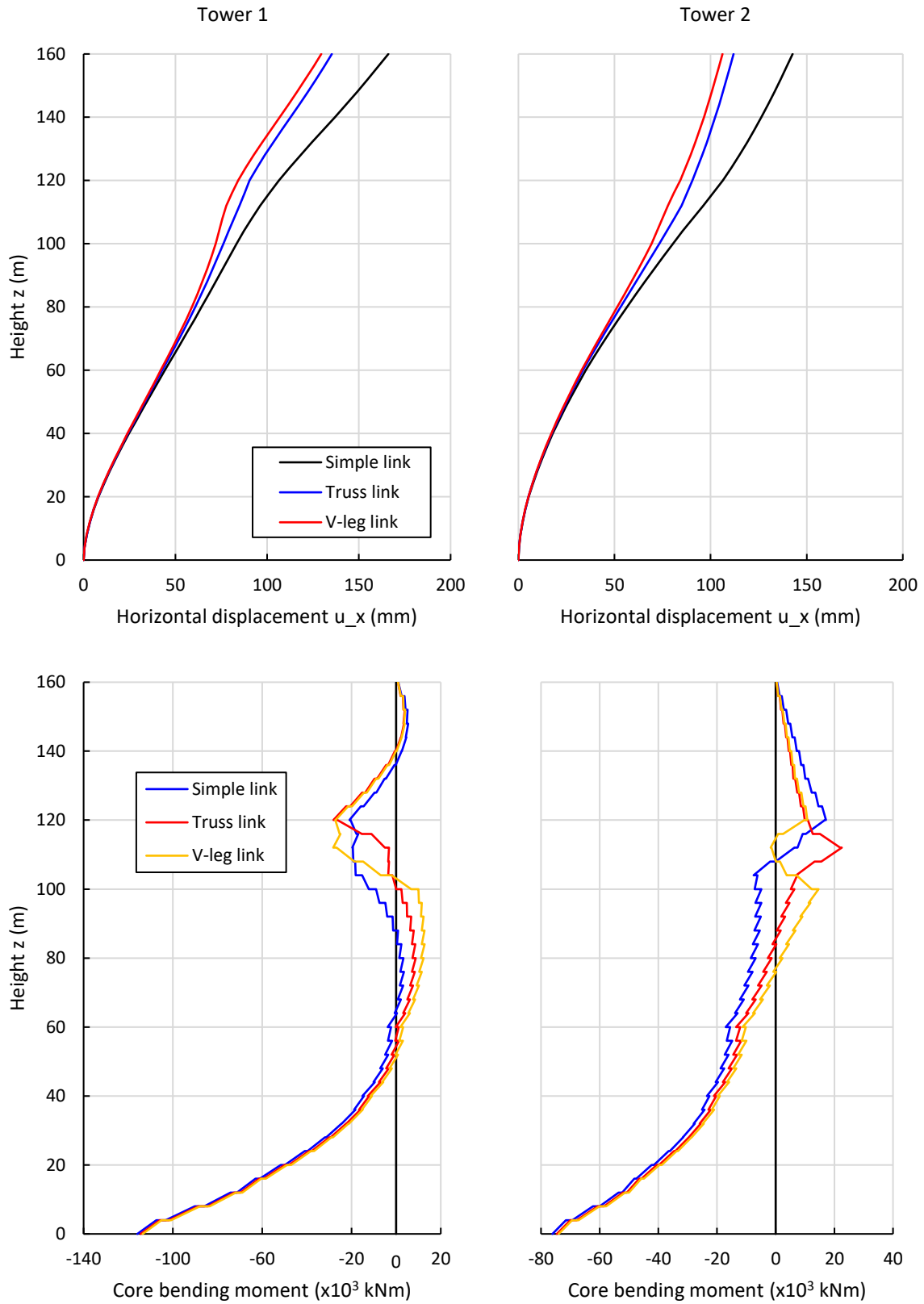


Figure 4.27 Displacements and bending moments in the cores for towers 1 and 2 for the links at $h'=120m$.

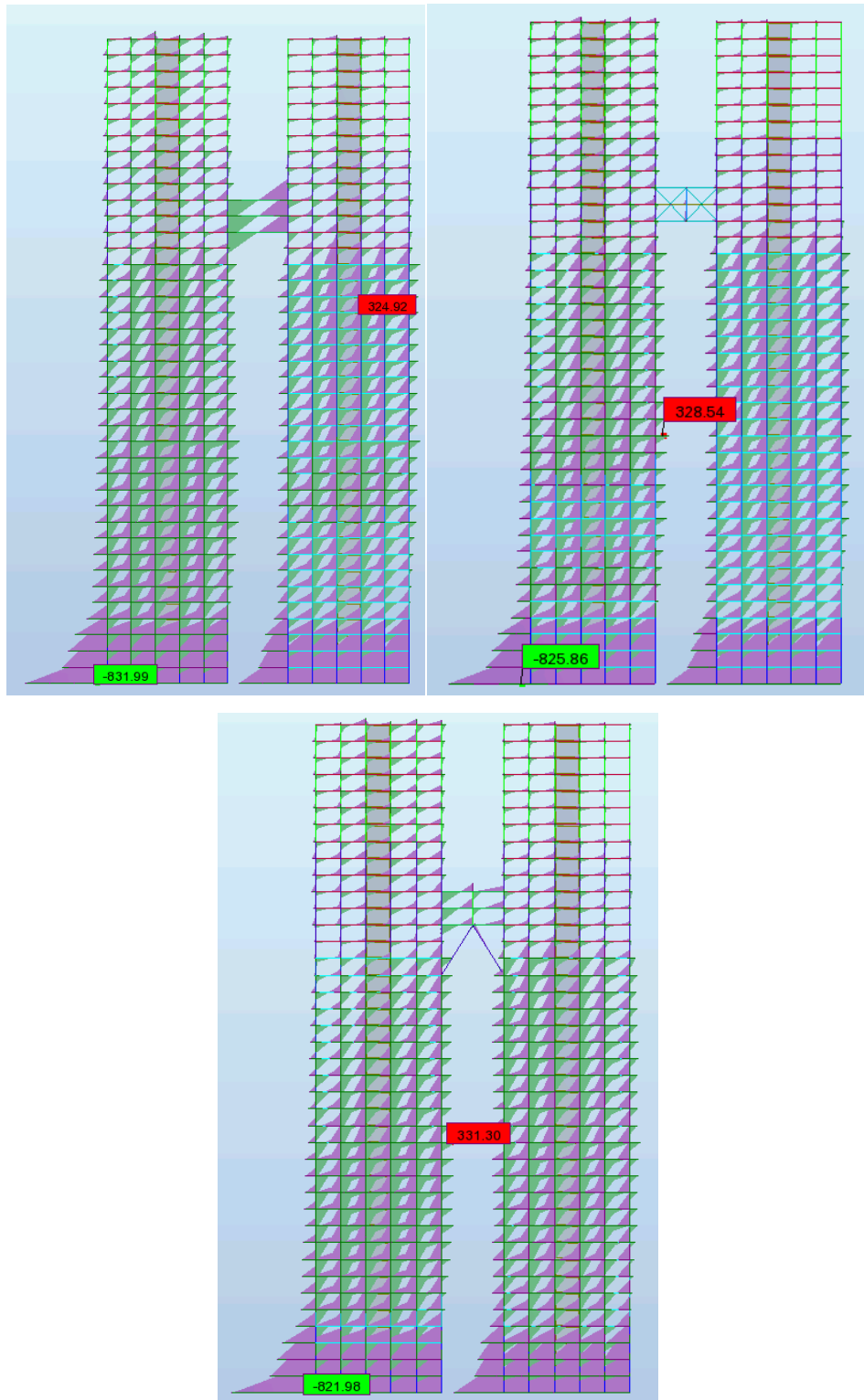


Figure 4.28 Bending moment diagrams for the rigid frames of the three different link types at $h=120\text{m}$. Note that the scale for each figure is not the same. In general, the distribution is similar for all the three models.

4.6 Links at $h'=80\text{m}$

The next models to consider are those with the structural link located with $h'=80\text{m}$. The three models are shown in Figure 4.29.

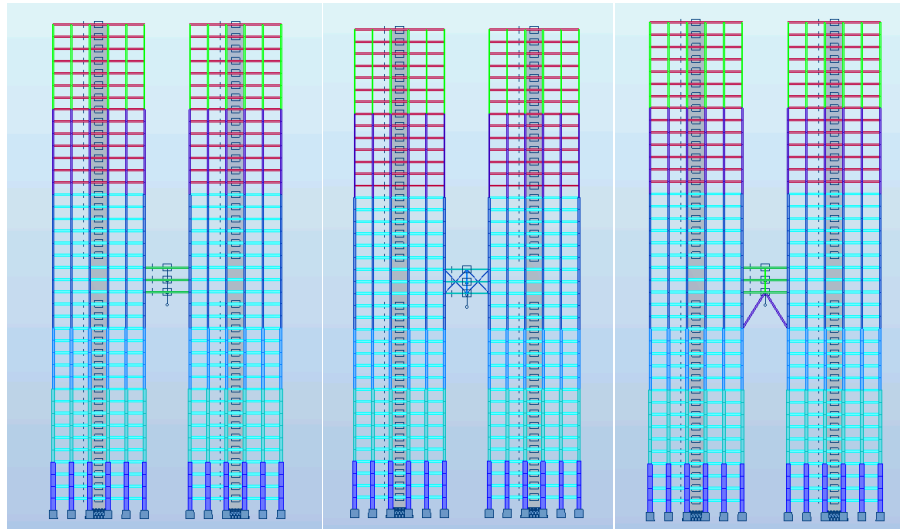


Figure 4.29 Structural models with links at $h'=80\text{m}$, showing the simple, truss, and V-leg links, respectively.

4.6.1 Dynamic characteristics and loading

The natural frequencies and “real” loads for the models are shown in Table 4.5. They show the same tendencies as for links at $h'=160\text{m}$ and 120m .

Table 4.5 Natural frequencies and loads for the three models with links at $h'=80\text{m}$. The discrepancies from the base model are small, with only a maximum 3,35% load reduction.

h'=80m Link type	Natural frequency $n_{1,x}$ (Hz)	Load $F_{w,D}$ (kN/m ²)	Load diff. from base model (%)	Peak acceleration a_{max} (m/s ²)
Simple	0,24	1,629	-0,04	0,01176
Truss	0,25	1,610	-1,20	0,01145
V-leg	0,27	1,575	-3,35	0,01090

4.6.2 Simple link

The structural diagrams for the simple link at $h'=120\text{m}$ model are shown in figures Figure 4.30 and Figure 4.31. From these figures, we observe that:

- The max displacement of tower 1 is 216mm. For tower 2 it is only 97mm. With the link so low, the second tower cannot help the first to resist its larger wind load, thus it deforms much less.
- The bending moments in tower one in the region above the link shows increased values than those in the frame below or above. This must be explained by the top of tower 1 cantilevering out from the link location, where the towers remain relatively level. Tower 2 has very little moment in the frame over the link due to the small load on it. Base moments for the frame of the two towers is very similar, with max moment of 732 kNm in tower 1 and 587 in tower 2. The moment in the link beams is around 210 kNm.
- Largest axial force is 1805 kN and max stresses around 19 MPa, both in tower 1.
- Bending moment in the cores give max 102219 kNm at the base of tower 1, and 89736 kNm at base of tower 2. The moment at height for tower 1 shows two peaks, one at the link and the other at $z=104\text{m}$, where the frame softens. Tower 2 only has a peak near the link. Max moments near the links is 41574 kNm for tower 1 and 32680 kNm for tower 2.
- A very large shear force is transferred to the two cores by the link, with 4193 kN for tower 1 and 5270 kN for tower 2. This shear force is so large because all the load going to tower 1 above the link wants to transfer over to tower 2.

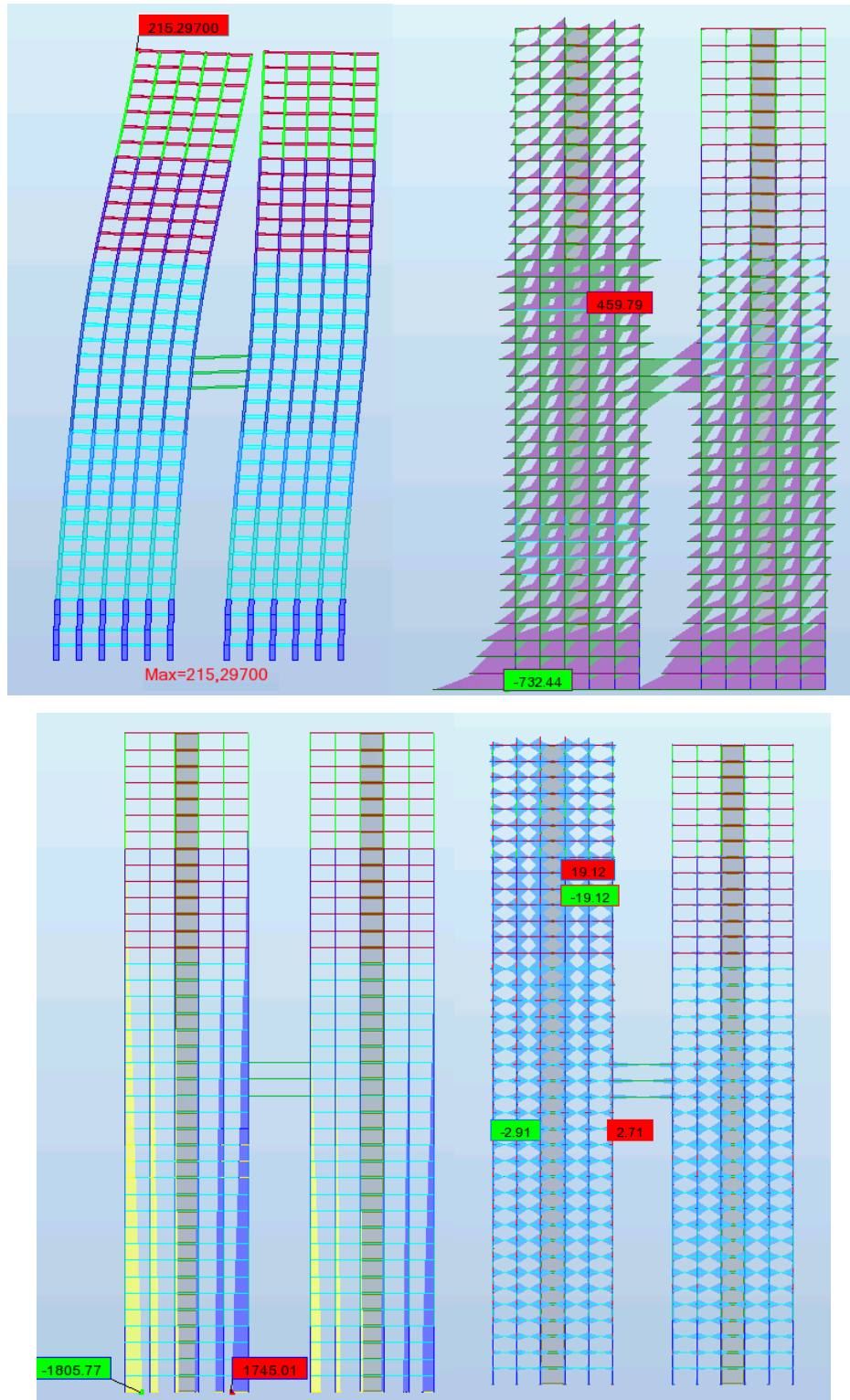


Figure 4.30 Deformed shape, bending moment, axial force and stress diagram for the frame of the simple link at $h' = 80\text{m}$ model, respectively. Units in mm, kNm, kN and MPa.

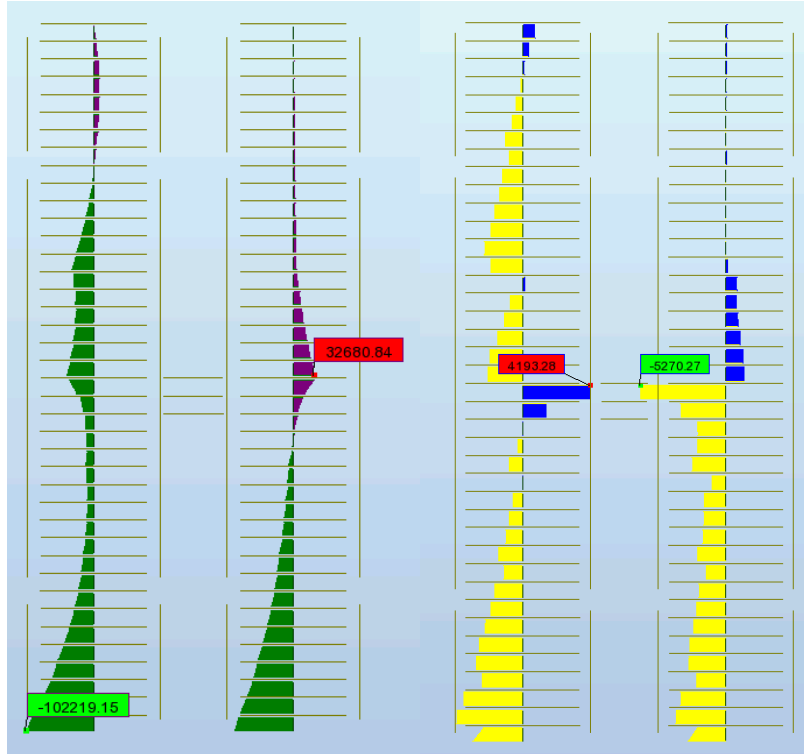


Figure 4.31 Bending moment and shear force diagram for the core of the simple link at $h'=80\text{m}$ model, respectively. Units in kNm and kN.

4.6.3 Truss link

The structural diagrams for the truss link at $h'=80\text{m}$ model are shown in Figure 4.32 and Figure 4.33. From these figures, we observe that:

- The max displacement is 194mm in tower 1 and 77mm in tower 2.
- The bending moment, axial force and stress distribution in the frame is similar to that of the simple link, the main difference being the truss' axial forces affecting the load in the columns like we also saw for the truss link at $h'=120\text{m}$.
- The peak bending moment of the core near the link is again very large, at 51786 kNm for tower 1. For tower 2 it is interestingly spread over two peaks, with the max at 23237 kNm.
- The shear force into the core tower 1 is very large, 7582 kN, much larger than the shear force in tower 2, 1873 kN. This is unlike the simple link, which had similar value shear for both cores near the link.

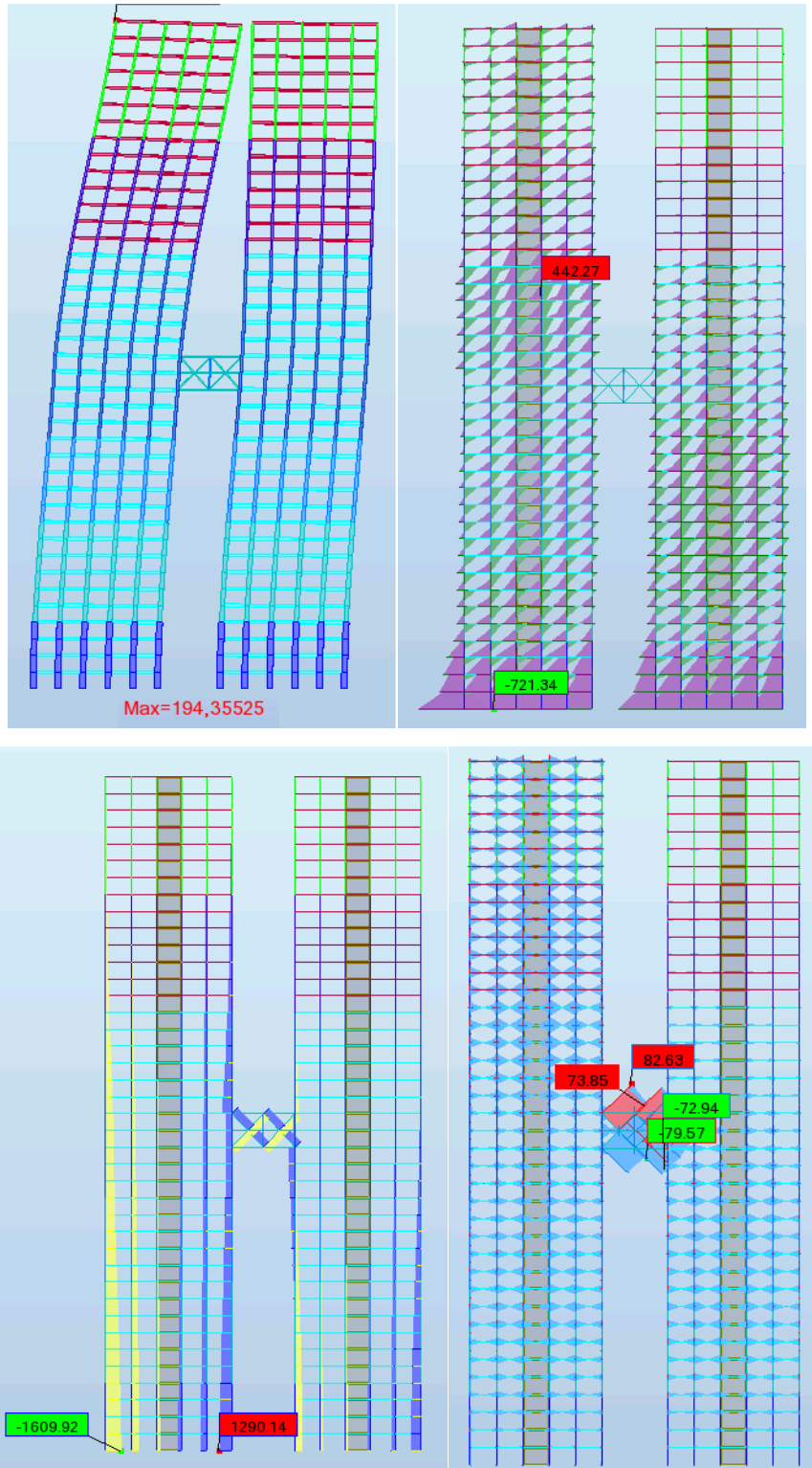


Figure 4.32 Deformed shape, bending moment, axial force and stress diagram for the frame of the truss link at $h' = 80\text{m}$ model, respectively. Units in mm, kNm, kN and MPa.

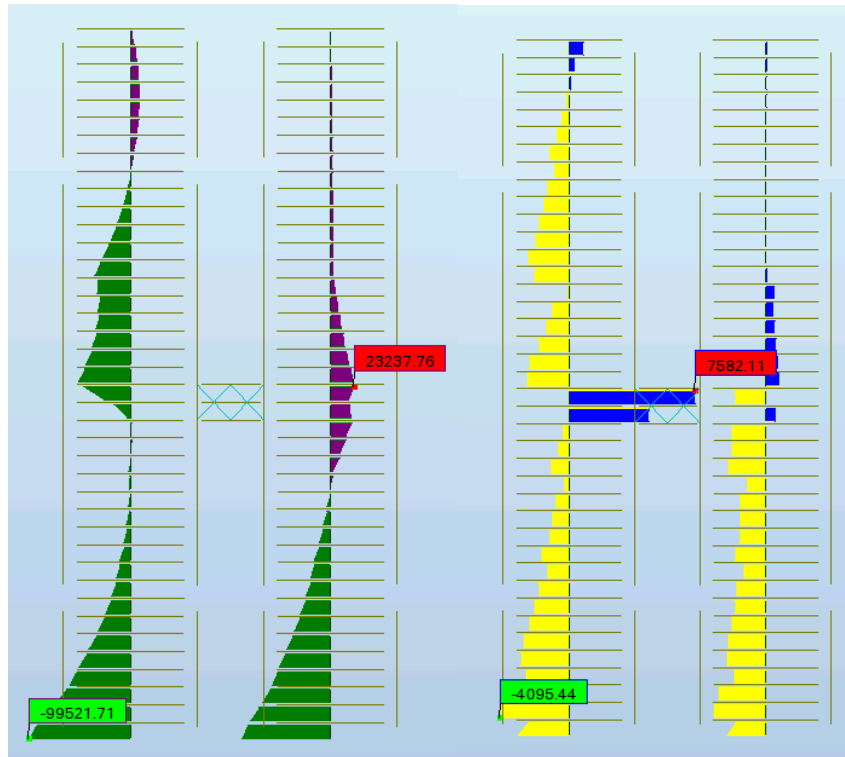


Figure 4.33 Bending moment and shear force diagram for the core of the truss link at $h'=80\text{m}$ model, respectively. Units in kNm and kN .

4.6.4 V-leg link

The structural diagrams for the truss link at $h'=120\text{m}$ model are shown in Figure 4.34 and Figure 4.35. From these figures, we observe that:

- The maximum displacement is 190mm in tower 1 and 73 mm in tower 2, 4mm less than the values for the truss link.
- Bending moment in the frame as before, with the change that the moment in the frame of tower 1 between the diagonal column base and the link having reduced moments compared to the surrounding areas.
- Max axial force is 2063 kN in the right leg of the V, max stress in frame is 19 MPa. Max axial force
- The shear forces in the core are much smaller near the link, with a max of 5685 kN. The shear force is distributed over more storeys.

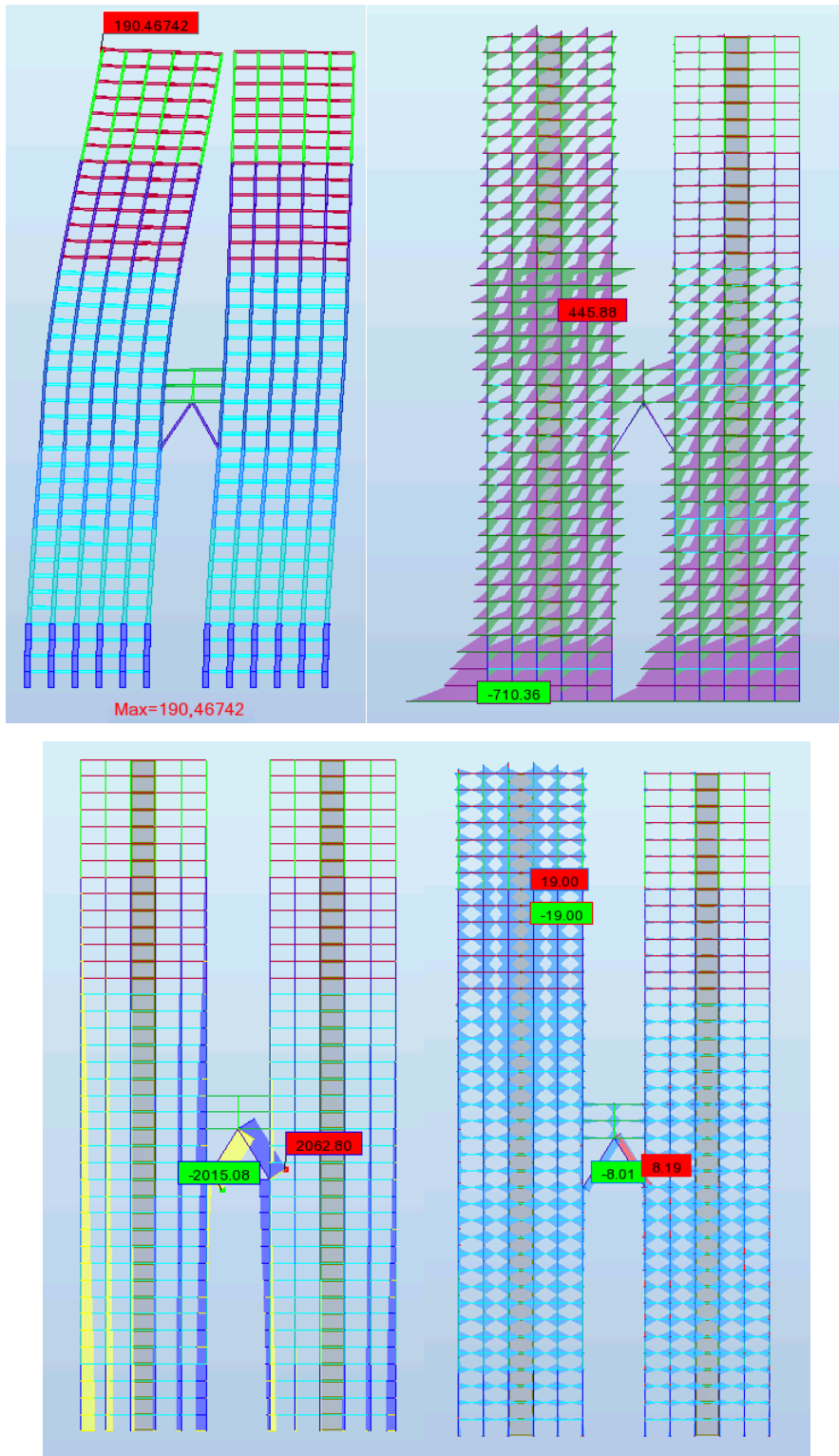


Figure 4.34 Deformed shape, bending moment, axial force and stress diagram for the frame of the V-leg link at $h'=80m$ model, respectively. Units in mm, kNm, kN and MPa.

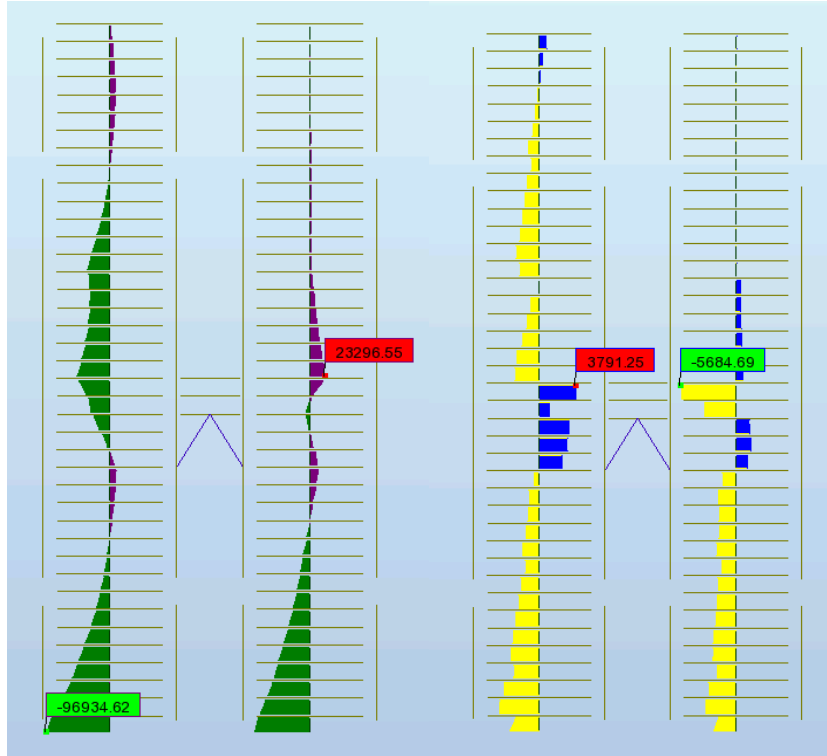


Figure 4.35 Bending moment and shear force diagram for the core of the V-leg link at $h'=80\text{m}$ model, respectively. Units in kNm and kN .

4.6.5 Summary

Figure 4.36 shows the displacements and bending moment in the cores for both towers. The displacements for the truss and V-leg links are almost identical throughout the height, with similar slopes above the link. The simple link models have a slightly lower gradient, increasing its displacement relative the other models as the building rises.

The moment in the core at the link is largest in tower 1 for the V-leg and truss links, but largest in tower 2 for the simple link. Above $z = 104\text{m}$ the bending moments in the cores for all three link types are the same.

Figure 4.37 shows the three models' frame bending moment diagrams. Note the decrease in frame moment in tower 1 between the top of the link and the base of the diagonal column.

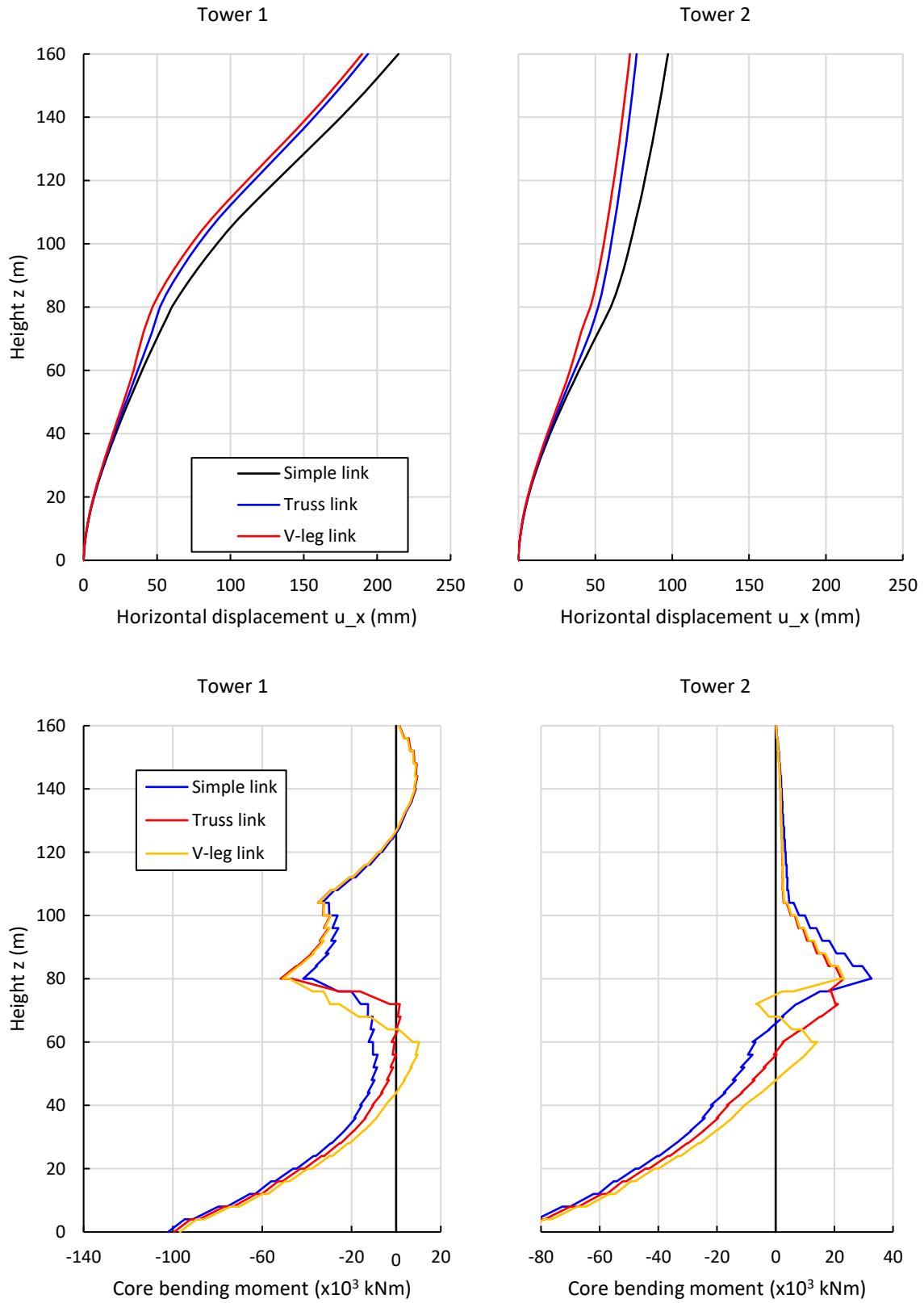


Figure 4.36 Displacements and bending moments in the cores for towers 1 and 2 for the links at $h'=80m$.

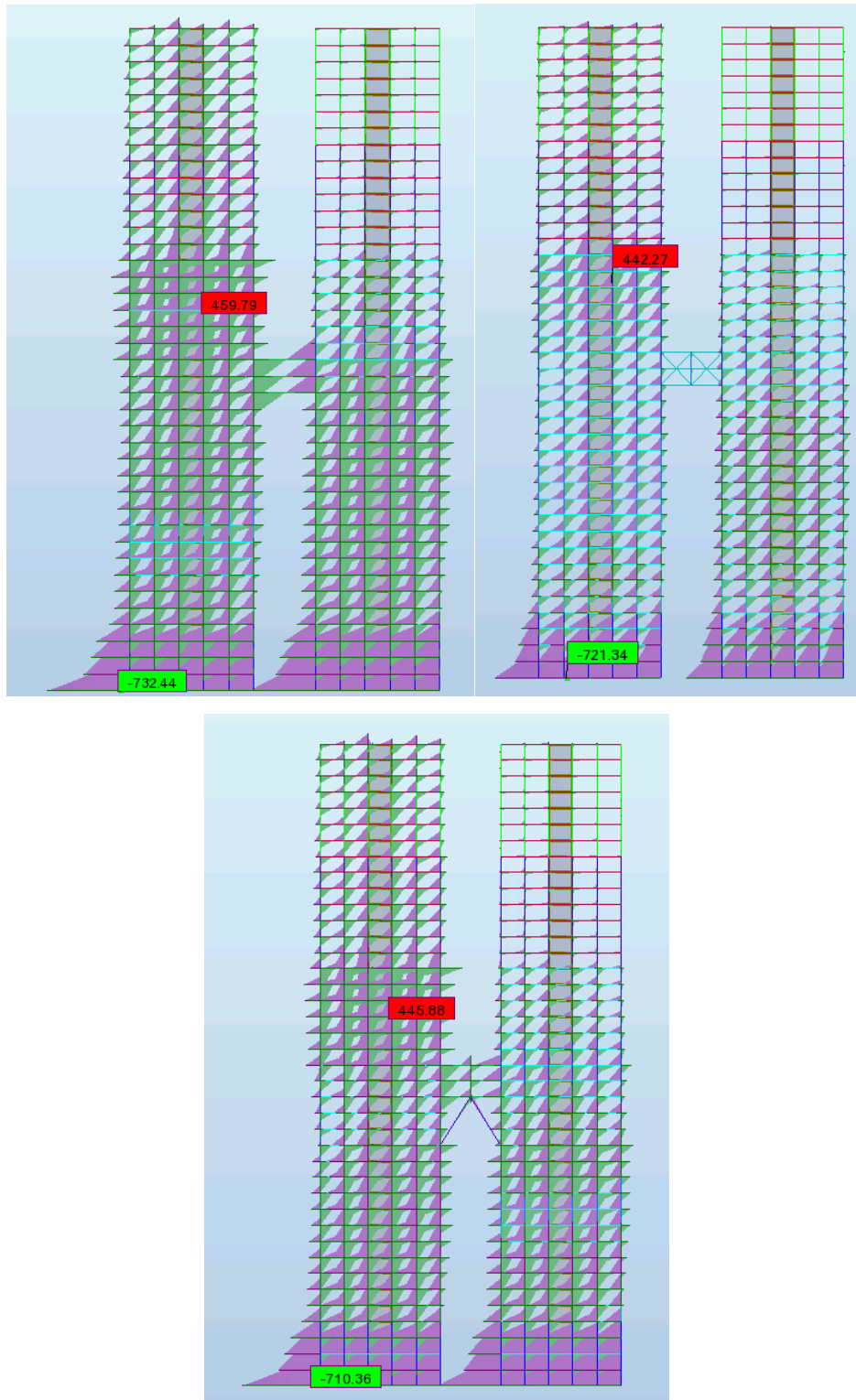


Figure 4.37 Bending moment diagrams for the rigid frames of the three different link types at $h=80\text{m}$. The scale for each figure is not the same. In general, the distribution is similar for all the three models. Note the increase in frame bending moment in tower 1, in the beams and columns above the link

4.7 Initial observations and conclusions

Having reviewed the results for the three different link types applied to the twin towers at heights $h' = 160\text{m}$, 120m and 80m , we can now observe the following trends:

Dynamic characteristics

- The natural frequencies are independent of link location, but vary with link stiffness. Stiffer links increase the natural frequency, e.g. for the simple link all models have a frequency of $0,24\text{Hz}$, while the V-leg link models all have $n_{1,x} = 0,27\text{ Hz}$, a $12,5\%$ increase.
- Link type or location does not meaningfully affect the acceleration of the buildings, which in general is very small. The limit for maximum accelerations given by ISO 10137 (ISO, 2007) gives a limit over $0,07\text{ m/s}^2$ for structures with natural frequencies less than $0,3\text{ Hz}$, this is almost 7 times as much as the accelerations induced by the wind. See Figure 4.38.

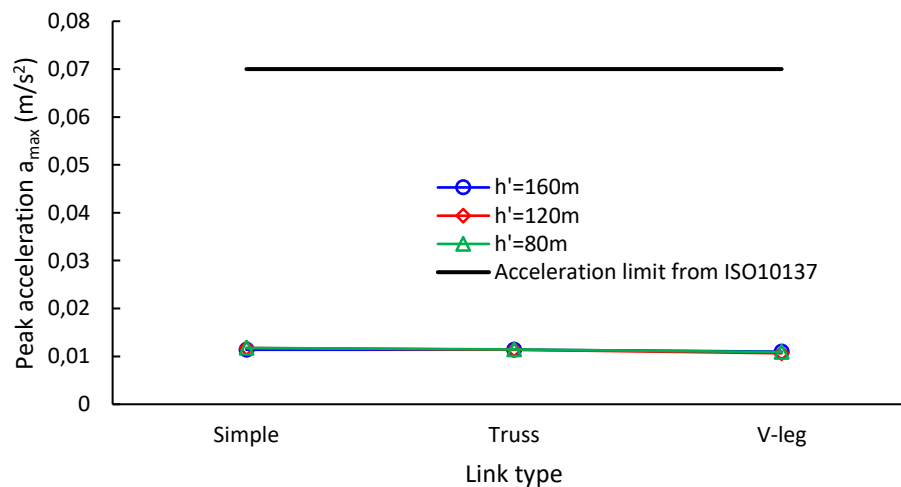


Figure 4.38 Max accelerations for models with structural links at $h' = 160$, 120 or 80m , compared to the maximum limit given by ISO 10137. The effect of the links is negligible, and the accelerations are well within acceptable values.

Stresses in the rigid frame

- Moment distribution in the frame is largely unaffected by link type.
- Link location does affect the moments, but this is due to the link's height determining if tower 2 helps carry tower 1's much larger load or not. This is expected from basic mechanics. What is interesting is how the link at $h'=80\text{m}$ causes the frames above the link to increase in moment as if the top of tower 1 is cantilevering out from it, which it practically is. This effect is not seen for link height $h'=120\text{m}$ in any significant capacity, probably due to the frame being much weaker at that height, because of the reduction in beam size.
- Max base column moment for tower 1 is around 950 kNm for $h'=160\text{m}$, 825 kNm for $h'=120\text{m}$, and 720 kNm for $h'=80\text{m}$. For tower 2 the corresponding column moments are ca 360 kNm, 480 kNm, and 570 kNm, respectively. This means that the moments at the base are more evenly distributed to each tower as the link moves closer to the ground.
- Stresses are largest where the moments in the frame are relatively large compared to the frame section sizes, which is as expected. The stresses in the base columns are very small even though the moments are by far the biggest there, because of the very large column sizes.
- The difference in axial load in a column of one side of a tower compared to a column on the other side of a tower is minimal for the simple links, but reach several hundred kilonewton for the truss and V-leg links. Take for example the link with $h'=160\text{m}$: the simple link has max axial load 1773 vs 1743 kN (30 kN difference) for the left and right side of tower 1, respectively, while for the V-leg link this is 1632 vs 1384 kN (248 kN difference). The same can be seen for links with $h'=120$ and 80m. This could be because the axial forces in the columns on the in-between faces have to change value in order to meet the axial forces generated in the truss and V-legs.

Stresses in the central core

- Core moments are very much dependent on link type around the link's location. The difference in moment can be over 10000 kNm, e.g. 24490 kNm for the simple link vs 35493 kNm with link $h'=160\text{m}$, a significant amount if the link is high up and the core walls are correspondingly thin. Which link type that gives the largest moments peaks depends on which tower is considered, and is generally not consistent. The largest moments usually come from the truss or V-leg links, but sometimes the simple link yield larger or just as large values.
- Base moments do not change significantly due to link type. However, the link's location has a significant effect, just like for the frame base moments. The moment for each tower grows more similar in magnitude as the link moves closer to the ground, with moments of 135 000 vs 55 000 kNm for $h'=160\text{m}$, 115 000 vs 75 000 kNm for $h'=120\text{m}$, and 100 000 vs 90 000 kNm for $h'=80\text{m}$, for towers 1 and 2, respectively.
- Core shear forces at link location changes drastically depending on link type, with the truss link consistently giving larger absolute values, sometimes over 2000 kN more than the shear force with the simple or V-leg links. The simple link generally gives the lowest shear force values. This suggests that with the simple link, which is relatively flexible, the shear force is distributed more to the frame compared to the columns than for the other, stiffer links.
- The direction and magnitude of the core shear forces near the link for either tower 1 or 2 change significantly from storey to storey, see Figure 4.39 and Figure 4.40.
- The link only changes the shear forces in the core in the storeys at the same height as the link, for the truss and simple links this is the two storeys that coincide with the link walkways, for the V-leg link this also includes the three storeys below. This means that outside the immediate height of the links, the shear forces from the core is transferred to the frame.

4. Structural behaviour

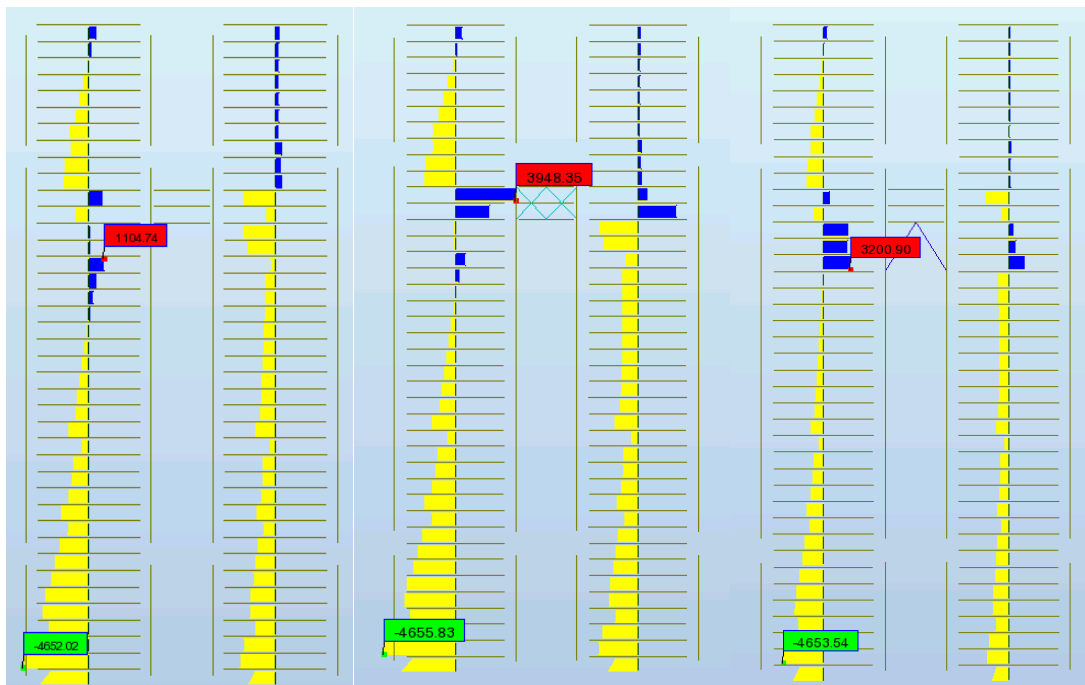
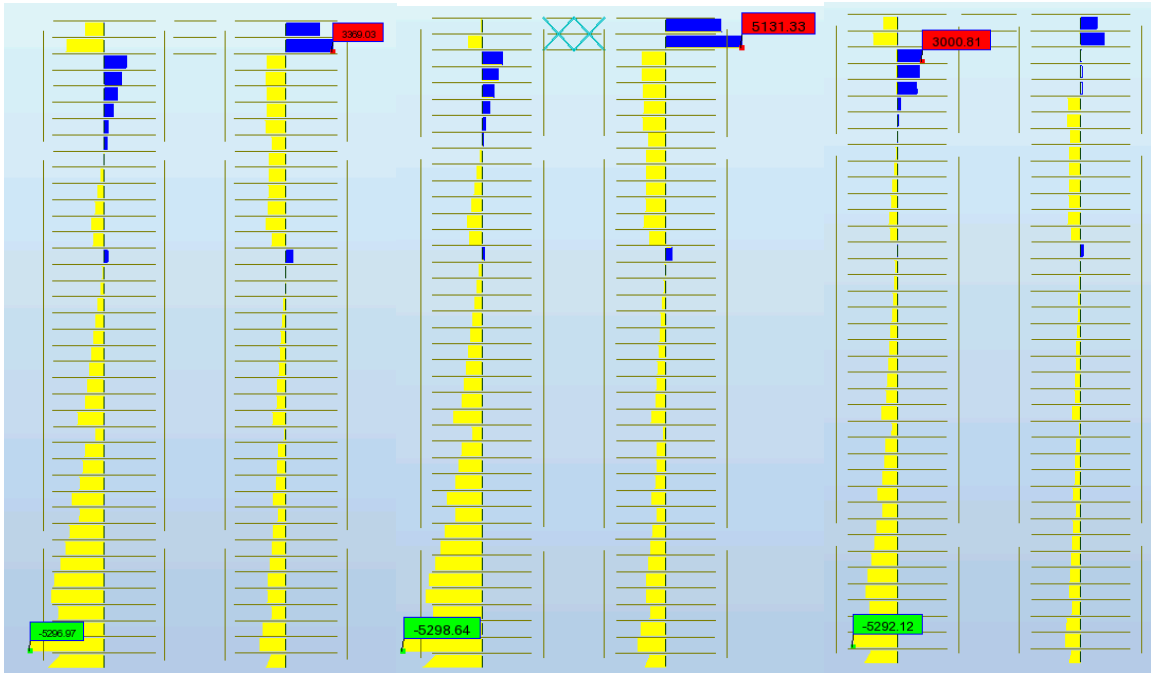


Figure 4.39 Shear force diagrams for the central cores of the towers for models with link height $h'=160\text{m}$ and 120m (for $h'=80\text{m}$, see next figure). The figures have different scales. Shear distribution near the link with $h'=160\text{m}$ is similar for all link types. For $h'=120\text{m}$ the direction of the shear forces are more confusing

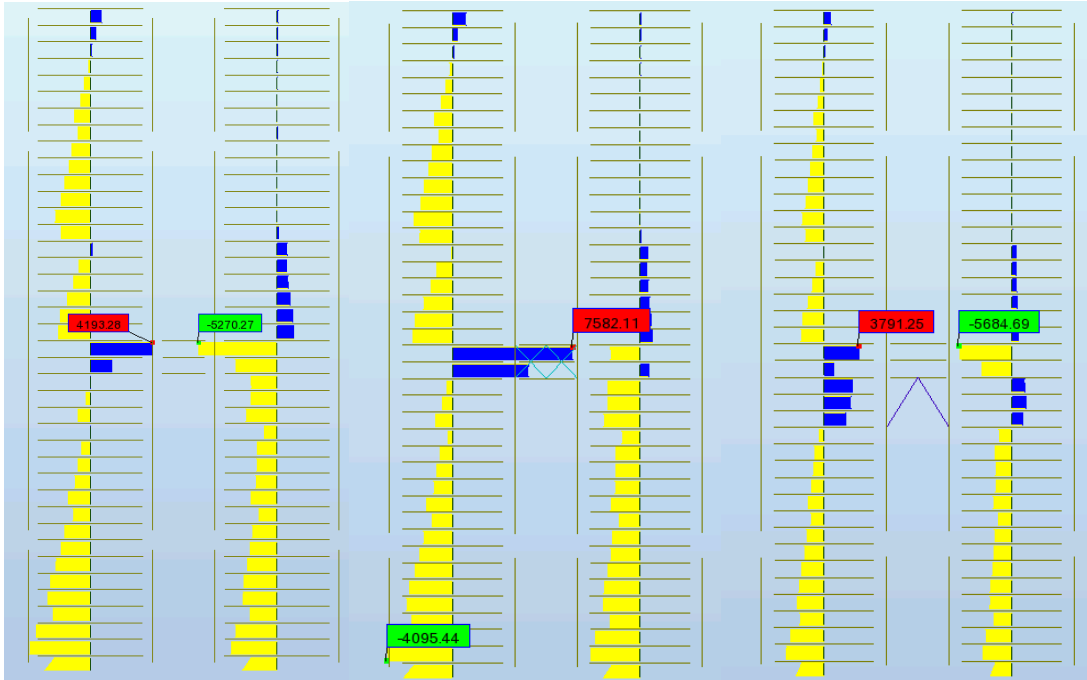


Figure 4.40 Shear force diagrams for the central cores of the towers for models with link height $h'=80\text{m}$. The figures have different scales. Tower 1 with the truss link experiences the largest shear force, of 7582 kN.

Deformations

- Deformations depend significantly on link stiffness. The V-leg link always gives the smallest displacements for both towers regardless of height, however the difference between the V-leg link and the truss link is minimal.
- The link's stiffness affects the top displacement the most for $h'=120\text{m}$, with a difference of 31mm between the truss and simple link models, for both towers 1 and 2, compared to a difference of 22mm for $h'=160$.
- The smallest top displacement is with $h'=160\text{m}$ for all link types, however for the truss link the difference between the link at 160m and 120m is minimal, only 2mm. For the V-leg link this difference is 6mm, while for the simple link this is 11mm.
- The stiffer links both create a noticeable change in curvature of both towers around their location, while the simple link does not. The towers with the simple link do change curvature because of the link, but this is because of the difference in load on

each tower, rather than the link itself straightening out the structure. This is as expected.

Based on these results, there are opportunities to use the links to alter the behaviour of the two towers to a desired effect, that will now be investigated further.

4.7.1 Opportunities

Shared reaction forces

The possibility of using both towers for resisting the lateral load that is acting on predominantly tower 1 is appealing, as the structural members at the base must deal with large axial forces from the self-weight of the building in addition to any shear and bending induced by the wind load. It was seen earlier that as the link location was lowered relative to the building's height, the moments in both the rigid frame and the central core was more evenly distributed to both towers.

To see how this relationship developed as the links moved further down than $h'=80\text{m}$ additional models were created with links ranging from $h' = 20$ to 140m . As previously stated the base moments in both columns and the central core were unaffected by link type, so only truss links were created for the additional link locations.

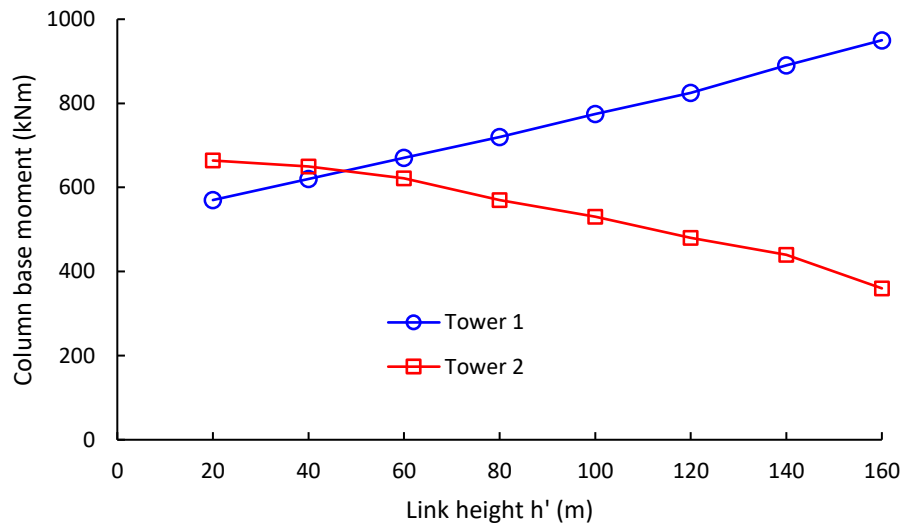


Figure 4.41 Column base moments in towers 1 and 2 for different link heights h' .

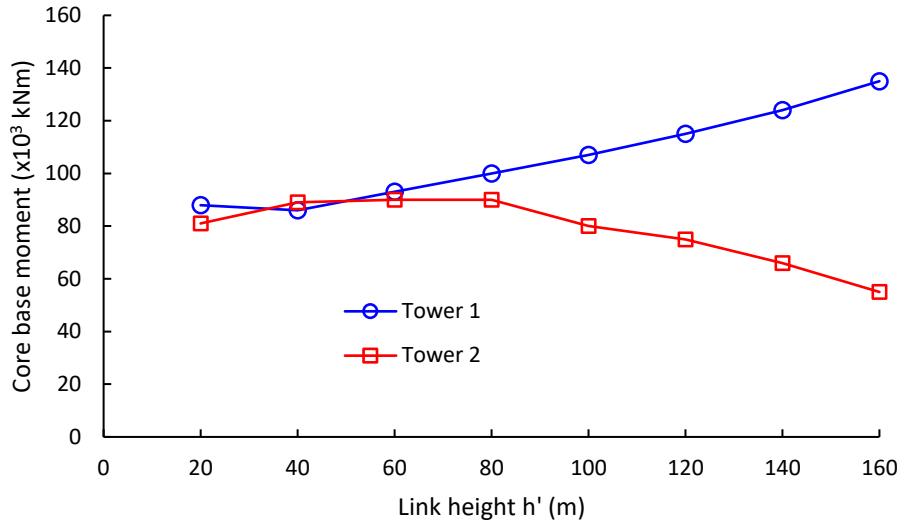


Figure 4.42 Central core base moments in towers 1 and 2 for different link heights h' .

The approximate bending moments in the bottom columns plotted against the height h' of the link is shown in Figure 4.41. The central core base moments are shown in Figure 4.42. The trend observed for the links with $h' = 160, 120$ and 80m is seen to continue as the links are lowered. The column base moment relationship with link height remains approximately linear even as the link reaches a h' of 20m , with the tower 2 columns actually carrying larger bending moments than those in tower 1 as h' goes below ca 50m .

The core base moments also decline with h' , but level out below $h' = 60\text{m}$, where the core moment in each tower is approximately equal. The values for $h' = 20\text{m}$ are not very useful, as the max moment in the core of tower 1 no longer occurs at the tower base but rather right above the link, due to it being so low. For $h' = 40$ and 60m the max moment is at the base for both towers. See Figure 4.43.

With this knowledge, it is possible for to use the link to create a bending moment distribution for the core, with the cores of both towers sharing the large moments at the bottom of the structure up to a certain height, so the cores above can be smaller because of less moment.

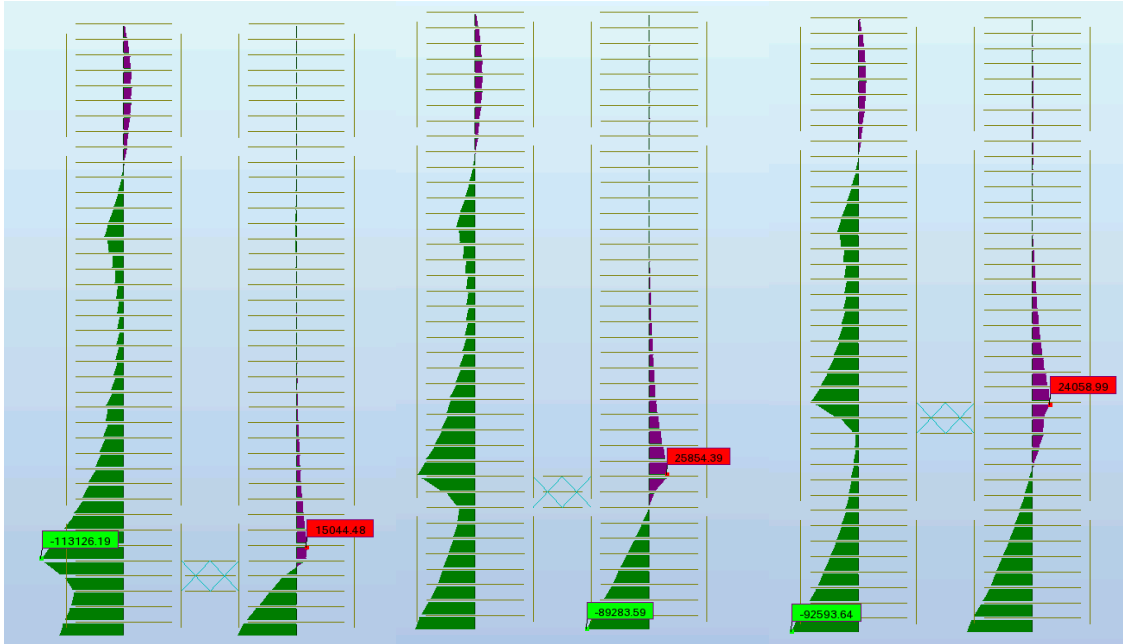


Figure 4.43 Core bending moment diagrams when $h'=20, 40$ and 60m , respectively. Note that the max moment is no longer at the base for $h'=20\text{m}$, but rather at the height corresponding to the top of the link.

The moment diagram for link $h'=40\text{m}$ for instance, makes this an appealing option, because the max moments at the base are approximately equal for each tower, and the max moment in tower 1 is located low, just above the link at $z=40\text{m}$. The cores could be stiff up to about 50 meters to take the moment to the lower core, then have much thinner walls above that.

Keep in mind that bottom cores can still be smaller than those with a link higher up, because the max moment at the base is around 90 000 kNm, which is a lot less than the base moment in tower 1 with the link at $h'=160\text{m}$, approximately 130 000 kNm, and about half of the base moment 180 000 kNm for the tower with no link.

Tower deformation shapes

The towers' deformation depends both on link type and location, like we saw earlier. What is interesting is if we can use the link to enforce a preferred deformation for one or both towers.

To see if we could use the links to minimize the towers' top displacement more models were created with links in the range of $h'=100\text{m}$ to 148m . As the V-leg and truss links both

deformed the towers in a very similar way, only truss and simple link models were created, to represent a stiff and a flexible link type, respectively. The results are shown in Figure 4.44.

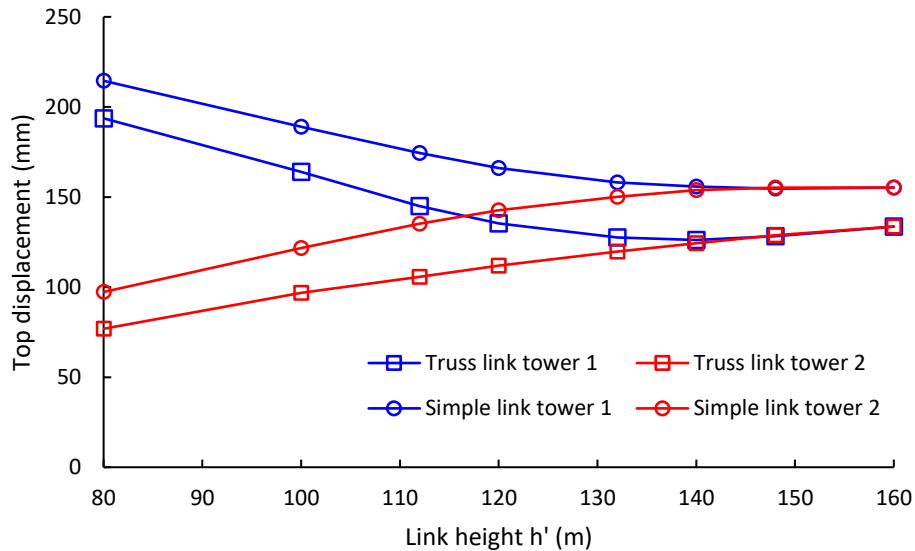


Figure 4.44 Change in top displacement for towers 1 and 2 with link height h' for the truss and simple link types. The minimum displacement for tower 1 with the simple link is 155mm with the link at the top, i.e. $h'=160m$, while for the truss link this is 126mm with the link at $h'=140m$.

From this figure, we see that for both link types the tower displacements at the top converge towards the link at $h'=160m$, as expected. For the simple link the minimum value for tower 1 corresponds to the link at the top, i.e. $h'=160m$, with a top displacement of 155mm. The top displacement also remains relatively constant for h' above 140m, then it gradually increases/decreases for either tower as the link moves downwards.

For the truss link the same is observed, however, the links with $h'=132m$, 140m and 148m give the lowest tower 1 top displacements, with $h'=140m$ giving the lowest of 126mm. As the link moves above or below these heights the trend is that the top displacement increases.

Figure 4.45 shows the deformed shapes for both towers with link heights varying from $h'=80$ to 160m, the top figures are for the simple link and the bottom are for the truss link. The crosses on each curve indicate the location of the link for that curve.

4. Structural behaviour

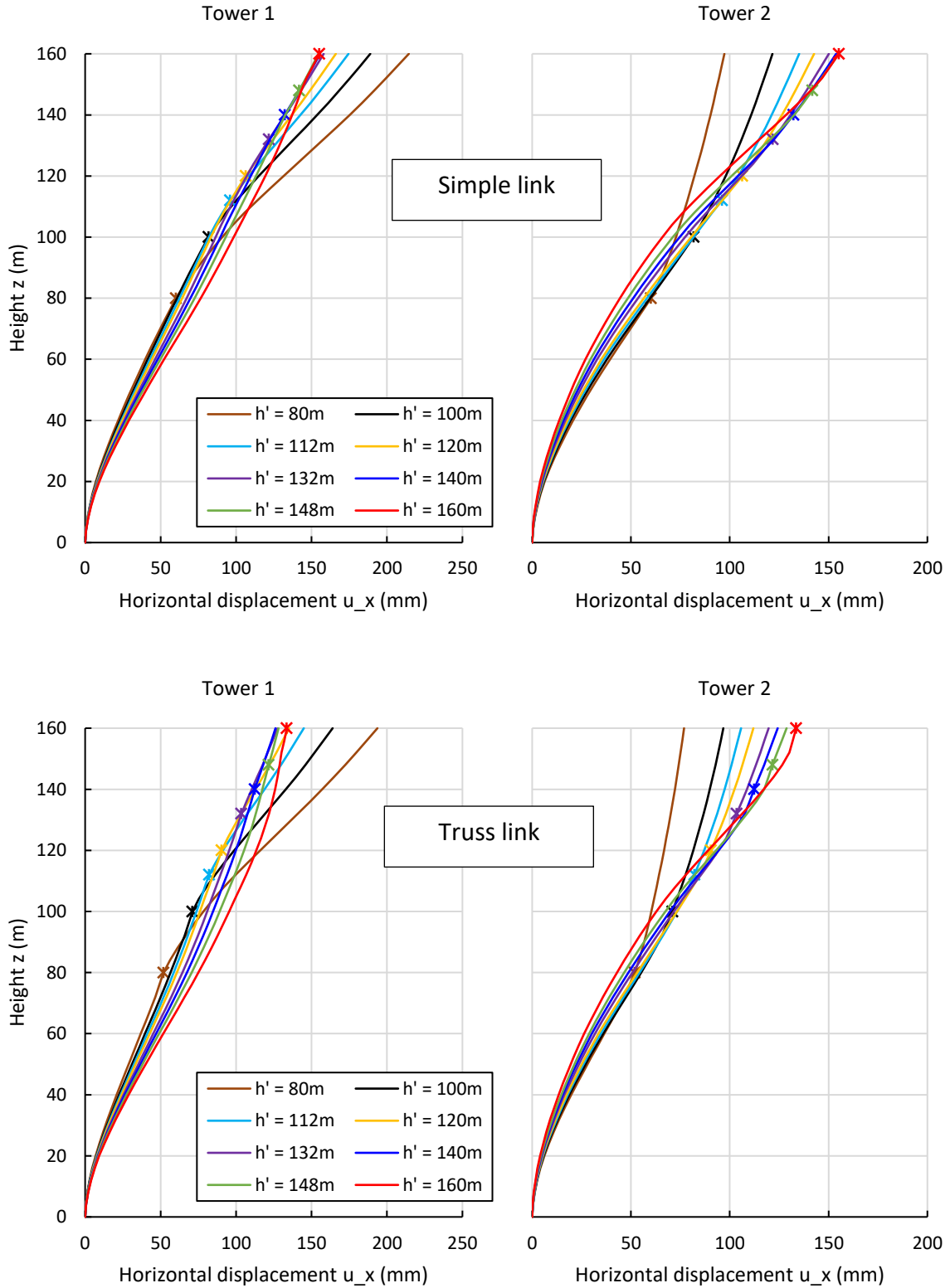


Figure 4.45 Displacement curves for towers 1 and 2 with varying link heights h' for the simple (top) and truss (bottom) links. The crosses indicate the location of the link for each curve.

Inter-storey drift, i.e. the displacement of one floor relative to the floors directly above or below, is usually a key design criteria in tall building design. From the above figure, this is how “flat” a curve is at any given height. Considering the top displacement of the free-standing tower was 296mm, and the top displacement for a linked system as low as 126mm, there is potential for the links to help keep this within limits due to both towers resisting the wind force instead of just tower 1. For all these links, the simple link at $h'=160\text{m}$ seem to give the most inter-storey drift for the linked building system, with tower 2's curve being the flattest out of any curve.

The link's location has a large impact on inter-storey drift regardless of link type, as we would expect. Having a link low lets tower 2 stand very upright at the cost of tower 1 gaining more drift.

We see from the crosses in Figure 4.45 that the displacement of the link varies approximately linearly with height, regardless of the displacements for the rest of the towers. At these locations both towers have equal displacement because the link holds them together. A plot of the displacement of both towers at link height, for different link heights, compared to the displacement of towers 1 and 2 when swaying unconnected, is shown in Figure 4.46, with data ranging down to $h'=20\text{m}$. From this figure, we see clearly that for both the truss and the simple link the relationship is mostly linear, and that the lines go parallel. It would be fair to assume that other links with different stiffnesses would produce other lines parallel to those obtained, with stiffer links moving the lines to the left.

With this a structural engineer could be able to determine certain fixed points along the height of the building, where they want to enforce a certain displacement for both towers. To do this they could apply a link with the right stiffness to fix a certain height to a maximum displacement. The curves shown in Figure 4.45 could be used along with it to let the structural engineer anticipate the displacement of both towers for the corresponding link type and location he has chosen, as Figure 4.46 says nothing about the displacement of either tower at heights other than the link height.

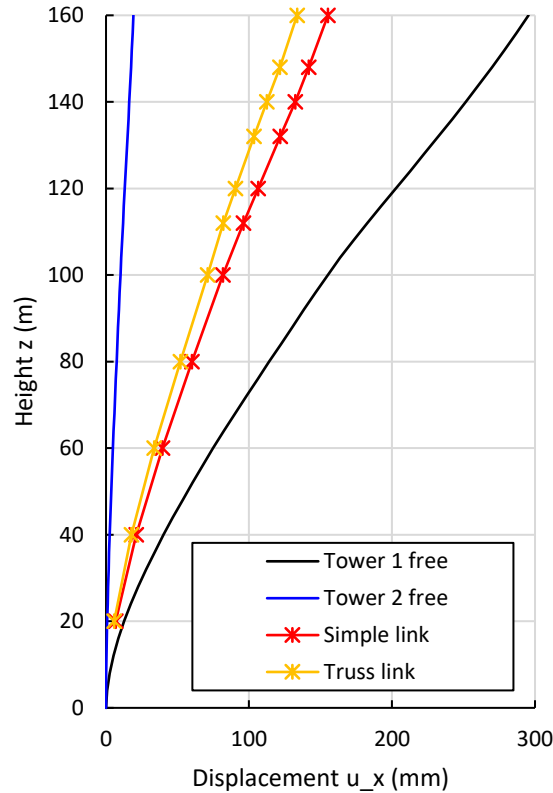


Figure 4.46 Displacement of both towers at link height for different link heights, compared with the displacements of towers 1 and 2 when they are free, i.e. unconnected.

4.7.2 Frame and core interaction

What has been clear from all the load effect diagrams so far, is that the stress distribution in the structure is highly dependent on the structure's system prior to adding any structural links. Knowledge of this distribution is thus relevant for deciding where a structural link will be beneficial or detrimental to the tower's structural effectiveness, and will vary depending on what structural system the buildings use, be it rigid frames, perimeter tubes, central cores, trussed frames, or any combination of the above.

For our model, the frame and shear walls interact in the way described in Figure 4.47. We have seen for all models that the core's moment changes significantly where the frame changes in stiffness.

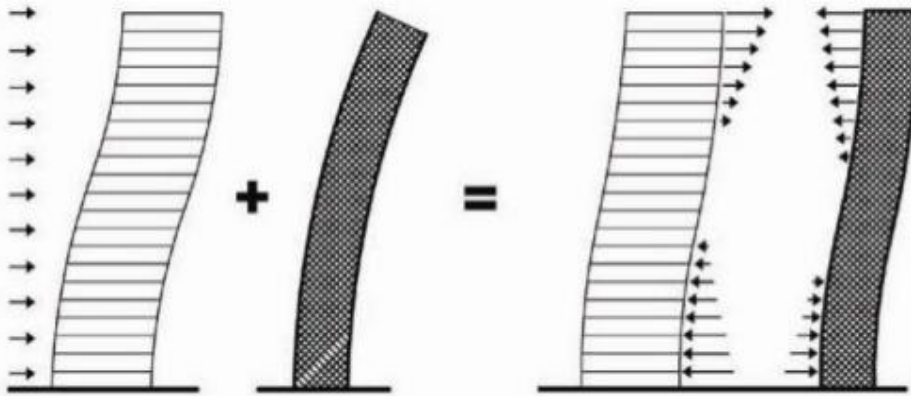


Figure 4.47 Interaction between a rigid frame (left) and a concrete core (centre). When swaying freely, a rigid frame will experience the largest gradient of displacement in the lower part of the frame, with little increase in deflection near the top. The concrete core on the other hand will have little displacement near the bottom, but with an increasing gradient of deformation near the top. Because of this, when these two systems are coupled, the core will restrain the frame near the bottom, while the frame will restrain the core near the top. Figure taken from Shahul (2017).

To better understand this, a model of a single tower was created with a completely homogeneous frame, i.e. all beam and columns sizes are equal throughout the height of the building. Additionally, the influence of core wall stiffness was also checked by creating a model with constant core walls, as the core's thickness changes with height at the same intervals as the columns in the standard model. The bending moment diagrams for the core are compared to the standard tower in Figure 4.48.

We see here that with the homogeneous frame the moment distribution in the core is very different from that of our standard tower. Now it basically has the shape of a normal propped cantilever subject to uniform loading. The change in core wall stiffness does not affect the bending moment diagram much, except for a reduction of base moment that must be attributed to the base walls being very thick, 55cm, compared to the constant core walls which are 35cm.

It seems reasonable to assume that a rigid frame that varies its stiffness differently than the frame of the base model would correspondingly result in a different moment distribution in both the frame and the core, and as such where a link will have the largest impact on structural behaviour.

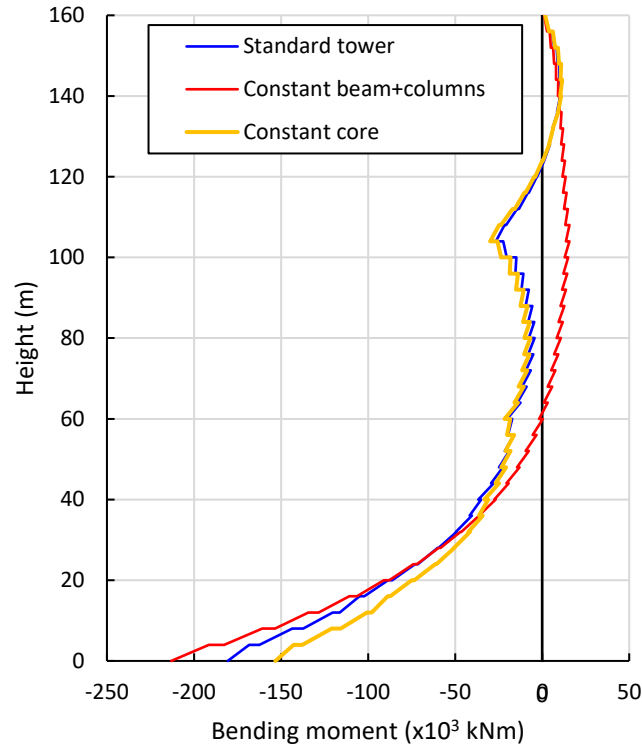


Figure 4.48 Bending moment diagrams for the central core for the standard tower, tower with constant beam and column sizes, and the tower with constant core wall thickness. The constant beams are all $30 \times 70 \text{ cm}^2$ while the columns are all $80 \times 80 \text{ cm}^2$. The constant core wall has a thickness of 35cm.

4.8 Links spacing for equal behaviour

Another thing to consider is how many structural links are needed to force the towers to behave identically, or put in another way: how far apart can multiple links connecting the towers be, while still making them behave equally. To find out, several models were created, which linked the towers together by simple beams pinned at each end only. The models had these links connecting the towers at every storey, every 2nd storey, every 4th storey, and so on, up to every 20th storey, see Figure 4.49. With links at every storey, it is assumed that both towers will behave essentially as one. The goal is to identify how many links we can remove before the towers show significantly altered behaviour from one another.

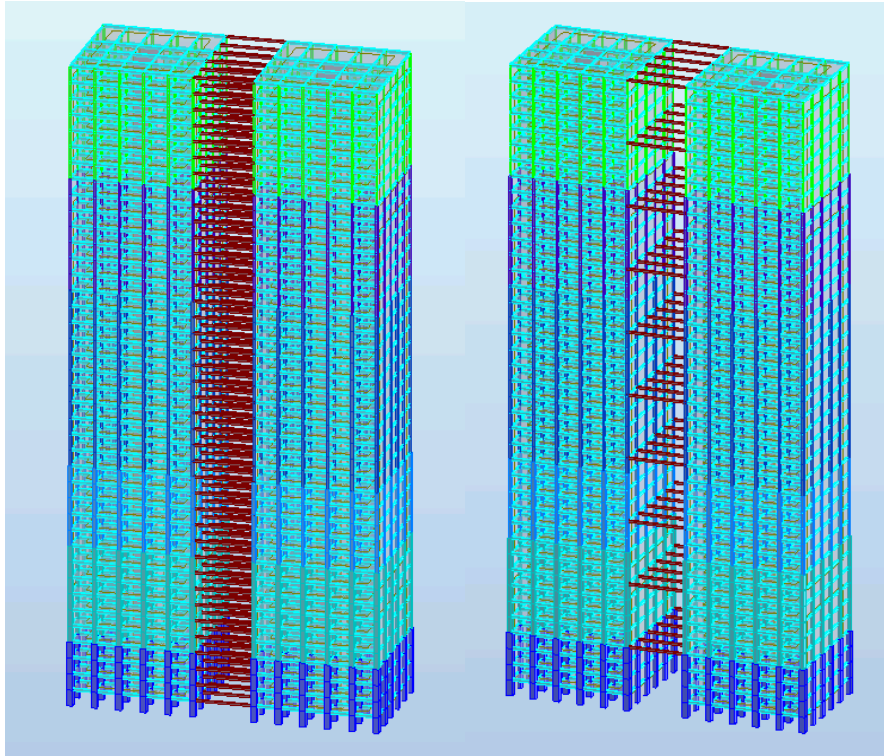


Figure 4.49 Models with links connected at every storey (left) and every 4th storey (right).

The bending moment diagrams for both the frame and the core for the models created are shown on the following pages. As we see from Figure 4.50, the towers have practically identical bending moment diagrams until the link moves more than 6 storeys, 30m, apart. However, the moment magnitude and shape remains very similar for both towers until the links are 10 storeys apart. When the links are 12 or more storeys apart, the bending moment diagram for each core can be described as dissimilar enough to conclude that they do not behave the same way.

From Figure 4.51 it seems like there are some small local variations in moment tower 1 to tower 2 even when the links are attached at every single storey of the building, however, further inspection reveals that this is just a visual glitch in Robot, and that the values are practically the same (with differences around 5 kNm). Ignoring this, the images indicate that the bending moments in the frames of both tower 1 and 2 are almost identical, even for the links as far as 20 storeys (80m), apart. For the models with the links 12 or more storeys apart

4. Structural behaviour

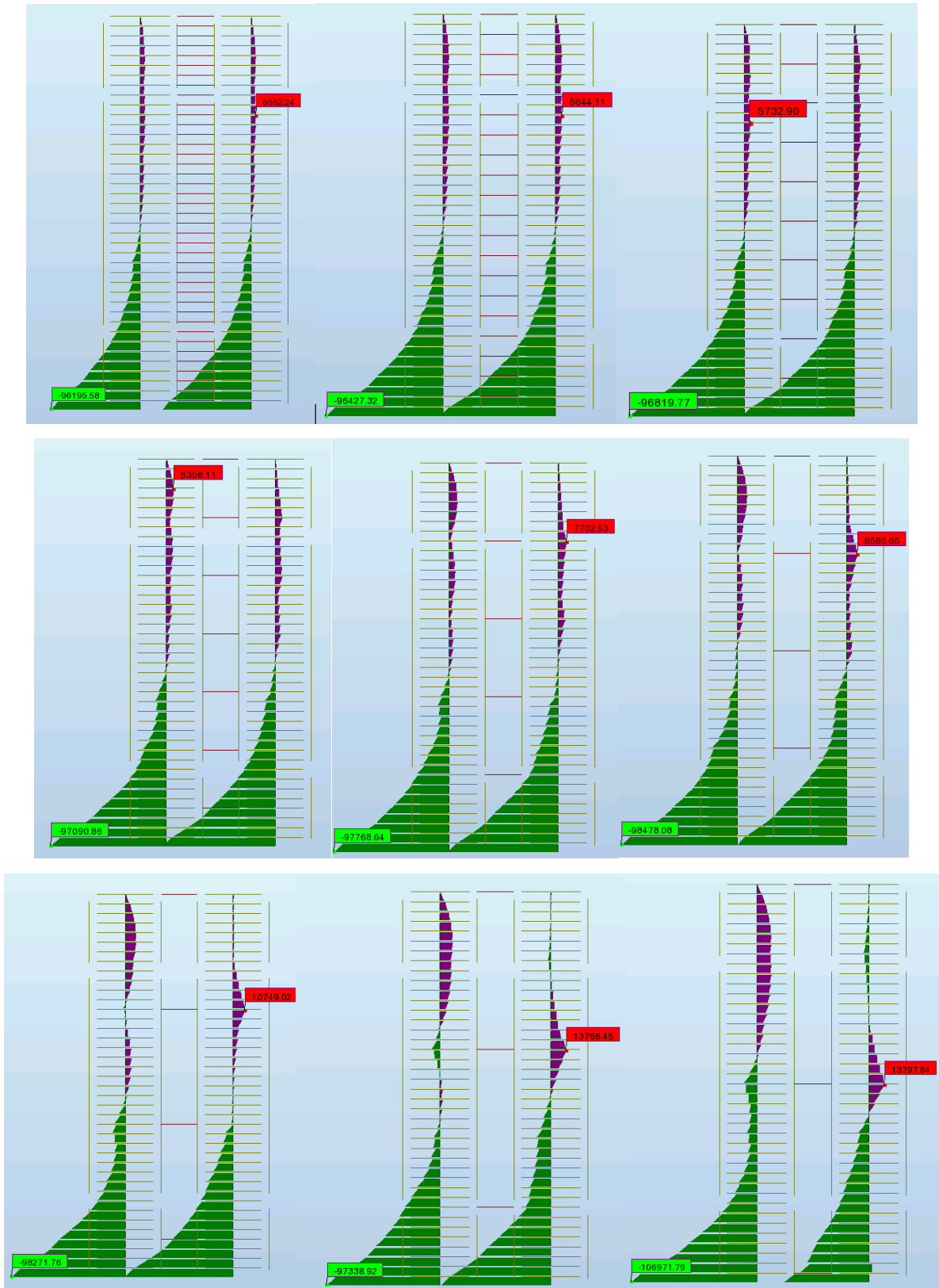


Figure 4.50 Bending moment diagrams for the core for the models with links at varying number of storeys apart. The links are connected at every storey, then every 2nd, 4th, 6th, 8th, 10th, 12th, 16th and 20th storey, respectively.

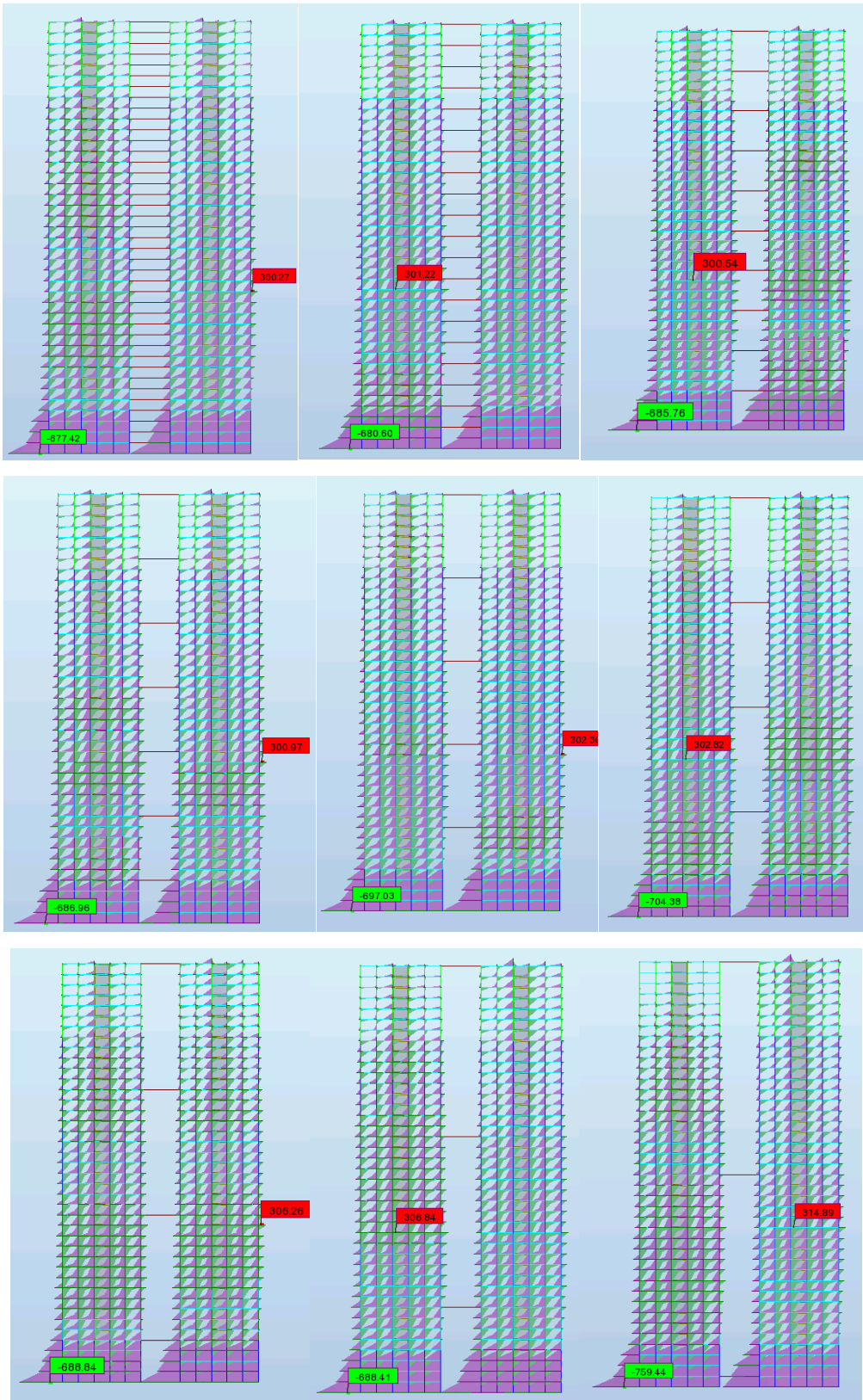


Figure 4.51 Bending moment diagrams for the frame for the models with links at varying number of storeys apart. The links are connected at every storey, then every 2nd, 4th, 6th, 8th, 10th, 12th, 16th and 20th storey, respectively.

tower 2 has much larger moment magnitudes in the top compared to tower 1, namely 108 kNm vs 33 kNm in the beams at the top of the respective towers, but this difference of 75 kNm is likely negligible compared to the moments generated by the gravity loads, and as such will not have much of an impact. Thus, we can conclude that the rigid frame is more or less unaffected by the long spacing between the links, while the core can have significant differences when the links move more than 40 meters, 1 quarter of the building height, apart. We have seen this same trend for all previous models as well, that the core is affected while the frame remains unaffected, so this is as expected.

As for the deformation of the towers

The deformed shapes of both towers are approximately equal even with links 20 storeys apart, see Figure 4.52.

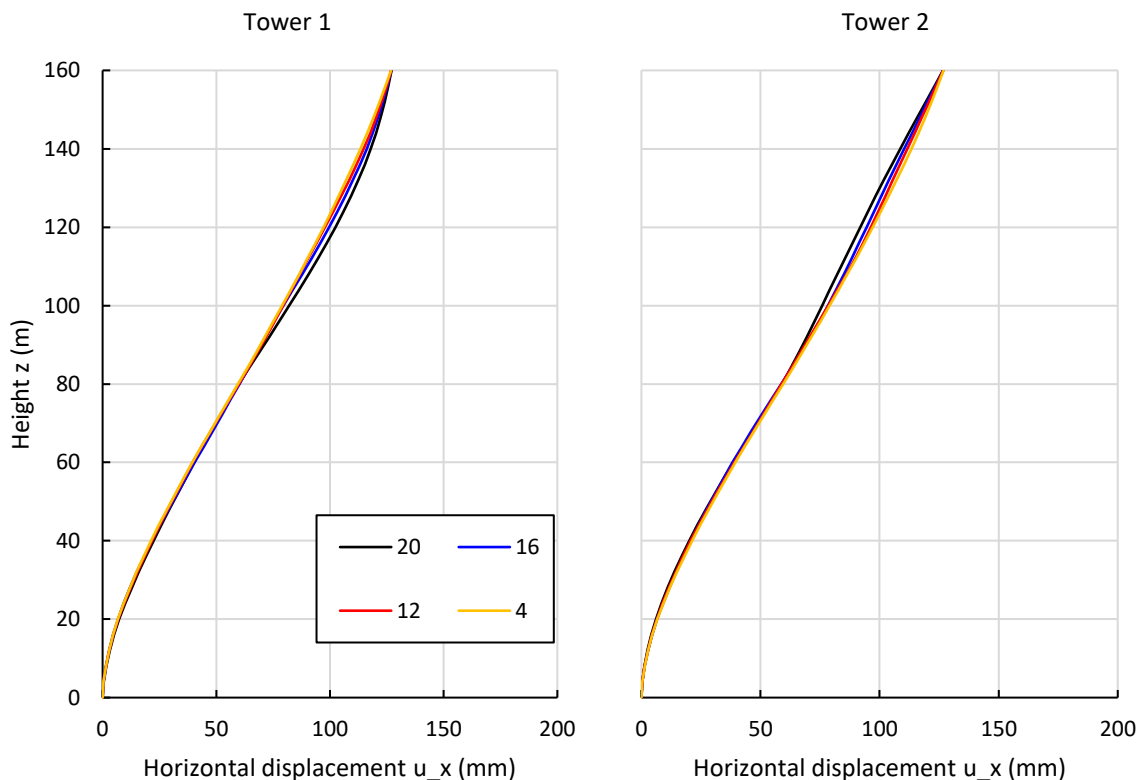


Figure 4.52 Deformed shapes for towers 1 and 2 for links 20, 16, 12 and 4 storeys apart, respectively. Overall the curves are the same. We see a slight increase in displacement for the links 20 and 16 storeys apart between $z = 100$ and 160m .

4.9 Errors

4.9.1 *Wrong modal mass*

Unfortunately, a simple algebraic error was made when calculating the modal mass, not dividing by 4, for the wind load calculation that was not detected before all calculations had been carried out. However, the effect is only that the load has been overestimated by approximately 3% throughout, which is not significant. The effect this had on the acceleration was corrected.

4.9.2 *Omission of skybridge mass in modal mass calculation*

The mass of the skybridges unfortunately had to be neglected when calculating the modal mass for each structure, appendix C explains why.

Song and Tse (2014) found that the mass of the link could have a substantial effect on the natural frequency of the system, especially for heavy links located high in the building, reducing the systems natural frequency by about 30% for a link mass equal to 0,1 the total mass of the building when located at the top of the building. The link mass for the simple link used in calculations is 610 885 kg, compared to a single tower's mass of 30 580 044 kg, meaning the link's mass is equal to ca 0,02 the tower's mass. Thus, the effect of the link mass is likely not this large, likely reducing the natural frequency by less than 10%. However, as we saw in section 3.5.1, the load increases as the natural frequency decreases, and we can assume that the load has been slightly underestimated due to this error.

5 Concluding remarks

To sum up the results of these analyses, the key points to take away are

- The stability system of the towers greatly influences how a link will benefit the structural behaviour. Knowledge of the behaviour of the towers prior to connecting them is important, as it will depend a great deal on how stiff different elements of the system are.
- For a rigid frame and shear wall system: the frame will see much smaller variances in moments and forces compared to the core walls. These variances are generally minor and likely to not cause critical design condition compared to the effects caused by the gravity loads.
- The core's shear and moment diagram varies greatly by both link type and location, in the same way a cantilevered column would by the addition of a concentrated force and moment.
- The base moments of both the core and frame grow equal for each tower as the link moves downwards. At and below the link height $h'=50\text{m}$ ($h'/h=0,3$) the base of each tower practically carry the same loads from wind.
- The minimum top deflection for the simple link happens when the link is at the top of the towers. The minimum top deflection for the truss link occurs when the link is at approximately 140m, or $h'/h = 7/8$.
- The displacement of the towers at the skybridge height are approximately linearly correlated to the skybridge height. This can potentially be used to fix towers at certain max displacements through the use of appropriately stiff links at relevant heights.
- The two towers start behaving as separate towers when unconnected for a distance of ca 40 meters, or 10 storeys, with the cores at this stage reaching dissimilar enough moment distributions for them to be considered different from a design point of view.

5.1.1 Limitations and further work

The knowledge obtained through the work on this thesis does not by any means give a complete picture of how a link might affect the structural behaviour of two tall towers. Important dynamic wind effects such as buffeting and vortex shedding could all have a more significant impact on the behaviour of the systems. Loads going in the across-wind direction have also not been considered, which are also of interest in seeing how the links behaviour creates a lateral torsional moment behaviour in the linked towers. Additionally, the load itself used in the along-wind direction is based on the simplified methods of the Eurocode, and not the more accurate measures provided by wind-tunnel testing. The effect of both combined wind and gravity loads have also not been considered. A more detailed non-linear analysis could also be carried out. Thus, there are several cases to tackle when going forward with further work.

Aside from the suggestions for further work just mentioned, it would also be interesting to see if the results obtained in this thesis hold true for a similar linked building system, but this time with different heights, distances apart, structural systems, etc. to see if the results could be normalized, and the findings could be applied in a more general sense. At the current stage, while the conclusions for this thesis are interesting, unfortunately it cannot be certain if they hold true to systems with a different arrangement of the parameters just mentioned, before further investigation is carried out.

References

- Blum, A. (2007) *Engineer Bill Baker is the King of Superstable 150-storey Structures*.
Wired.com. <https://www.wired.com/2007/11/mf-baker/> (Accessed: 09.06.2017).
- CTBUH (2009) *Linked Hybrid, Beijing*.
<http://www.ctbuh.org/TallBuildings/FeaturedTallBuildings/Archive2009/LinkedHybridBeijing/tabid/4222/language/en-GB/Default.aspx> (Accessed: 09.06.2017).
- CTBUH (2017a) *Raffles City Chongqing Complex*.
<http://www.skyscrapercenter.com/complex/398> (Accessed: 09.06.2017).
- CTBUH (2017b) *SkyHabitat Block 7*. <http://www.skyscrapercenter.com/building/skyhabitat-block-7/14281> (Accessed: 09.06.2017).
- DIVISARE (2006) *Steven Holl Architects, Linked Hybrid*. <https://divisare.com/projects/16691-stein-holl-architects-linked-hybrid> (Accessed: 09.06.2017).
- Dyrbye, C. and Hansen, S. O. (1997) *Wind Loads on Structures* England: John Wiley & Sons Ltd.
- European Committee for Standardization (2009) *NS-EN 1991-1-4:2005+NA:2009: Eurocode 1: Actions on structures. Part 1-4: General actions. Wind actions*.
- ISO (2007) *ISO 10137: Bases for design of structures - Serviceability of buildings and walkways against vibrations*.
- Mainstone, R. (1998) *Developments in Structural Form*. 2 edn. Oxford: Architectural Press, p. 294-315.
- Moon, K. S. (2015) 'Supertall Asia/Middle East: Technological Responses and Contextual Impacts', *buildings*, 5, pp. 814-833.
- NTNU (2014) *Stålkonstruksjoner - Profiler og Formler*. 2 edn. Trondheim: Fagbokforlaget Vigmostad & Bjørke AS.
- Sev, A. and Özgen, A. (2009) 'Space Efficiency in High-Rise Office Buildings', *METU JFA*, pp. 69-89.
- Shahul (2017) *Structure, Technology and Materials of High Rise Buildings*.
<https://www.slideshare.net/shahul130103/structure-technology-and-materials-of-highrise-buildings> (Accessed: 09.06.2017).

Song, J. and Tse, K. T. (2014) 'Dynamic characteristics of wind-excited linked twin buildings based on a 3-dimensional analytical model', *Engineering Structures*, (79), pp. 169-181.

Steenbergen, R. D. J. M., Vrouwenvelder, A. C. W. M. and Geurts, C. P. W. 'Dynamics of Tall Buildings under Stochastic Wind Load: applicability of Eurocode EN 1991-1-4 procedures 1 and 2'. *EACWE 5*, Florence, Italy.

Wikipedia (2017) *The Pinnacle@Duxton*.

https://en.wikipedia.org/wiki/The_Pinnacle@Duxton (Accessed: 06.09.2017).

Wood, A. (2003) 'Pavements in the Sky: the Skybridge in Tall Buildings', *Urbanism*, 7, pp. 325-332.

Photo credits

All photos were accessed on 09.06.2017.

[p, 1] King's vision for New York, <http://stuffnobodycaresabout.com/2015/01/26/old-new-york-in-postcards-11/>

[p, 2] The Monadnock Building, https://en.wikipedia.org/wiki/Monadnock_Building

[p, 3] The Reliance Building, <http://www.architecture.org/architecture-chicago/buildings-of-chicago/building/reliance-building/>

[p, 4] The Empire State Building, https://en.wikipedia.org/wiki/Empire_State_Building

[p, 5] IBM Office building in Pittsburgh,
<https://no.pinterest.com/pin/308707749429474291/>

[p, 6] Johnson Wax Research Tower,
https://commons.wikimedia.org/wiki/File:Administration_Building_and_Research_Tower;_Johnson_Wax_Headquarters;_Racine,_Wisconsin;_June_9,_2012.JPG

[p, 7] Brasilia National Congress Complex, <http://openbuildings.com/buildings/brazilian-national-congress-profile-44692#!buildings-media/2>

[p, 8] Rigid frame bending and shear sway, <https://www.slideshare.net/chuhonsan/15-vertical-structure-pt-3> slide 11.

[p, 9] Bottom of a World Trade Center tower,
<http://archive.doobybrain.com/2013/08/26/world-trade-center-towers-1977/>

[p, 10] Willis Tower, https://en.wikipedia.org/wiki/Willis_Tower

[p, 11] John Hancock Center, <https://no.pinterest.com/pin/323555554458795796/>

[p, 12] Tube structural systems, <http://fgg-web.fgg.uni-lj.si/~pmoze/esdep/master/wg01b/l0720.htm>

[p, 13] Petronas Towers, <http://blog.123hotels.com/experience-the-magic-of-the-majestic-petronas-towers-in-malaysia/>

[p, 14] Burj Khalifa, <http://1001nattreiser.no/en/Utflukter/item/44>

[p, 15] Jeddah Tower, <http://english.alarabiya.net/en/features/2017/02/05/Skyscrapers-Will-Jeddah-Tower-be-the-tallest-in-the-world-.html>

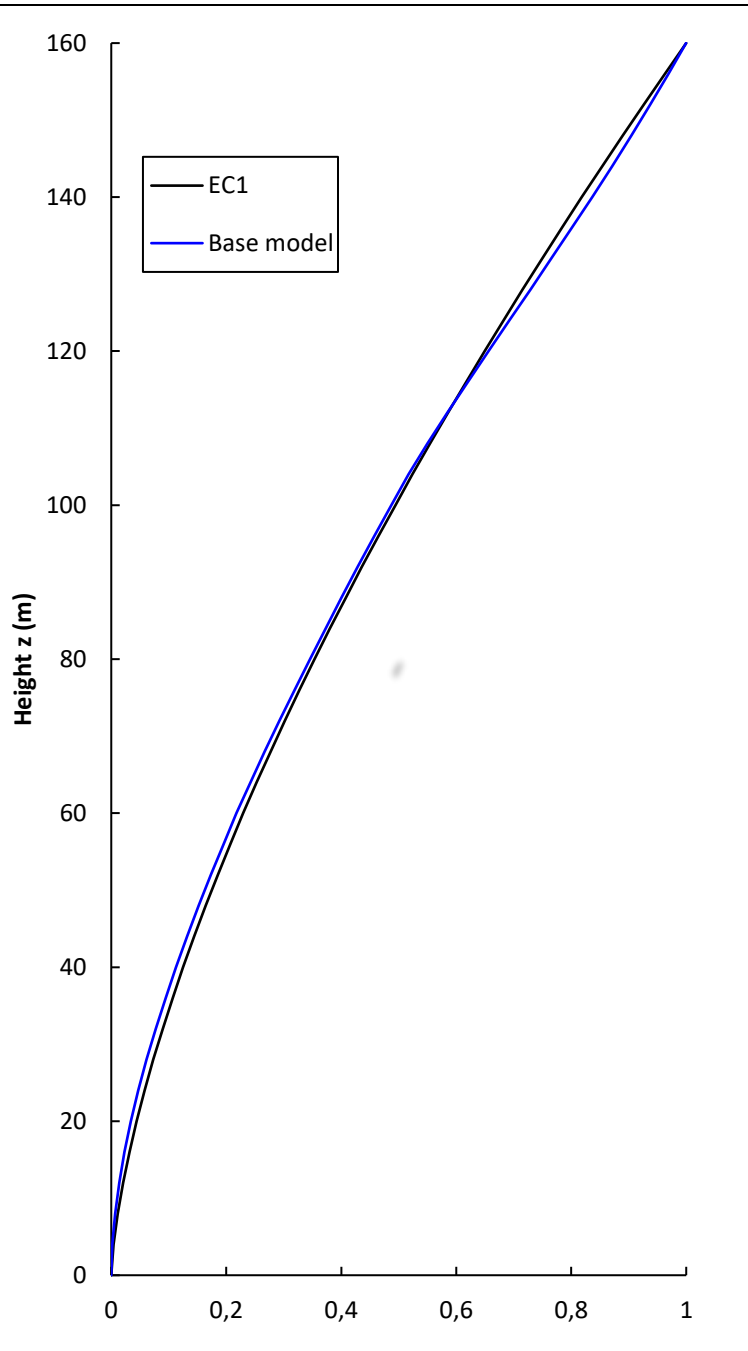
- [p, 16] Nakheel Tower, <http://www.designcurial.com/news/nakheel-tower-in-dubai-by-woods-bagot-exhibits-islamic-design-elements>
- [p, 17] Linked Hybrid 1, <http://www.ctbuh.org/TallBuildings/FeaturedTallBuildings/Archive2009/LinkedHybridBeijing/tabid/4222/language/en-GB/Default.aspx>
- [p, 18] Linked Hybrid 2, <http://www.archdaily.com/34302/linked-hybrid-steven-holl-architects>
- [p, 19] Pinnacle @ Duxton, <http://www.visitsingapore.com/see-do-singapore/architecture/modern/pinnacle-at-duxton.html>
- [p, 20] Sky Habitat, <https://www.dezeen.com/2016/02/09/sky-habitat-moshe-safdie-architects-singapore-housing/>
- [p, 21] Dancing Copper Apartments, <https://www.6sqft.com/live-in-shops-american-copper-buildings-for-833month-lottery-launching-for-160-affordable-units/>
- [p, 22] Umeda Sky Building, <http://japan-highlightstravel.com/en/travel/shin-osaka/160001/>
- [p, 23] Marina Bay Sands, https://no.wikipedia.org/wiki/Marina_Bay_Sands
- [p, 24] Golden Dream Bay, <http://www.propagandastudio.asia/asia/china/photographer/commercial/news/2015/12/20/safdie-architecture-photography-qinhuangdao-china>
- [p, 25] Raffles City Chongqing, <http://www.cladding.com/?project=raffles-city-chongqing>

Appendix

A. Base model mode shape

Table A.1 Mode shape for the base model, taken from Autodesk Robot. The EC1 graph is from the function $\Phi(z) = \left(\frac{z}{h}\right)^\zeta$, with $\zeta = 1,5$, suggested by the Eurocode.

Height (m)	Mass (kg)	Phi_1,x Base model
0	0	0
4	1296162	0,002
8	1296162	0,00692
12	1296162	0,01406
16	1296162	0,02294
20	964781	0,03402
24	964781	0,04701
28	964781	0,06154
32	964781	0,07741
36	964781	0,09445
40	964781	0,11241
44	825506	0,13177
48	825506	0,15206
52	825506	0,17325
56	825506	0,19524
60	825506	0,21779
64	711844	0,24203
68	711844	0,26694
72	711844	0,29256
76	711844	0,31878
80	711844	0,34552
84	711844	0,37274
88	711844	0,40044
92	711844	0,42864
96	711844	0,45742
100	711844	0,48693
104	711844	0,51714
108	565564	0,55002
112	565564	0,5847
116	565564	0,62026
120	565564	0,65637
124	565564	0,69271
128	565564	0,72905
132	565564	0,76508
136	565564	0,80121
140	524742	0,83656
144	524742	0,87108
148	524742	0,90469
152	524742	0,93729
156	524742	0,96892
160	531714	0,99982



B. Portal frame theory

This section explains how statically indeterminate frames are affected by the stiffness of structural members.

Bending stiffness

When talking about portal frame behaviour, we are mostly interested in its deformed shape and bending moment diagram, as these are usually the dominant design criteria in the serviceability and ultimate limit states, respectively. Shear and axial deformations also occur, but these are very small compared to bending deformations in most situations, and have therefore been ignored. Both bending moments and deformations depend strongly on the bending stiffness of the beams and columns making up the frame, so let us begin by introducing this relationship.

Note: a portal frame is as mentioned before made up of horizontal beams and vertical columns. Analytically, beams and columns behave identically, and as such only the term “beam” has been used in the following sections, but all the formulas for a beam also apply to columns. Additionally, the terms “node”, “joint” or “support”, and “beam end” all refer to the same thing and are used interchangeably.

Rotational bending stiffness

Let us define the rotational bending stiffness $k_{b,\theta}$ of a beam with any given boundary conditions as the ratio between an applied end moment M and the rotation θ caused at that end due to said moment, i.e.

$$k_{b,\theta} = \frac{M}{\theta} \quad (\text{B.1})$$

which is the formula for a rotational spring, analogous to Hooke’s famous law: force equals spring stiffness times spring displacement, $F = kx$ ($\Leftrightarrow k = \frac{F}{x}$). Equation (B.1) yields $M = k_{b,\theta} \cdot \theta$, in other words: the end moment of a beam due to a given end rotation is proportional to the rotational bending stiffness of said beam.

It can be shown that the rotational stiffness $k_{b,\theta}$ of a beam depends on its length, L , second moment of area, I , and modulus of elasticity, E , with the relationship

$$k_{b,\theta} = a \frac{EI}{L} \quad (\text{B. 2})$$

where a is an arbitrary constant depending on the boundary conditions of the beam. This yields that the end moment of a member due to an applied rotation is given by

$$M = a \frac{EI}{L} \cdot \theta \quad (\text{B. 3})$$

Translational bending stiffness

Similarly, the relationship for the translational bending stiffness $k_{b,\Delta}$, end moment M and end transverse displacement Δ is defined as

$$k_{b,\Delta} = \frac{M}{\Delta} \quad (\text{B. 4})$$

The translational stiffness $k_{b,\Delta}$ is related to L, I and E by

$$k_{b,\Delta} = b \frac{EI}{L^2} \quad (\text{B. 5})$$

where b is another arbitrary constant depending on the beam boundary conditions. Thus,

$$M = b \frac{EI}{L^2} \cdot \Delta \quad (\text{B. 6})$$

Values for a and b for four standard boundary conditions are shown in Figure B.5.1.

	Moment M
	$\frac{3EI}{L} \cdot \theta$
	$\frac{4EI}{L} \cdot \theta$
	$\frac{3EI}{L^2} \cdot \Delta$
	$\frac{6EI}{L^2} \cdot \Delta$

Figure B.5.1 Relationship between end rotations or translations and moments in a beam for four standard boundary conditions. The first row shows both ends restrained from translation, but free to rotate, corresponding to $a = 3$. The second row shows the left end restrained in both rotation and translation, while the right end is allowed rotate, corresponding to $a = 4$. The third row has the left end fixed, with the right end free to rotate and subject to lateral displacement, giving $b = 3$. Finally, the bottom row shows both ends restrained from rotation, with the right end subject to a lateral translation, corresponding to $b = 6$. Figure taken from NTNU (2014), p. 29.

Bending moment and deformations

The exact numerical relationship between moments and stiffness is not what is of primary importance here however; what is important to take away from this section is that *stiffness attracts moments*.

Realistically, for a portal frame allowed to sway freely, any horizontal load will cause a deformation which includes both a rotation and lateral displacement of the nodes. As we can see from equations (B.3) and (B.6), the moment caused by any given value for either is proportional to a beam's stiffness. Thus,

- The stiffer a beam is relative to other structural members subject to the same deformation, the more moment it will experience relative to the other members.

Furthermore, if we assume that L and E are kept constant, we see that the stiffness is directly proportional to a beam's second moment of area I . As we know from basic mechanics, the second moment of area for a square cross-section is directly related to the section's height h and width b by

$$I = \frac{bh^3}{12} \stackrel{b=h}{\iff} I = \frac{h^4}{12} \quad (\text{B.7})$$

In other words, *the bending moment in a beam due to a given deformation is directly related to the size of the beam*.

Using this knowledge as a basis, we can investigate some portal frames where the structural members have different relative sizes. Assume that all beams and columns have equal lengths and elasticity moduli. The terms "size" and "stiffness" will be used interchangeably.

Normal portal frame

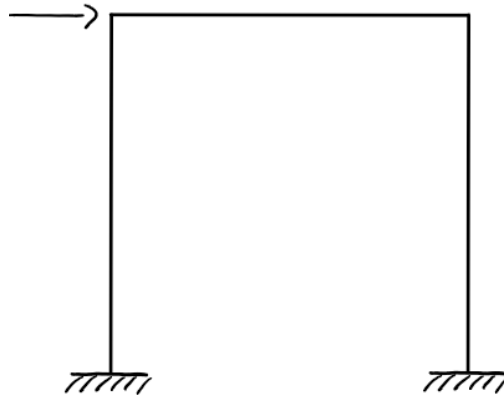


Figure B.5.2 Fixed base portal frame subject to a horizontal load in the top left corner.

Let us begin by considering the basic example, that we will call the normal frame: a simple portal frame with constant beam and column cross-sections, standing on fixed supports, subject to a horizontal load, H , in the top left corner. The frame has six unknown support reactions, F_{X_A} , F_{Z_A} , M_{Y_A} and F_{X_B} , F_{Z_B} , M_{Y_B} , corresponding to the reaction forces in the horizontal, F_X , and vertical, F_Z , directions, and the base moment about the Y -axis (which is perpendicular to the paper plane), M_Y , of columns A and B , respectively. Figure B.5.3 shows the frame reaction forces with the direction of the arrows corresponding to their positive values, i.e. the right, upwards, and clockwise directions, for F_X , F_Z and M_Y , respectively.

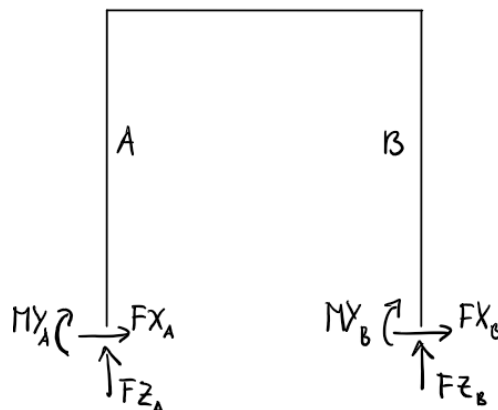


Figure B.5.3 Fixed base portal frame with six unknown support reactions, F_{X_A} , F_{Z_A} , M_{Y_A} , F_{X_B} , F_{Z_B} , and M_{Y_B} . The direction of the arrows indicates the positive direction. Thus, vertical forces going up, horizontal forces going right, and moments going with the clock are all positive values.

Because we only have three equations of equilibrium; horizontal, vertical, and moment equilibrium, see equation (B.8), the frame is three times statically indeterminate, meaning we have three too many unknowns to solve for using only equations of equilibrium.

$$\sum FX = 0 \therefore \sum FZ = 0 \therefore \sum MY = 0 \quad (\text{B.8})$$

However, we can intuitively understand in what direction the support reactions must act, i.e. if they will be positive or negative, because we realize that they will always resist whatever effect is caused by the load.

To illustrate, let us first consider the horizontal reactions, FX_A and FX_B . The applied load is trying to move the frame to the right, and as such they should both resist this, by acting to the left. Additionally, we know both columns are the same size, and from this we can assume that each column will resist the horizontal load an equal amount, i.e. $FX_A = FX_B$. Using horizontal equilibrium, we see that the left and right supports must carry half the shear force each:

$$\sum FX = 0 \Rightarrow H - FX_A - FX_B = 0 \xrightarrow{FX_A=FX_B} FX_A = FX_B = H/2$$

Now let us consider the vertical reactions, FZ_A and FZ_B . We see that the applied load will try to overturn the frame by causing a moment in the clockwise direction. Taking moment about the left support, we see that if the vertical reaction in B, FZ_B , acts in the upwards direction, it will resist this overturning moment, thus we can assume it will. We also know that the sum of vertical forces on the frame must be zero, and with the absence of a vertical load, this means that the vertical reaction in A must be equal but opposite to that in B, and thus act downwards.

$$\sum FZ = 0 \Rightarrow FZ_A + FZ_B = 0 \Rightarrow FZ_A = -FZ_B$$

Finally, by the same logic applied to the vertical reactions, the base moments of each column must also resist the overturning moment, by acting in the opposite, anti-clockwise, direction. And because the columns are equally stiff, we can assume that $MY_A = MY_B$. Thus, the reaction forces must act in the directions shown in Figure B.5.4.

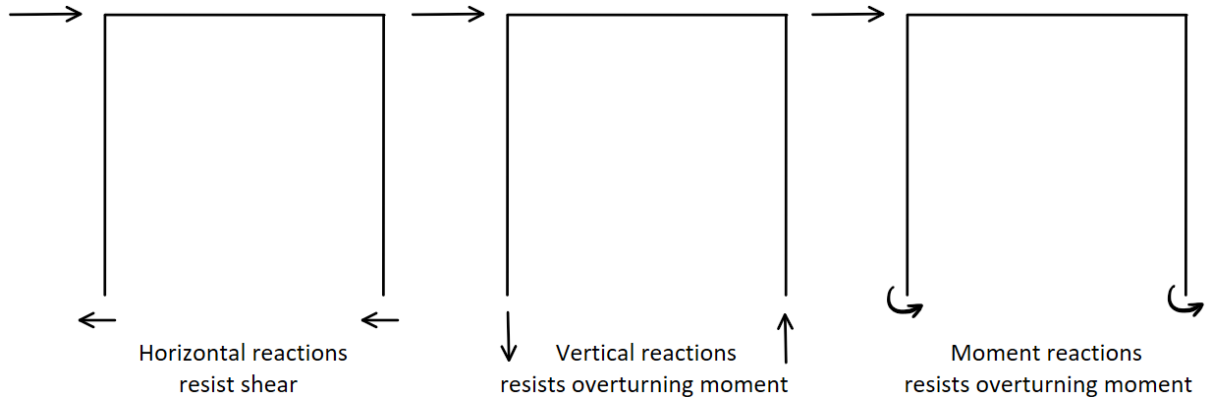


Figure B.5.4 Illustration of how the support reactions for a portal frame will resist a horizontal load action. Left figure: the horizontal support reactions counteract the load by acting to the left. Centre figure: the vertical reactions counteract the clockwise moment from the load by creating a counter-clockwise force couple. Right figure: the fixed moments counteract the clockwise overturning moment by acting in the anti-clockwise direction.

We do not yet know the magnitude of the support reactions, but from knowing their directions we can begin to piece together the shape of the bending moment diagram.

Let us begin by considering column A, which is subject to $H/2$ acting as a shear force to the right at the top of the column, and an equal shear force F_{X_A} acting to the left at the bottom. We also know the column is subject to a counter-clockwise moment M_{Y_A} at the base from the support, creating tension in the left side of the cross-section. At the top, the load will try to bend the column to the right, which will cause the column end to rotate in the clockwise direction. However, the column will want to stay 90 degrees at the corner with the beam, and to achieve this, the beam must apply a counter-clockwise rotation on the column. From equation (B.3) we know that this is done by a counter-clockwise moment. Let us call this moment M_{Y_C} , where the C denotes that it is the corner of the frame. Unlike M_{Y_A} , the corner moment M_{Y_C} will not prevent rotation at the end of the column entirely, and M_{Y_C} must be smaller than M_{Y_A} .

Knowing all this, we can draw the bending moment diagram for column A, see Figure B.5.5. Column B is subject to the same shear force ($H/2$) and base moment ($M_{Y_A}=M_{Y_B}$) as column A, and its bending moment diagram must therefore be identical to column A's.

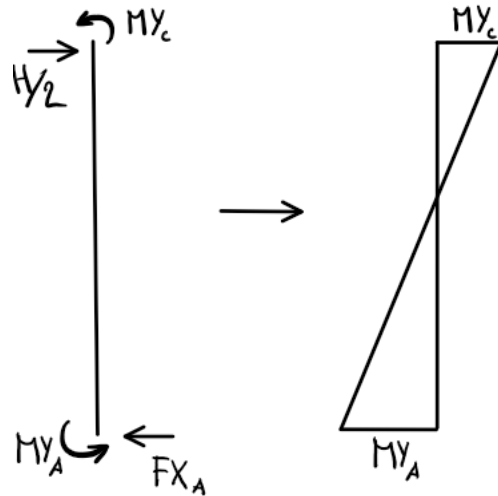


Figure B.5.5 Free-body (left) and corresponding bending moment diagram (right) for column A. The free-body diagram shows the forces $H/2 = FX_A$ and moments $MY_A > MY_C$ acting on the column. The beam prevents the column top from rotating freely, causing the restraining moment MY_C . The beam will not prevent rotation completely, unlike the support at the base, and the restraining moment MY_C will be smaller than MY_A , i.e. $MY_A > MY_C$. This moment diagram is also valid for column B, which is subject to the same load and boundary conditions. Axial forces in the columns have been omitted as they are irrelevant to the bending moment.

Now let us consider the beam. To ensure moment equilibrium of the corners, the beam is subject to the same end moments as the columns, MY_C , but acting in the opposite, clockwise, direction. The reaction force FZ_A goes through column A in tension and pulls down as a shear force on the left end of the beam. Likewise, the force FZ_B goes through column B in compression and pushes up as a shear force on the right end of the beam. The forces, moments and bending moment diagram for the beam seen in Figure B.5.6.

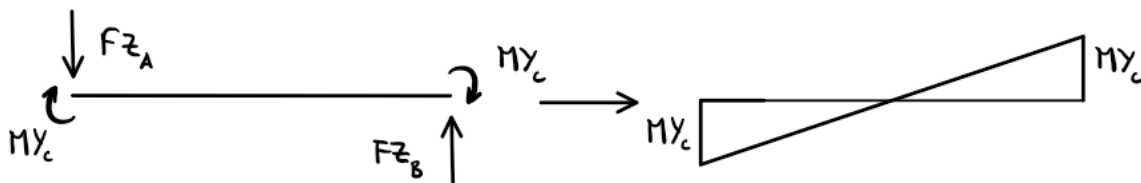


Figure B.5.6 Free-body (left) and bending moment diagram (right) for the beam. The free-body diagram shows how the support reactions FZ_A and FZ_B act as shear forces on the beam. The moments MY_C are transferred from columns A and B (see Figure B.5.5), and must act in the opposite direction to ensure moment equilibrium of the corners. The axial force $H/2$ in the beam has been omitted as it has no impact on the bending moment.

By combining figures Figure B.5.5 and Figure B.5.6, we obtain the bending moment diagram for the frame, which lets us draw its deformed shape. We know that the side the moment

diagram is drawn relative to the structure, indicates which side of the frame is in tension. Figure B.5.7 shows the bending moment diagram for the full frame, with the corresponding deformed shape. The T's mark the tensile zones of the frame.

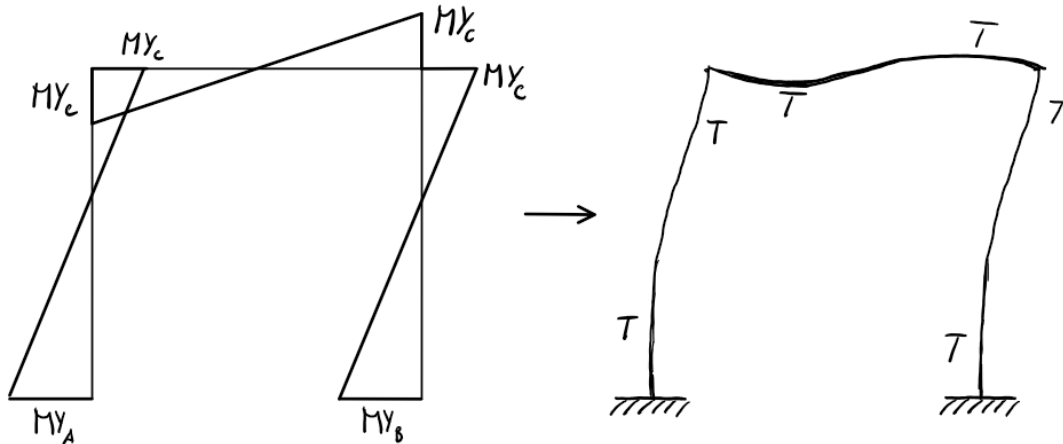


Figure B.5.7 Bending moment diagram and deformed shape for a fixed base portal frame with equal member sizes subject to a horizontal load in the top left corner. MY_A , MY_B and MY_C are the bending moments at the base of columns A or B, or at the frame corners, respectively. The T's in the deformed shape drawing indicate which side of the frame is in tension at their location.

Stiff columns frame

So far, we have found the direction of the support reactions for the portal frame subject to a horizontal load, and we have established the relative magnitude of the horizontal, vertical and moment reactions at A, compared to the horizontal, vertical and moment reactions at B, respectively, by making educated assumptions and applying the equilibrium equations.

We have however not discussed the relative magnitude between the horizontal, vertical and moment reactions themselves, e.g. what size is the horizontal reaction compared to the vertical, and how big is the moment at the base compared to the axial force in the column.

To investigate this relationship, let us consider the same portal frame as in section 0, but this time assume that the columns are much stiffer than the beam. Like the normal frame, we can assume both columns will be subject to a shear force equal to $H/2$.

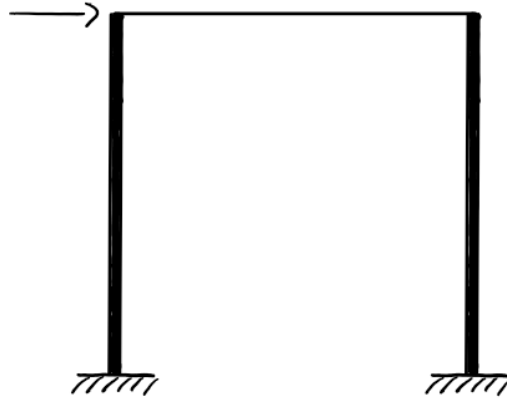


Figure B.5.8 Fixed base portal frame with columns significantly stiffer than the beam, subject to a horizontal load in the top left corner.

Knowing that an increased stiffness attracts an increase in moment, we can assume that the base moments MY_A and MY_B are greater in the stiff column frame than for the normal frame.

Let us also introduce another concept: it can be proven that the change in moment between the ends of a beam subject to a constant shear force, is equal to the shear force times the length of the beam, i.e.:

$$\Delta M = V \cdot L \quad (\text{B. 9})$$

where V is the shear force in the beam. If we consider column A, where MY_A acts counter-clockwise at one end, and MY_C acts clockwise at the other, the total change in moment ΔM is equal to the sum of MY_A and MY_C , $\Delta M = MY_A + MY_C$. Thus, we see that the corner moment MY_C is equal to the base moment MY_A minus the shear force $H/2$ times the length:

$$MY_A + MY_C = \frac{H}{2}L \Rightarrow MY_C = MY_A - \frac{H}{2}L \quad (\text{B. 10})$$

As MY_A and MY_C have opposite signs, this means that by increasing the base moment, we equally decrease the corner moment, and by extension the moment in the beam. The effect this has on the frame's bending moment diagram can be seen in Figure B.5.9.

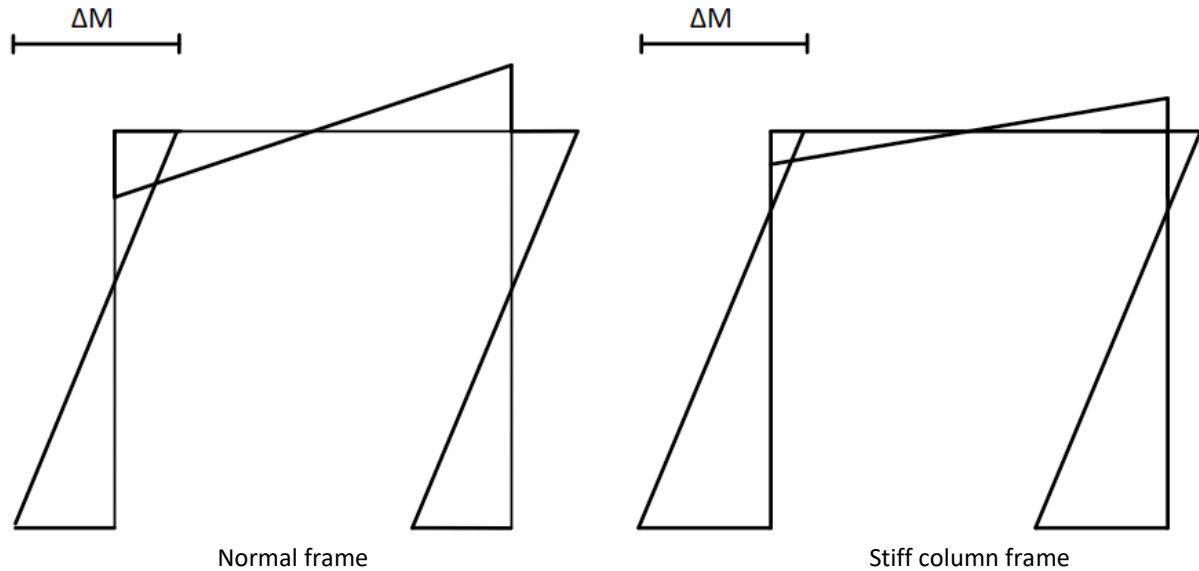


Figure B.5.9 Bending moment diagrams for the normal and stiff column frame, respectively. Note the increased moment in the column and reduction in the beam for the stiff column frame. Also note that the change in moment ΔM for both frames is equal, because the columns are subject to the same shear force $H/2$.

By decreasing the moment in the beam, the beam shear force is also reduced, see equation (B.9). And as we established earlier, the shear force in the beam was equal to the vertical reactions at the base, FZ_A and FZ_B . This means that by increasing the column stiffness,

- The bending moment at the base and in the column is increased.
- The bending moment at the corners and in the beam is decreased.
- The vertical support reactions, and by extension the axial force in the columns, are decreased.

By increasing the stiffness of the columns towards infinity, the beam moment will keep reducing and the behaviour of the frame will go towards the extreme case where there is no moment in the beam at all, which is equal to a hinged frame that allows no moment transfer at the corners, see Figure B.5.10.

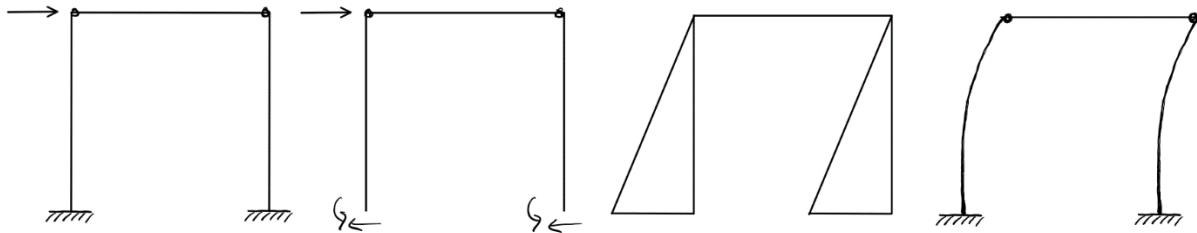


Figure B.5.10 Portal frame with fixed supports and hinged corners, subject to a horizontal load in the top left corner, with the corresponding support reactions, bending moment diagram, and deformed shape, respectively. The pinned corners transfer no moment to the beam, and with no bending in the beam there can also be no axial force in the columns. The columns essentially act as two individual cantilever beams, resisting the overturning moment entirely by the fixed moment at the base.

Stiff beam frame

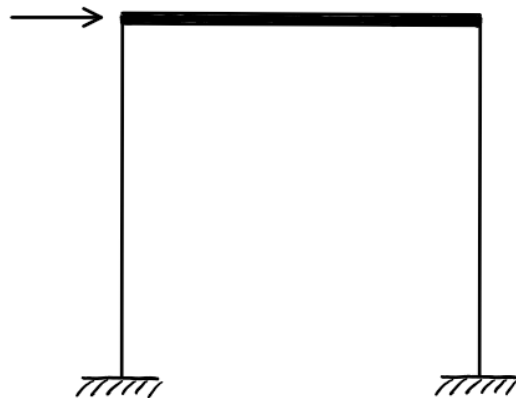


Figure B.5.11 Fixed base portal frame where the beam is significantly stiffer than the columns subject to a horizontal load in the top left corner.

If we now consider a frame where the beam is much stiffer than the columns, we can apply the same logic in and see that an increase in the beam stiffness relative to the columns results in the bending moment diagram of Figure B.5.12.

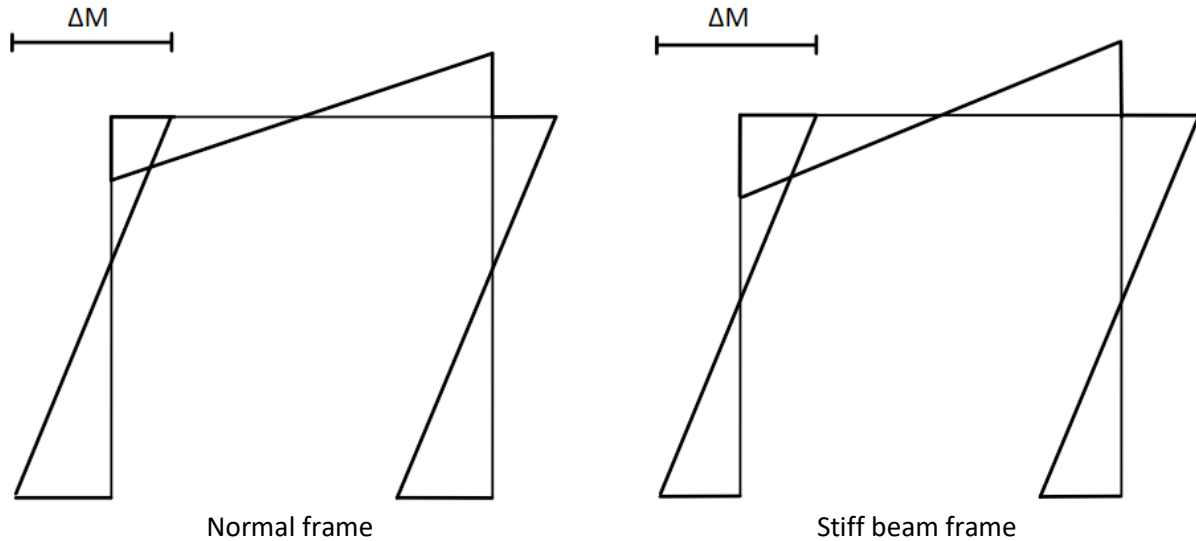


Figure B.5.12 Bending moment diagrams for the normal and stiff beam frame, respectively. Note the increased moment in the beam and reduced moment at the column base for the stiff beam frame. Also note that the change in moment ΔM for both frames is equal, because the columns are subject to the same shear force $H/2$.

We can understand that an increase in stiffness for the beam relative to the columns is the same as a reduction in column stiffness relative to the beam, and we can thus conclude that by increasing the beam stiffness,

- The bending moment at the base and in the column is decreased
- The bending moment at the corners and in the beam is increased
- The vertical support reactions, and by extension the axial force in the columns, are increased

As the beam tends towards infinite stiffness, the rotation at the corners will tend towards zero, which means the restraining moment MY_C will become equal to the base moment MY_A , i.e.

$$k_b \rightarrow \infty \Rightarrow MY_C \rightarrow MY_A \quad (\text{B.11})$$

Where k_b is the beam's bending stiffness. This is analogous to a loading condition for the column equal to the bottom row of Figure B.5.1, see also Figure B.5.13.

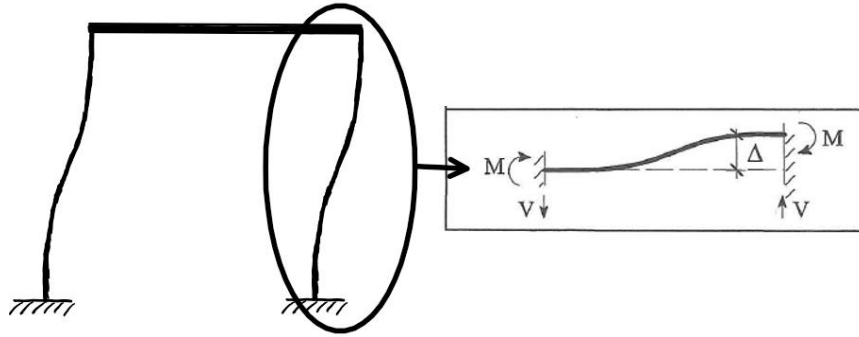


Figure B.5.13 Deformed shape for an infinitely stiff beam frame. The figure shows how the column behaviour is identical to the case shown in the bottom row of Figure B.5.1, with the beam restraining the top end of the column like a fixed support.

One stiff column frame

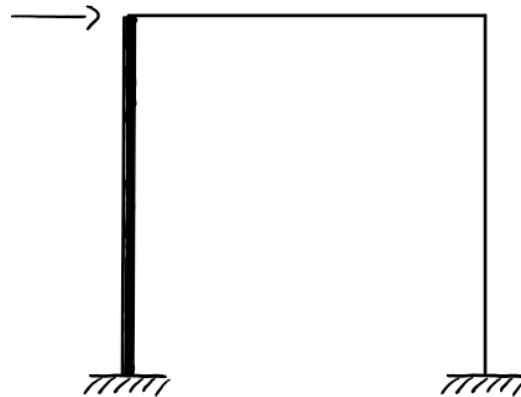


Figure B.5.14 Fixed base portal frame where the left column is significantly stiffer than the right column and the beam, subject to a horizontal load in the top left corner.

Applying what we have learned so far in this chapter, we can also understand how the force distribution in the frame changes if we make one column much stiffer than the other. Let us consider the frame shown in Figure B.5.14, where column A is much stiffer than column B. If we assume the axial deformation of the beam is negligible, then we realize that each column must be subject to the same lateral sway at the column ends, Δ . As we stated in section 0, and as we see from equation (B.3), the base moment in each column is directly proportional to the stiffness of the columns. This means that column A must be subject to a greater base moment than column B, proportional to the relative stiffness of A and B. Let us illustrate by

assuming the second moment of area for column A is twice that of column B, i.e. $I_A = 2I_B = 2I$. Then we see that the base moment in A must be twice that of B.

$$MY_A = b \frac{EI_A}{L^2} \Delta = 2b \frac{EI}{L^2} \Delta, MY_B = b \frac{EI_B}{L^2} \Delta = b \frac{EI}{L^2} \Delta \Rightarrow MY_A = 2MY_B \quad (\text{B.12})$$

However, we have not considered the end rotation of each column. The stiff column will restrain the left corner rotation more than the weak column restrains the right corner, which means that the end rotation of column A must be smaller than the end rotation of column B. This will reduce the moment of column A relative to column B, such that $MY_B \leq MY_A \leq 2MY_B$.

So far, we have assumed the shear in each column is the same, but in the case with one column stiffer than the other, we can assume that the shear force in column A is greater than in B. Thus, the change in moment for column A will be greater than the change in moment for column B, see equation (B.9). Due to vertical equilibrium, the vertical reaction forces must still be equal and opposite. Figure B.5.15 shows the frame with relative magnitude of reaction forces, and Figure B.5.16 shows the resulting bending moment diagram compared with the normal frame.

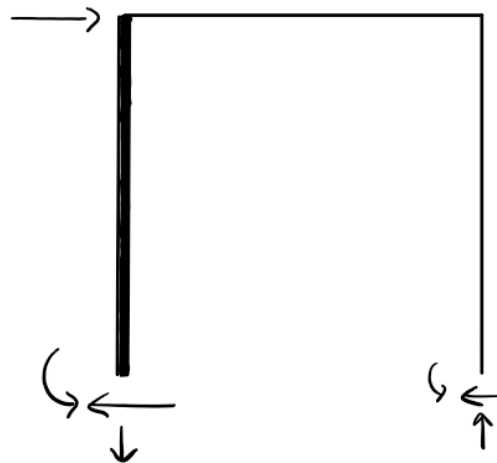


Figure B.5.15 Reaction forces for a fixed base portal frame where the left column is significantly stiffer than the right column and the beam, subject to a horizontal load in the top left corner. The size of the arrows for the support reactions indicate their relative size, i.e. the left shear force is greater than the right, likewise for the moment. The vertical reactions are equal in magnitude, thus the vertical arrows are the same size.

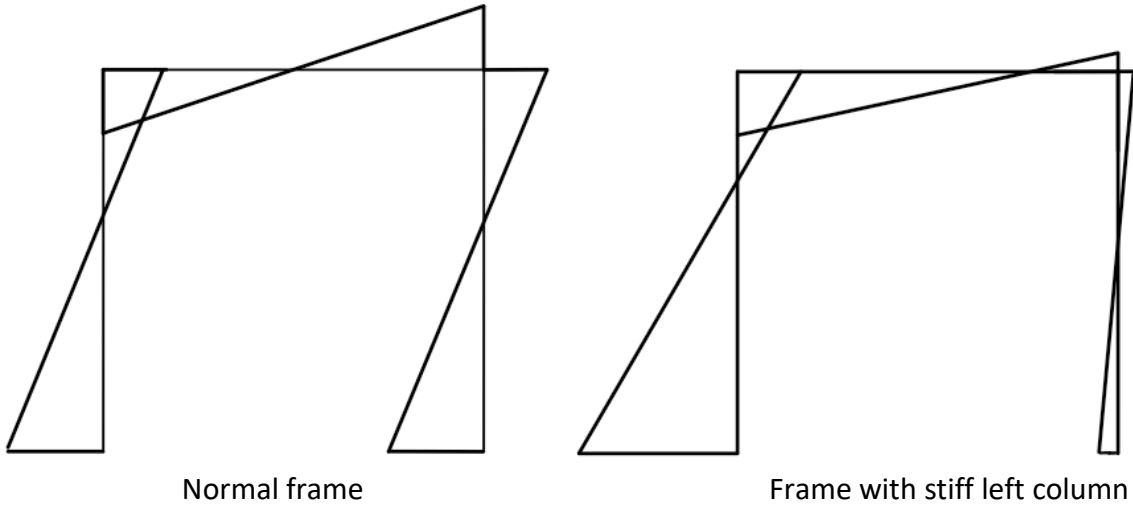


Figure B.5.16 Bending moment diagrams for the normal frame and the stiff left column frame, respectively. The left column carries greater moments both at the base and at the corner than the right. Note the total change in moment from the base to the corner is greater for column A than column B, due to column A carrying a larger shear force.

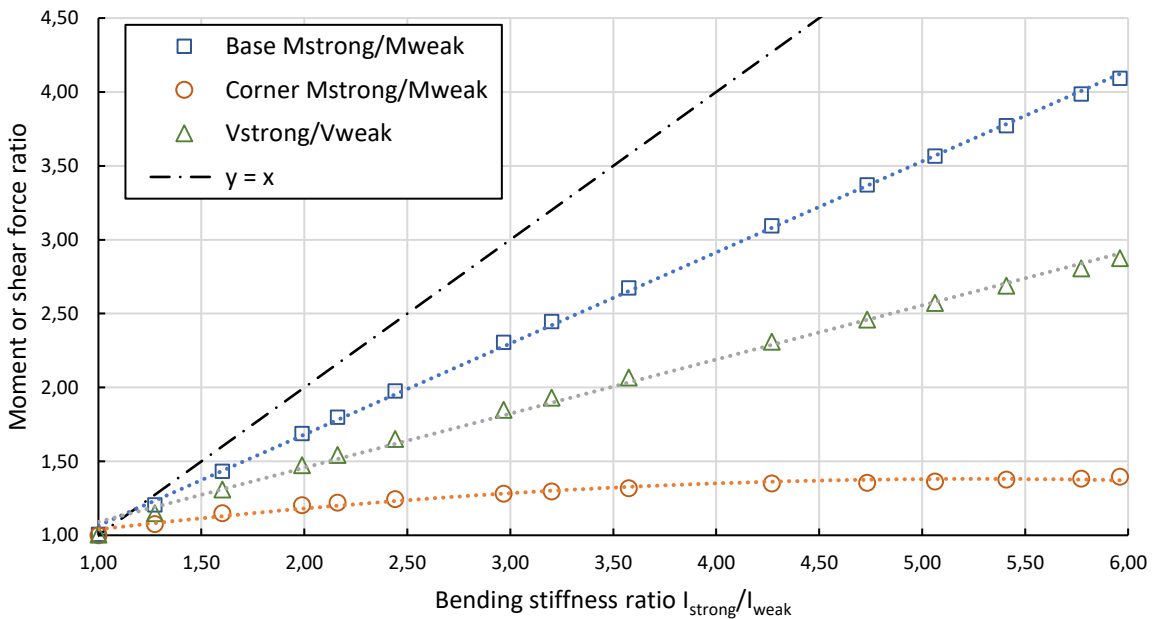


Figure B.5.17 Relationship between bending stiffness ratio, $I_{ratio} = I_{strong}/I_{weak}$, and the ratio of base moments, corner moments, and shear forces for the strong column compared to the weak column, respectively. The black dashed-dotted line indicates a 1-to-1 relationship. The base moment and shear force ratios are approximately equal to 0,616 and 0,366 times the stiffness ratio, respectively. The corner moment ratio levels off and remains constant at about 1,4 the bending stiffness when the strong column becomes 4 or more times stiffer than the weaker column.

Figure B.5.17 shows a plot of how the moment and shear force magnitudes vary with column stiffness ratio $I_{ratio} = I_{strong}/I_{weak}$. The base moment ratio is calculated by dividing the base moment of the strong column by the base moment of the weak column. Likewise for the corner moment and shear force ratios.

As we can see from the figure, both the base moment and shear force ratios vary approximately linearly with the stiffness ratio. We also see that there is less than a 1-to-1 correlation between the base moment ratio and the stiffness ratio, as we would expect. When column A is almost 6 times stiffer than column B, it is subject to a base moment about 4 times greater than B, and a shear force 3 times as large. The trendline for the base moment data points approximately follows the relationship $base\ moment\ ratio = 0,616I_{ratio}$, which means that the end rotation moment reduces the base moment ratio by almost 40%. The shear force ratio is approximately equal to $0,366I_{ratio}$. The corner moments level out at a ratio of around 1,4 when the stiffness ratio becomes greater than 4, implying that increasing the stiffness ratio further past this point will not change the relative size of the corner moments at each end of the beam.

Summary of findings

To summarize this chapter, we can report the following findings about a simple portal frame

- Increasing column stiffness will increase the base moment of the column and reduce moments in the beam. It will also reduce the axial forces in the columns.
- Increasing beam stiffness will decrease the base moment of the column and increase moments in the beam. It will also increase the axial forces in the columns.
- The shear force and base moment distribution in a column is linearly correlated with its relative stiffness compared to the other column.
- The axial force in one column must always be equal and opposite to the axial force in the other column.

We also now understand that in general, *the stiffer a beam or column is, the more moments, and thus stresses, it will attract relative to other structural members.* Figure B.5.18 summarizes the behaviour of the portal frames that we have investigated in this chapter.

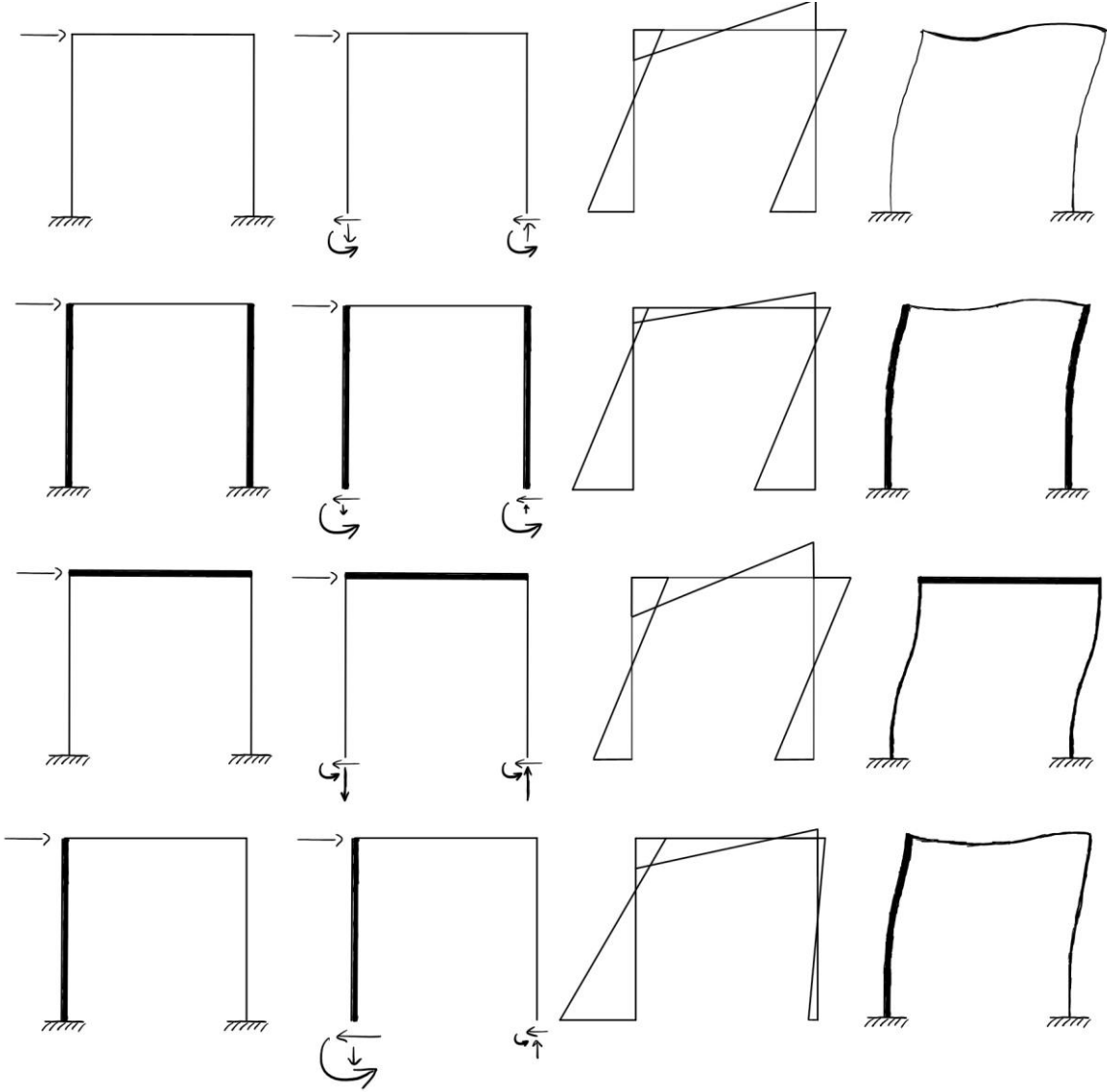


Figure B.5.18 Simple portal frames with varying relative beam and column stiffnesses, standing on fixed supports, subject to a horizontal point load in the top left corner, and their corresponding support reactions, bending moment diagrams and deformed shapes, respectively.

C. Skybridge mass omission

Modal mass, m_e , is a function of mass per meter at any given height, $m(z)$ [kg/m], see equation (3.14):

$$m_e = \frac{\int_0^h m(z) \cdot \Phi^2(z) dz}{\int_0^h \Phi^2(z) dz}$$

Therefore, we see that it depends on the link mass and location along the height of the towers. As mentioned before, to calculate m_e , $m(z)$ is obtained from Robot. The way Robot handles the vertical axis in building modelling is assigning height segments into stories, in our case 40 stories at 4 meters each. All model objects that are inside this 4m envelope belong to that storey, and Robot then returns the total mass of all objects in that storey. That way we find the mass along the building height for every 4m intervals, essentially giving us the value of $4 \cdot m(z)$ at these heights, which we can easily convert to $m(z)$ by dividing by 4. However, when plotting the mass for each storey against the height for a structural model with a truss link over the top 3 stories (i.e. $h' = 160\text{m}$), it was found that the mass for certain stories were differing from other identical stories, see Figure C.15.19, which they should not.

Upon investigating this model, it was found that Robot had incorrectly assigned structural objects belonging to other storeys to storey 28, causing an increase in mass for storey 28 and subsequent decrease in mass for the other storeys affected, see Figure C.25.20. Attempts to remedy this proved to be unsuccessful, as fixing one storey would cause another to break. Equally unfortunate was the fact that this had happened for all the other model permutations. Not being able to solve this problem, it was decided to neglect the mass of the skybridge entirely, and rather use the mass distribution for the twin towers without any skybridge. This way it was possible to ensure that all model permutations remained equally unaffected by this modelling error. Unfortunately, it also means that the mass of the structural links had to be ignored when calculating the dynamic load, and more importantly, the building peak acceleration.

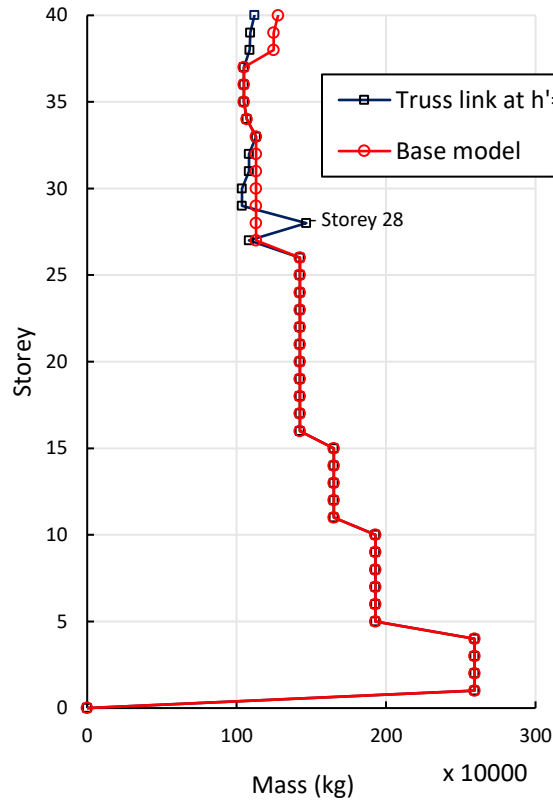


Figure C.15.19 Mass per storey for the base model and the model with a truss link at $h' = 160\text{m}$. The mass distribution for the base model is correct, with equal mass for storeys with equal member sizes. The mass distribution for the truss model is incorrect. This can be seen around storey 28, which has a much higher mass than the floors above it, even though they contain the same structural elements.

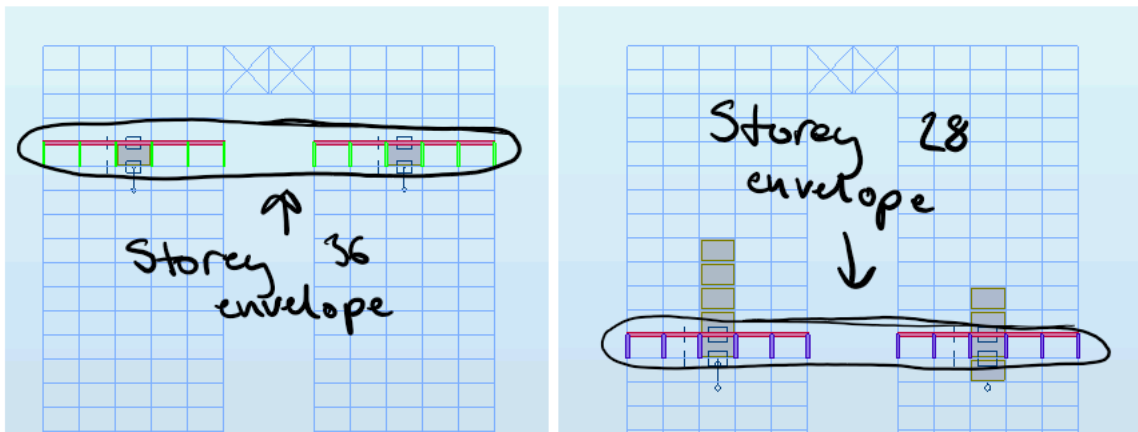


Figure C.25.20 Example of the storey assignment in Robot for twin towers connected by a truss bridge. To the left: only the contents of storey 36 showing. This storey and its objects are assigned correctly, as evidenced by none of the visible objects being outside the envelope of storey 36. To the right: only the contents of storey 28 showing. The objects in this storey are assigned incorrectly, with walls belonging to storeys up to storey 32 showing as being a part of storey 28.